PULSE MODE PERFORMANCE MODEL

W. D. Chadwick, et al

Rocketdyne

Prepared for:

Air Force Rocket Propulsion Laboratory

November 1972

AFRPL-TR-72-16

PULSE MODE PERFORMANCE MODEL

FINAL REPORT

W. D. Chadwick
L. P. Combs

Rocketdyne
A Division of North American Rockwell Corporation
6633 Canoga Avenue
Canoga Park, California

Technical Report AFRPL-TR-72-16
November 1972

Air Force Rocket Propulsion Laboratory
Director of Laboratories
Air Force Systems Command
United States Air Force
Edwards, California

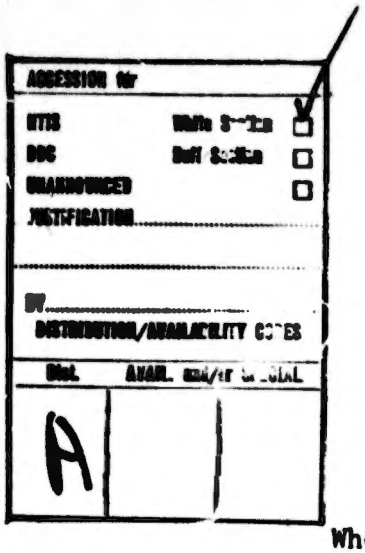

When U. S. Government drawings, specifications, or other data are used for any purpose other than a definitely related Government procurement operation, the Government thereby incurs no responsibility nor any obligation whatsoever, and the fact that the Government may have formulated, furnished, or in any way supplied the said drawings, specifications, or other data, is not to be regarded by implication or otherwise, or in any manner licensing the holder or any other person or corporation, or conveying any rights or permission to manufacture, use, or sell any patented invention that may in any way be related thereto.

UNCLASSIFIED

Security Classification

DOCUMENT CONTROL DATA - R & D

(Security classification of title, body of abstract and indexing annotation must be entered when the overall report is classified)

1. ORIGINATING ACTIVITY *(Corporate author)*

ROCKETDYNE
a division of North American Rockwell Corporation
6633 Canoga Avenue, Canoga Park, California 91304

2a. REPORT SECURITY CLASSIFICATION

Unclassified

2b. GROUP

3. REPORT TITLE

PULSE MODE PERFORMANCE MODEL

4. DESCRIPTIVE NOTES *(Type of report and inclusive dates)*

Final Report

5. AUTHOR(S) *(First name, middle initial, last name)*

W. D. Chadwick and L. P. Combs

6. REPORT DATE	7a. TOTAL NO. OF PAGES	7b. NO. OF REFS
November 1972	196	83

8a. CONTRACT OR GRANT NO.	9a. ORIGINATOR'S REPORT NUMBER(S)
F04611-70-C-0074	R-8864
b. PROJECT NO.	
c.	9b. OTHER REPORT NO(S) *(Any other numbers that may be assigned this report)*
d.	AFRPL-TR-72-16

10. DISTRIBUTION STATEMENT

Approved for Public Release: Distribution Unlimited

11. SUPPLEMENTARY NOTES	12. SPONSORING MILITARY ACTIVITY
	Air Force Rocket Propulsion Laboratory Edwards, California

13. ABSTRACT Development of a computerized Pulse Mode Performance Model (PMPM) is described consisting of three distinct technical phases: model formulation, model programming, and model evaluation. The model was formulated and coded for digital computer solution to accurately simulate pulse mode performance operation of liquid bipropellant attitude control engines. The model consists of three primary subprograms that are fully integrated. The first subprogram (PMDER) is an adaptation of an earlier Distributed Energy Release combustion model, which is comprised of smaller models to analyze steady-state operation of spray formation and distribution, stream tube combustion, and two-dimensional kinetic nozzle flow. The second subprogram (PULSE) characterizes transient performance of short pulses by generating time traces of thrust and propellant flowrates, integrating these variables, varying the operating conditions for each pulse, and setting up parametric performance tables. Transient performance is solved using subprograms for modeling transient combustion, feed system dynamics, feed system bbiloff, and ignition. In the third primary subprogram (DCYCLE), a mission duty cycle is analyzed by synthesizing individual pulse performance using the parametric performance data generated from the first two primary subprograms and then calculating cumulative and mean duty cycle performance. Sample output data from the computer model are presented and discussed. Model evaluation consisted of conducting many computer runs (modifying the model as required) that simulated the performance of two rocket engines for which performance parameters and characteristics were known from hot-fire tests. Most performance parameters obtained using the PMPM computer program agreed accurately with hot-fire test data when appropriate values were used for empirical correlation coefficients

DD FORM 1 NOV 68 1473

UNCLASSIFIED

Security Classification

14. KEY WORDS	LINK A		LINK B		LINK C	
	ROLE	WT	ROLE	WT	ROLE	WT
Liquid Propellant Rocket Engines						
Restartable Rocket Engines						
Pulse Mode						
Combustion Analysis						
Injectors						
Thrust Chambers						
Rocket Nozzles						
Performance, Efficiency						
Programs (Computers)						
Performance, Efficiency						
Transient Response						

AFRPL-TR-72-16

PULSE MODE PERFORMANCE MODEL

FINAL REPORT

W. D. Chadwick
L. P. Combs

Rocketdyne
A Division of North American Rockwell Corporation
6633 Canoga Avenue
Canoga Park, California

Technical Report AFRPL-TR-72-16

November 1972

Air Force Rocket Propulsion Laboratory
Director of Laboratories
Air Force Systems Command
United States Air Force
Edwards, California

FOREWORD

This report, prepared by the Advanced Programs Division of Rocketdyne, a division of North American Rockwell Corporation, 6633 Canoga Avenue, Canoga Park, California, summarizes the work performed under Contract F04611-70-C-0074, Pulse Mode Performance Model (Project No. 3058, Program Element No. 6.23.02F), during the period 1 July 1970 to 21 September 1972. The Air Force Project Officer was Capt. S. Rosen, who replaced Dr. Clark Hawk. Initially Mr. T. A. Coultas was the Rocketdyne Program Manager, with Mr. L. P. Combs replacing him just prior to the program extension. Before being assigned as Program Manager, Mr. Combs actively participated in the technical effort.

This report has been assigned the Rocketdyne identification number R-8864.

This technical report has been reviewed and approved.

Walter A. Detjen, Chief
Engine Development Branch

CONTENTS

ILLUSTRATIONS

TABLES

NOMENCLATURE

A	area
a	local sound speed
$a, b, c_1 \text{---} c_6$	empirical spray coefficients (Eq. 9)
C	valve flowrate coefficient
C_0, C_1	valve opening or closing rate coefficients (Eq. 46 and 47)
C_D	drag coefficient
C_F	thrust coefficient
$C_{k'}$	approximate evaporation coefficient
C_{ND}	nozzle discharge coefficient
c	mixture ratio
c^*	characteristic exhaust velocity
c_p	specific heat at constant pressure
D	diameter
$\overline{D}$	mass median droplet diameter
E_m	Rupe mixing efficiency factor (Ref. 17)
F	drag force or thrust
g_c	gravitational coefficient
I_s	specific impulse
K	flow entrance loss coefficient
k_g	thermal conductivity (gas)
k'	droplet evaporation coefficient
L	length of a flow system component
ℓ	length of fluid column in a flow component
M_w	molecular weight

MR	mixture ratio
m	droplet mass or spray size group mass
$\dot{m}$	rate of change of mass
N	droplet concentration (no/volume)
$\dot{N}$	number flowrate of droplets
N_{EL}	number of injection elements
Nu	Nusselt number
n_t	number of stream tubes
P, p	pressure
$\dot{Q}_{SB}$	heat soakback rate
$\dot{q}$	volumetric flowrate
R	universal gas constant or injection oxidizer mass fraction
R_f	flow component frictional loss coefficient
R_p	ambient to nozzle stagnation pressure ratio
R_r	nozzle throat radius ratio (curvature/opening)
Re	Reynolds number
r, θ, z	cylindrical coordinates
r	radius or local oxidizer mass fraction
s	stream tube path length
T	temperature
t	time
u	velocity
V	volume or voltage
W; $\dot{W}$; $\hat{W}$	overall or integrated weight; flowrate; weight flux
w; $\dot{w}$; $\hat{w}$	local or instantaneous weight; flowrate; weight flux
w_{001}	normalization factor equivalent to weight flux at (x=0, y=0, z=1)

X	nondimensional distance from throat plane
X_v	fraction of feed system volume occupied by vapors
x, y, z	rectangular coordinates
z_0	LISP collection plane and PMSTC start plane

Greek Letters

α	nozzle wall angle (from chamber axis)
γ	ratio of specific heats or adiabatic expansion coefficients
Δ	increment or interval
ε	local area ratio (local/throat)
ε_c	chamber contraction ratio
ε_e, ε	nozzle expansion area ratio
λ_c, λ_h	exponential cooling, heating coefficients
λ_v	heat of vaporization
η	efficiency factor
θ	angular coordinate
μ	viscosity
ρ	density
σ	surface tension
τ	time period
τ_n	off-time for the n^{th} pulse
τ_{ign}	ignition delay time

Superscripts

$-$	average value or concerned with one-dimensional solution
n	concerned with the n^{th} droplet size group
$'$	value reduced by evaporation
$*$	value at sonic flow condition

Subscripts

a, amb	ambient
c	chamber or cooling
d	droplet
de	de-energize
E, EL	element
EC	energy conservation
e	expansion section, energize or entrance
enr, ENR	energy
ens	ensemble
exh	exhaust
F	fuel or thrust
f	fuel
fs, FS	feed system
g	gas
h	heating
I, inj	injection
IE	injection end
i	i^{th} stream tube or integer index
j	j^{th} propellant or integer index
ℓ	liquid
m	mixture, midpulse, or mean
mix	mixing
NS	nozzle stagnation
n	integer index
o, O	oxidizer, initial value, or stagnation value

off	at off signal or during off-time
p	pulsing
s	surface, stream tube or separation (also sepr)
ss, SS	steady-state
t	throat
th	theoretical
v	valve or vapor
vac	vacuum
vap	vapor or vaporization
w	wall

INTRODUCTION

Moderate-to-low thrust rocket engines used for attitude control of spacecraft are generally operated in a repeated on-off or pulsed manner. They are usually developed through the use of extensive hot-fire test programs which, although expensive, allow the performance and repeatability characteristics of these engines to be measured. However, such empirical evaluations do not directly indicate the design changes necessary to achieve a specific set of characteristics. No general relationships between engine design and performance characteristics have been available. Therefore, tailoring the performance and repeatability characteristics of an engine for the needs of a particular mission generally requires each trial design adjustment to be evaluated in a series of hot firings.

During the past several years, significant advances have been made toward understanding of, and ability to analytically model, the elemental processes involved in combustion generation of small impulse bits. Computer programs have been developed for analyzing propellant feed system and injection dynamics, liquid propellant spray distribution in a combustor, spray evaporation and ignition phenomena, transient combustion (starting and stopping) dynamics, and steady-state performance. The existing capabilities were examined in the current program. Selected methods, with appropriate modifications, were assembled into an analytical formulation for pulse mode performance analysis and programmed for numerical solution on digital computers.

The importance of some operating conditions on pulsing performance is shown in Fig. 1, which was obtained from actual tests of a development engine. This figure clearly shows that both the pulse width (or on-time) and pulse spacing (or off-time between pulses) have significant effects on performance, and that the steady-state performance forms an upper limit. Therefore, ability to predict the substantial effects of these parameters is considered essential to prediction of pulse-mode performance.

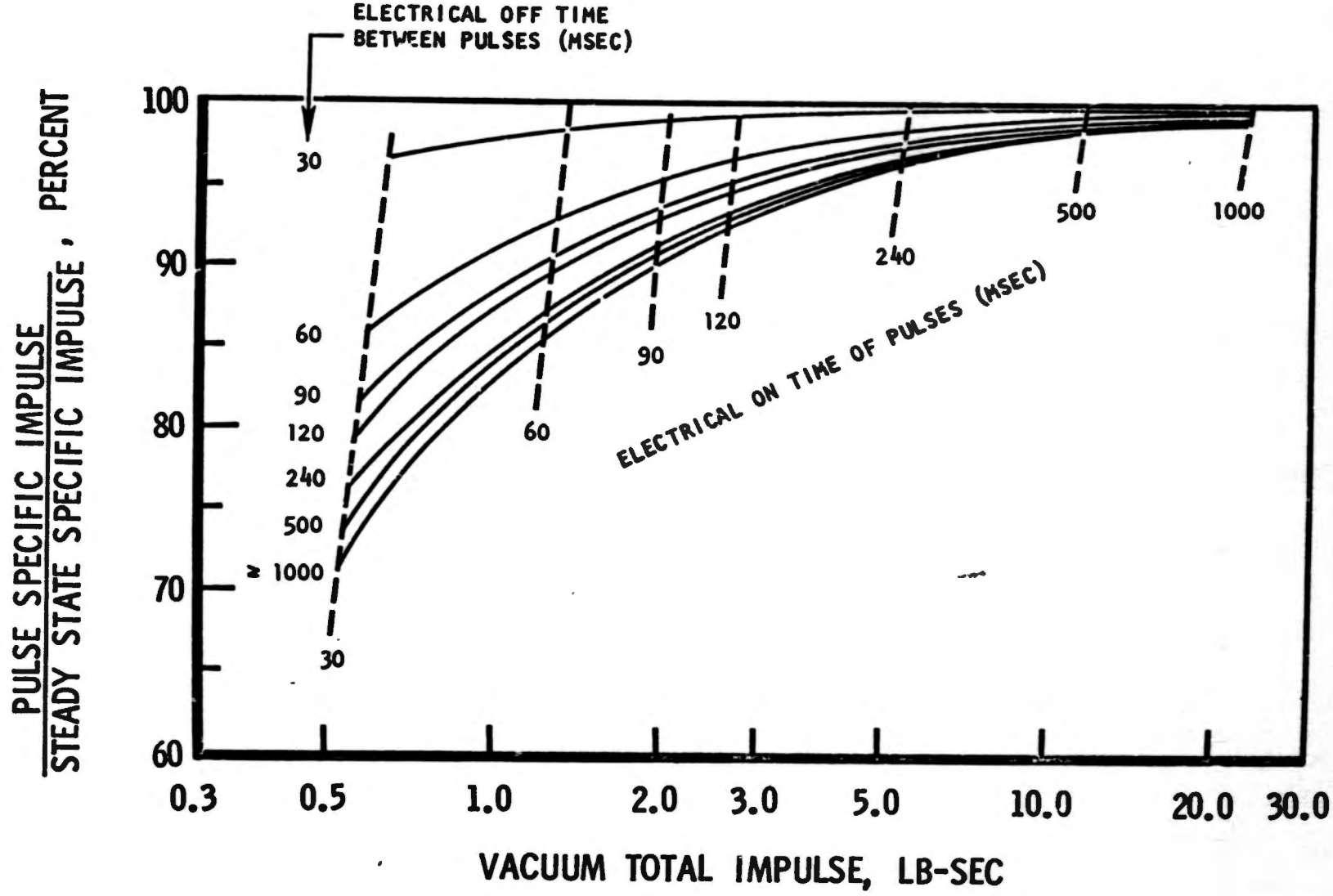

Figure 1. Effects of Pulse Parameters on Performance (Empirical)

TECHNICAL APPROACH

PROGRAM OBJECTIVES

The main objective of the Pulse Mode Performance Model (PMPM) program has been the development of an accurate computerized model for analyzing liquid rocket performance during pulse mode operation. The model accuracy goal was to predict average specific impulse, impulse per pulse, and mean injection mixture ratio within 3 percent of experimentally observed values for pulse rates varying from a single isolated pulse to 100 pulses per second and for pulse durations of 5 milliseconds to steady-state operation.

It was recognized that achieving this kind of accuracy would require as realistic modelling as possible of many physical phenomena and that the computer program inevitably would be large and complicated. A second important goal was to obtain a practical balance between formulation detail and the cost of running the program on a computer.

Another important objective was to make use, to the maximum extent possible, of existing formulations and computer models for the various physical processes involved. These are referred to herein as "component" models.

Three distinct technical phases comprised the program: model formulation, model programming, and model evaluation. In this section, a general description of the technical approach taken in the model development is subdivided according to those three phases.

MODEL FORMULATION

The technical approach taken to model formulation considers pulse mode performance to be determined by the overall nature of a specified engine duty cycle, i.e., details regarding the number of pulses to be fired, pulse durations, and

pulse-to-pulse spacings (off-times). The duty cycle, in turn, is considered to be uniquely determined by its individual pulses, so that a duty cycle analysis can be synthesized by performing, sequentially, detailed analyses of the individual pulses. Then, proceeding a step further, each pulse is considered to consist of discreet phases during which the engine behavior is predominently governed by one (or several) physical or chemical processes which are amenable to quantitative, detailed analysis. A single pulse can be broken down, for example, into valve actuation, feed system priming, spray formation and evaporation, ignition, chamber pressurization, steady-state combustion, valve closure, chamber blow-down, and residual propellant boiloff phases. The model formulation, ultimately, rests on the sequential analysis of the pulse phases.

Many of these pulse phases have obviously been examined analytically prior to this program. The first model formulation task, therefore, was to identify the phases that could be analyzed by adapting existing component models, and the phases that would need to be analyzed with new component models. To aid in this selection, a review was conducted of the technical literature concerned with transient and steady-state rocket combustion. A second task was to formulate the appropriate modifications for existing models, and the required equations and solution methods for the new pulse phase models.

The final model formulation task was to structure the computer programs which, building from computed pulse phase data, calculate performance parameters for individual pulses and then progress to the prediction of duty cycle performance.

Selection of Existing Component Models

The preignition processes that transpire when hypergolic propellants are injected into an evacuated combustion chamber were analyzed by Agosta, Seamans et al. (Ref. 1, 2, and 3). From the inception of the Pulse Mode Performance Model development, it was planned that Seaman's model be adopted for modeling these processes. This primary selection is used as a baseline for discussion selection of other component models.

Feed System/Propellant Injection Model. Seaman's model treats the initial propellant injection very simply: the injection rate of each propellant is increased linearly from zero at time zero to a prescribed steady-state value at some prescribed "steady-state-flow" time. A more realistic injection rate model, capable of responding to chamber pressure variations and of accounting (approximately, at least) for manifold filling phenomena, was desired for the pulse mode formulation. It was decided to consider only short feed systems, so that feed system acoustic wave phenomena need not be analyzed.

The model selected, therefore, considers each propellant to be supplied at constant pressure to a flow control valve which is close-coupled via a short feed line to an injection manifold. Each injection manifold is connected to the combustion chamber by one or more injection orifices.

Feed systems of this kind have been analyzed many times in rocket combustion instability models (Ref. 4 , 5 and 6). Usually, however, the systems are considered to be full of liquids, with injection rates oscillating in response to some pressure oscillation. These models are inadequate when the feed system contains some gas, such as occurs during initial priming or during flow reversals (such as might result from long duration surges in chamber pressure). One example of a more appropriate model for partially liquid-filled systems is that used by Webber (Ref. 7) who discussed concepts and presented model equations, but whose computer program was not available.

An extensive search for an adaptable existing feed system model was not undertaken. Rather, it was decided to program a new component model for this area, adapting concepts and equations of other models as appropriate. Valve response consists of actuation delay times and valve opening and closing rates. The feed system model is used to compute valve and injection flow rates during all phases of pulsing operation.

Preignition Combustor Model. Given propellant injection rates as functions of time, Seamans' model was modified to analyze propellant atomization, vaporization,

reaction, condensation, and flow during the period from beginning of flow into the chamber to the instant of ignition. A major function of this component model is computation of how chamber conditions vary with time until they satisfy an ignition criterion. An option was also provided to use a constant ignition time delay, supplied as input data, rather than the full ignition model.

Transient Combustion. Seamans' model ends with the occurrence of ignition in the combustion chamber. Subsequently, the chamber contents are burned rapidly, and the chamber pressure rises abruptly. Liquid inertia, however, causes the injection rate to remain high for some time. Typically, a chamber pressure spike is produced which is substantially higher than the eventual steady-state pressure level. Particularly for short duration pulses, it is important that this transient chamber pressurization period be analyzed accurately. To aid in selecting an appropriate model for this pulse phase, a brief literature review of transient combustion models was conducted; the findings are summarized in Appendix I.

It was concluded that one model, that of Webber (Ref. 7), offers the greatest potential for physical and, perhaps, computational validity. However, for repetitive analyses of pulses in a sequence, total computer execution times would be prohibitively expensive. Most of the other models were considered to be inadequate for the current use because their equations have been linearized. One model, developed at Rocketdyne but unpublished, was similar to Webbers' in concept except for the analysis of spray gasification. Whereas Webber calculated complete spatial and temporal behavior of several spray size groups for each propellant, the Rocketdyne model used a simple Gaussian function with an empirical rate constant to prescribe the decay of the weight of a propellant liquid spray element with its residence time in the combustor. The approach selected was to adopt the Rocketdyne time-distributed type combustion model, but with the empirical Gaussian gasification functions replaced with computed spray gasification time functions to be generated in the steady-state combustion model.

Steady-State Combustion. Performance during the steady-state phase of a pulse, even if it is of short duration, bears a strong influence on the mean pulse

performance. Selection of a steady-state combustion model was considered to be a relatively important task. Here, too, the technical literature regarding this subject were reviewed, as discussed in Appendix II.

The model selected for steady-state performance analysis is the Distributed Energy Release (DER) model of Ref. 8 . This model encompasses, in a single integrated computer program, calculations of propellant spray mass flowrate distributions and droplet sizes produced by the injector, spray burning along the chamber length, and subsonic, transonic and supersonic gas dynamics of axisymmetrically striated combustion products flow. The DER computer program was modified substantially to form the pulse mode version PMDER. Among those changes, some were made to permit bypassing its TDK subprogram, which consumes substantial computer time in analyzing the kinetically limited nozzle expansion, while still calculating all required performance parameters.

Pulse Decay Transient. The pulse decay transient period, following closure of the propellant valves, includes blowdown of combustion chamber gases from steady-state chamber pressure and boiloff of residual propellants left downstream of the valves when they were closed.

When the program began, it was intended that a new model for the pulse decay transient, which was to have been developed under a concurrent AFRPL contract, would be utilized. As that contract was not consummated, it was necessary to develop a pulse decay transient model for the pulse mode performance model. The approach taken was to use the same transient combustion model as developed for the chamber pressurization phase preceding steady-state operation, but with propellant injection rates into the combustor calculated by a feed system boiloff model instead of the feed system flow model.

New Component Models

From the foregoing discussion, it is seen that, insofar as analyses for the pulse phases are concerned, completely new component models were needed only for analyzing propellant injection rates as follows.

1. A propellant feed system model capable of analyzing partially filled systems and including valve actuation dynamics and reverse flow through the system. A rather simple feed system consisting of a valve (with constant, known, propellant supply pressure), a short connecting line, an injection manifold, and injection orifices was deemed appropriate.

2. A feed system boiloff model accounting for boiling of residual propellant downstream of a propellant valve when it is closed. Relationships among chamber pressure, residual propellant temperatures and vapor pressures, boiloff rates, heat soakback from the combustor, and heats of vaporization were formulated.

Additionally, new component models were required for deriving pulse and duty cycle performance predictions from the pulse phase data. One straightforward approach that might have been taken is to conduct a complete analysis of every pulse in a duty cycle, using the entire array of pulse phase physical models. It was anticipated, however, that such a "brute force" method applied to a long or complicated engine duty cycle would be very uneconomical. Therefore, a more sophisticated formulation was conceived which will perform the duty cycle analysis very rapidly, using parametric performance data from full analyses of a relatively limited number of pulses. Essentially, the approach is to:

1. Determine steady-state performance with subprogram PMDER, generating tables of steady-state combustion parameters and performance data to be used by the subsequent subprograms

2. Characterize pulse transient performance by performing a transient analysis of specified sequences of "standard" width pulses and by setting up tables of parametric performance data with subprogram PULSE for use in the next subprogram

3. Synthesize the performance of each pulse in a specified engine duty cycle by subprogram DCYCLE as well as summing and averaging appropriate parameters over all previous pulses

The main program (PMPM) contains the executive logic which calls for and controls computations by these three subprograms (PMDER, PULSE, and DCYCLE). Each of these subprograms in turn contains the logic for inputing data into and obtaining solutions for smaller component models.

COMPUTER PROGRAMMING

Throughout the computer programming effort, the following objectives were implemented, within practical limits, to provide: a modular structure, simplicity of logic, ease of input, readily comprehensible output, efficient coding for minimum execution time, compatibility of coding between FORTRAN IV and FORTRAN IV H, and, in general, a program well suited for "production" operation.

Program Adaptation to AFRPL Facility

The comprehensive PMPM computer program was developed and operated at Rocketdyne on an IBM System/360 Model 65 computer. An H version of FORTRAN has been used in-house, to be compatible with the System/360. A FORTRAN IV version was prepared for delivery to AFRPL. The conversion process required the generation of a BCD source deck from the FORTRAN IV H EBCDIC source deck. Then a visual check was made to make sure features only available in FORTRAN IV H were eliminated. FORTRAN IV is essentially a subset of FORTRAN IV H, making it possible with very few exceptions, to write a FORTRAN IV H program with the same coding as a FORTRAN IV version.

The AFRPL CDC 6400 computer is more limited in core storage capacity than the Rocketdyne computer. In order to fit the computer program within the usable core capacity of approximately 48K words, the program was structured to allow maximum overlay. Also, the CRT plotting routines were removed from the AFRPL program deck because CRT plotting is not supported there. When these plotting routines are used, the required core size is approximately 52K words.

Input/Output Features

Input data consists of engine design parameters, empirical constants, propellant properties, feed system characteristics, and duty cycle description. Output includes a time history of engine operation and summary data. The Rocketdyne in-house program plots these data using CRT equipment. The coding for plotting appears in separate subroutines, facilitating adaptation to other plotting equipment.

MODEL EVALUATION AND DEMONSTRATION

Designs of two rocket engine thrustors were chosen as evaluation cases for the PMPM computer model. These engines were the Rocketdyne RS1402 and the Marquardt R-1E, which were selected because extensive test data were available for each engine. This evaluation was conducted: (1) to demonstrate the adequacy of the model formulation, (2) to uncover any computer execution problems, (3) to determine the effects of variations in critical input parameters on performance, and (4) to adjust the values of model parameters to obtain agreement of predicted performance with test data, as nearly as possible.

COMPUTER MODEL DESCRIPTION

This section provides a comprehensive technical description of the Pulse Mode Performance Model (PMPM) computer program. The model is comprised of major subprograms that are coupled with an executive control main program. The primary subprograms are PMDER, PULSE, and DCYCLE, with PMDER containig subprograms LISP, STC, and TDK. Pertinent physical processes, analytical equations, digitized construction, and computer program structure are described in this section.

MAIN AND AUXILIARY CONTROL PROGRAMS

MAIN CONTROL PROGRAM (PMPM)

The PMPM main program is a very short executive program which calls subroutines and appropriate subprogram blocks, as required, to perform all data input, analysis, and data output functions. Figure 2 is a PMPM flow chart. First called is subroutine PMPMID which prints out a run heading page, identifying the program used, and reads and writes a number of primary program control indicators. These integer control indicators are used by PMPM (and throughout its subprogram blocks) to denote which subprogram blocks are to be called and whether initialization data are to be supplied. Indicators with initial letter I (e.g., ILISP, IPULSE, c.) are used for subprogram flow control, while those with initial letter J (e.g., JLISP, JPULSE, etc.) are used for data input control. Subroutine PMPMID tests for consistent values of the several indicators before permitting execution to proceed. Allowed indicator combinations are detailed below.

Model Indicator	Allowable Combinations					
	1	2	3	4	5	6
ILISP	1 or 0	1 or 0	0	1	0	0
ISTC	1	1	0	0	±1	0
ITDK	1 or 0	1 or 0	0	0	0	0
IPULSE	1	0	1	0	0	0
IBOIL	1 or 0	0	1 or 0	0	0	0
IIGN	1 or 0	0	1 or 0	0	0	0
IDCYCL	1 or 0	0	1 or 0	0	0	1

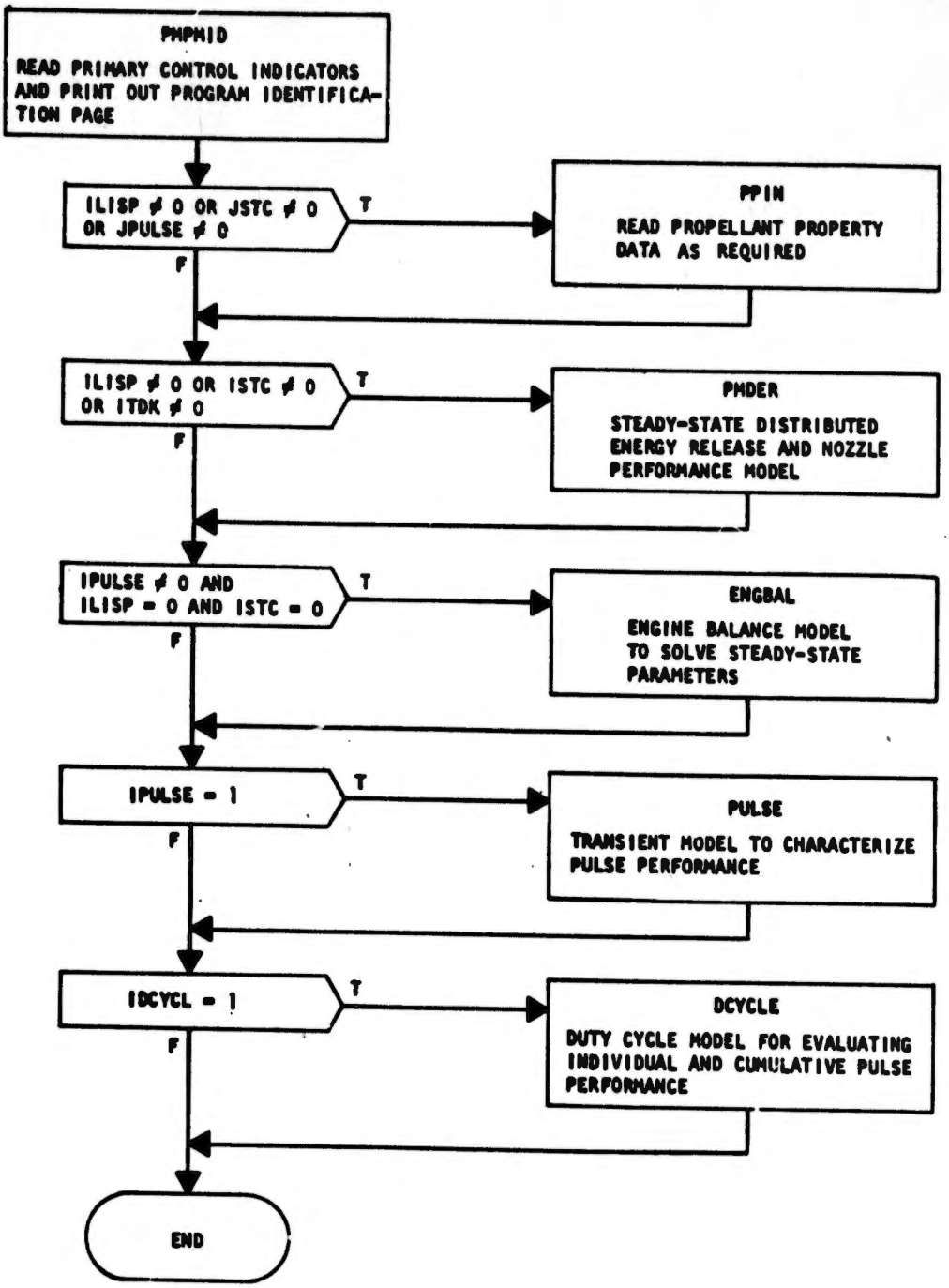

Figure 2. Flow Chart of PMPM Control Program

Broad versatility in running all or selected portions of the PMPM program is provided by the primary program control indicators. For example, it is possible to begin analyzing a case in one run, examine the output and, using punched-card data generated during that run, resume the analysis in a later run without having to repeat the earlier analysis. As another example, it may be desirable to analyze a number of candidate duty cycles using data from a single run of PMDER and PULSE. Also, once a thrust coefficient efficiency has been established for a particular nozzle, TDK subprogram analyses will probably be bypassed, routinely.

PROPELLANT PROPERTIES INPUT DATA (PPIN)

Subprogram blocks PMDER and PULSE require a substantial quantity of propellant and combustion gas properties data. To eliminate redundancies, their input is consolidated in subroutine PPIN, called by PMPM if any of JLISP, JSTC, or JPULSE are non-zero. Within PPIN, read-in of particular blocks of data are bypassed if certain "J" indicators have zero values. For example, if the physical ignition model (IGN) were not to be run, there is no need for thermochemical and kinetic rate data on preignition reactions, so JIGN=0 would be input and these data would be omitted.

ENGINE BALANCE CALCULATIONS (ENGBAL)

The PMPM computer model is designed to be used in either of two ways to satisfy particular run objectives. In an engine design study, for example, the objective might be for the engine to operate with preselected values of certain parameters, such as thrust, impulse per pulse, steady-state chamber pressure, and mixture ratio. In this case, some other parameters, such as propellant supply pressures, propellant injection rates, or even number of injection elements or element orifice diameters, may be allowed to vary to maintain the desired parameters constant in spite of engine inefficiencies. However, quite a different objective may be desired in an engine evaluation program, for example. Here, the engine design and propellant supply conditions may be firmly fixed so that the objective is to predict all engine operating parameters. In this case, inefficiencies will affect thrust, chamber pressure level, propellant injection rates, mixture ratio,

etc., in a complicated manner which the performance model should reproduce in determining calculated engine performance.

The ability to run PMPM in either manner is provided through subroutine ENGBAL; one option permits specifying the injection-end combustion chamber pressure and propellant injection mixture ratio (at steady-state), and the other option permits specifying the propellant valve inlet pressures. In either case, the engine balance solution is based on making best estimates of propellant vaporization and mixing efficiencies, nozzle discharge coefficient, and the ratio of chamber injection end to nozzle stagnation pressures. At key points in the PMPM analysis, computed values of these variables are compared with the estimates used in ENGBAL; if they differ by more than specified tolerances, they become new best estimates for another ENGBAL analysis and, perhaps, reiteration through (at least a portion of) the preceding component model analysis.

Subroutine ENGBAL performs an implicit solution of the following equations (or inversions of them):

$$\dot{W}_f = C_f\sqrt{P_{vf} - P_{IE}} \tag{1}$$

$$\dot{W}_o = C_o\sqrt{P_{vo} - P_{IE}} \tag{2}$$

$$\overline{MR}_g = \left(\frac{\eta_{vap,\,o}}{\eta_{vap,\,f}}\right)\left(\frac{\dot{W}_o}{\dot{W}_f}\right) \tag{3}$$

$$MR_I = \frac{\dot{W}_o}{\dot{W}_f} \tag{4}$$

$$c^* = \eta_{c^*}\, c^*_{th}(MR_I) = \eta_{c^*_{mix}}\, \bar{\eta}_{vap}\, \eta_{ENR}\, c^*_{th}(MR_I) \tag{5}$$

$$P_{IE} = \left(\frac{c^*\left(\dot{W}_f + \dot{W}_o\right)}{A_t\, g_c}\right)\left(\frac{P_{IE}}{P_{NS}}\right) \tag{6}$$

assuming best estimate values of $\eta_{vap,o}$, $\eta_{vap,f}$, $\eta_{c^*_{mix}}$, η_{ENR} and (P_{IE}/P_{NS}) and that C_f, C_o, c^*_{th} and A_t are known. (Default values of the best estimates are built-in if reasonable starting values are not known.)

Initial (estimated) values and computed values of variables are included in an engine balance summary printout.

STEADY-STATE MODEL (PMDER)

Steady-state performance is analyzed by subprogram block PMDER, which is an adaptation to the pulse mode application of the earlier DER (Distributed Energy Release) performance analysis computer program (Ref. 8). In this section, a verbal description is given of the general features of the PMDER subprogram before detailing the various major subprograms which make up PMDER.

PMDER performs a spatial analysis of pertinent processes occurring within a rocket combustion chamber during steady-state operation. In general, the analysis begins from known or estimated conditions at the injector and proceeds along the length of the combustor to a plane just downstream of the nozzle throat, solving for combustion field variables as it goes. In this analysis, the combustor is considered to contain a number of discrete zones, as shown schematically in Fig. 3 . A discussion of the physical natures of these zones is given in Appendix II.

The structure of the PMDER subprogram block essentially parallels that of the zonal approach to the combustion processes. One major subprogram, LISP, within

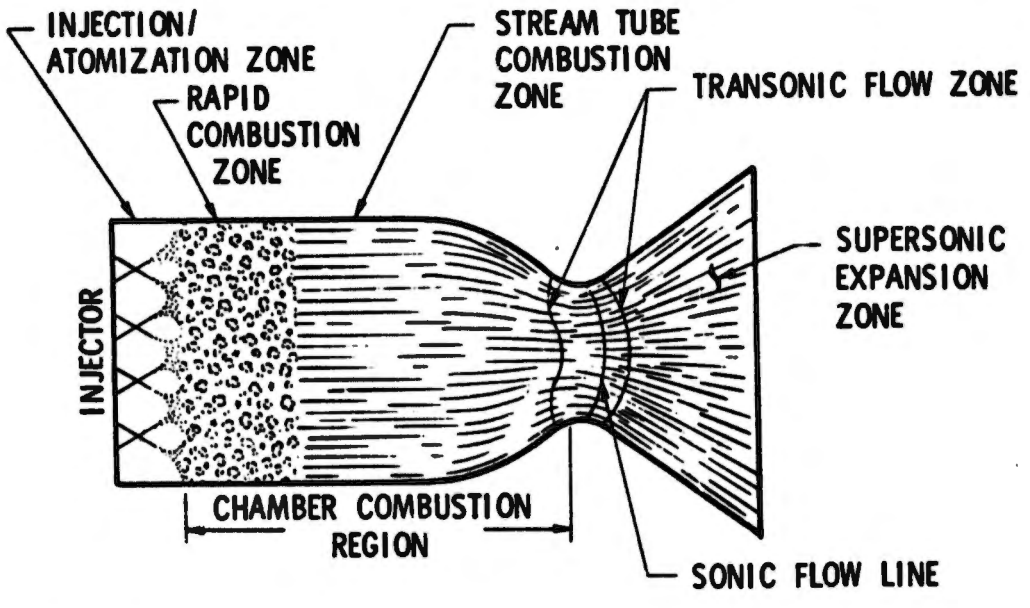

Figure 3. Subdivision of Combustion Chamber Into Zones for Steady-State Combustion Analysis

PMDER calculates propellant injection rates, spray mass flux profiles, spray velocity vectors, and mean droplet diameters in a prescribed plane within the initial combustion zone. These calculations are based on injector design data (number and types of injection elements, element designs, locations, and orientations), propellant data, and empirical parameters which correlate each element's spray mass flux distribution and mean droplet size with its design and operating parameters. LISP also approximates the partial spray vaporization which occurs upstream of its spray collection plane and forms a combustion gas stream therefrom.

The data computed by LISP are used to initialize a bipropellant spray combustion analysis, which starts at the LISP spray collection plane. In PMDER, this analysis is performed by subprogram PMSTC, a stream-tube combustion model. While the LISP data may exhibit both radial and azimuthal variations in mass flux and mixture ratio, the stream tubes usually are set up axisymmetrically so that their flows can feed directly into the exhaust nozzle analysis model. To avoid excessive degradation of the transverse gradients in initializing stream tube flows, a fairly complicated nonphysical method is used to combine LISP mesh points into an order-of-magnitude fewer stream tubes.

PMSTC is structured to analyze a single stream tube as well as multiple stream tubes. The single stream tube option is used extensively in conjunction with subroutine ENGBAL, to solve for compatible flow rates, vaporization efficiencies, and chamber pressure level prior to performing the multiple stream tube analysis. The multiple stream tube solution consists of a multiplicity of simultaneous, one-dimensional, single stream tube solutions which are coupled together by chamber pressure and flow area constraints. By imposing the pressure distribution for a homogeneous transonic flow on the stream tube solution in the nozzle, it is possible to carry the stream tube analysis past the throat plane. Thus the data are generated which are needed for initializing analysis of the supersonic exhaust nozzle flow.

The supersonic combustion gas flow downstream of the nozzle throat is analyzed by a Two-Dimensional Kinetic (TDK) computer program, which is a shortened and

somewhat modified (Ref. 8) version of the ICRPG reference TDK program (Ref. 9). This TDK program performs a method of characteristics solution for the expansion of an annularly striated gas flow with kinetically limited reaction chemistry. The supersonic start-line conditions are provided by PMSTC, except for the chemical species concentrations of the stream tubes, which are obtained by TDK equilibrium solutions before the expansion analysis is begun.

For the pulse mode application, the start-line interface between PMSTC and TDK was improved, the nozzle performance data of the TDK were made available to other PMPM subroutines, and an option was provided to bypass TDK entirely if a steady-state vacuum thrust coefficient is known for the nozzle.

Figure 4 is a flow chart for the PMDER subprogram block. Subroutine ENGBAL is called from PMDER prior to its call for LISP and after each pass through PMSTC single stream tube analysis. Before proceeding from single to multiple stream tube analyses, a tolerance check is made on the change in propellant flowrates used in LISP with the updated rates; if the tolerance is not met, an iteration loop back to the PMDER call for LISP is made, i.e., LISP and PMSTC are coupled, through ENGBAL, to ensure compatibility of their solutions. ENGBAL is also called at the end of each pass through the multiple stream tube analysis.

In addition to steady-state performance data, PMDER supplies propellant spray depletion functions to the PULSE subprogram block. Computed in subroutine CPM2 from data stored by CPM1 during PMSTC analysis, these functions express, for each propellant, the steady-state fraction of an injected element that is still in the liquid state as a function of its residence time in the combustor.

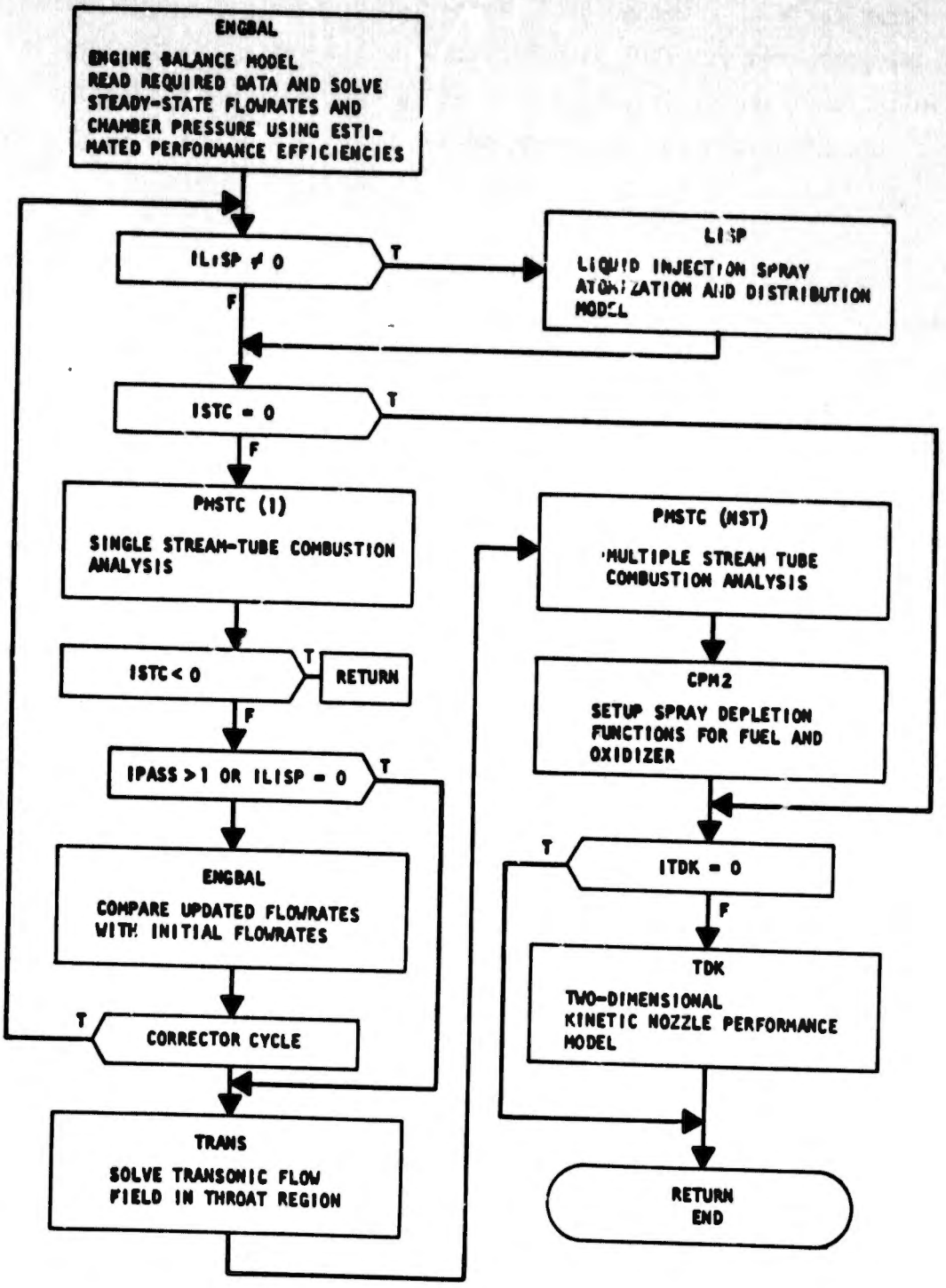

Figure 4. Simplified Flow Chart for PMDER Subprogram

PROPELLANT SPRAY FORMATION MODEL (LISP)

The LISP (Liquid Injector Spray Pattern) computer subprogram block analyzes the propellant spray distributions produced by the injector. Using injection element design, location and orientation data, and empirical correlations for elemental mass flux profiles, mean droplet sizes, and spray vaporization, LISP calculates spray and combustion gas mass fluxes, spray velocity vectors, and mean droplet diameters at a large number of mesh points in one or more "collection planes" at specified distance(s) downstream of the propellant injector. Up to a total of 60 injection elements, in as many as 10 different element types or designs, can be considered. As many as 400 combustion zone mesh points can be prescribed.

Mesh System and Injection Elements

LISP is formulated in cylindrical coordinates (r,θ,z) for analyzing combustors with circular cross sections. Propellant spray parameters are calculated at discrete mesh points ($1 \leq j \leq NMESH$) with coordinates r_j, θ_j, z_0, where z_0 denotes the collection plane. The program is designed to take advantage of radial planes of symmetry to reduce the amount of input required, the number of mesh points required in the analysis, and the computer run times. Normally, the mesh system is set up to analyze only a pie-slice-shaped sector of the injector and chamber flow.

Consider, for example, the injector sketched in Fig. 5, which has 36 unlike doublet elements. The injector pattern consists of the repeating set of elements contained between rays OA and OB. Careful examination shows that line COD represents a plane of symmetry. Rays OA and OC, therefore, define boundaries of symmetry across which there should be no gradients and, thus, they bound an appropriate sector for LISP analysis.

While there is no net flux through planes which are normal to the injector and pass through rays OA and OC, the flow from an individual element is obviously not constrained from flowing through these surfaces. For this reason, LISP must either "reflect" propellant fluxes from planes of symmetry, or enough elements

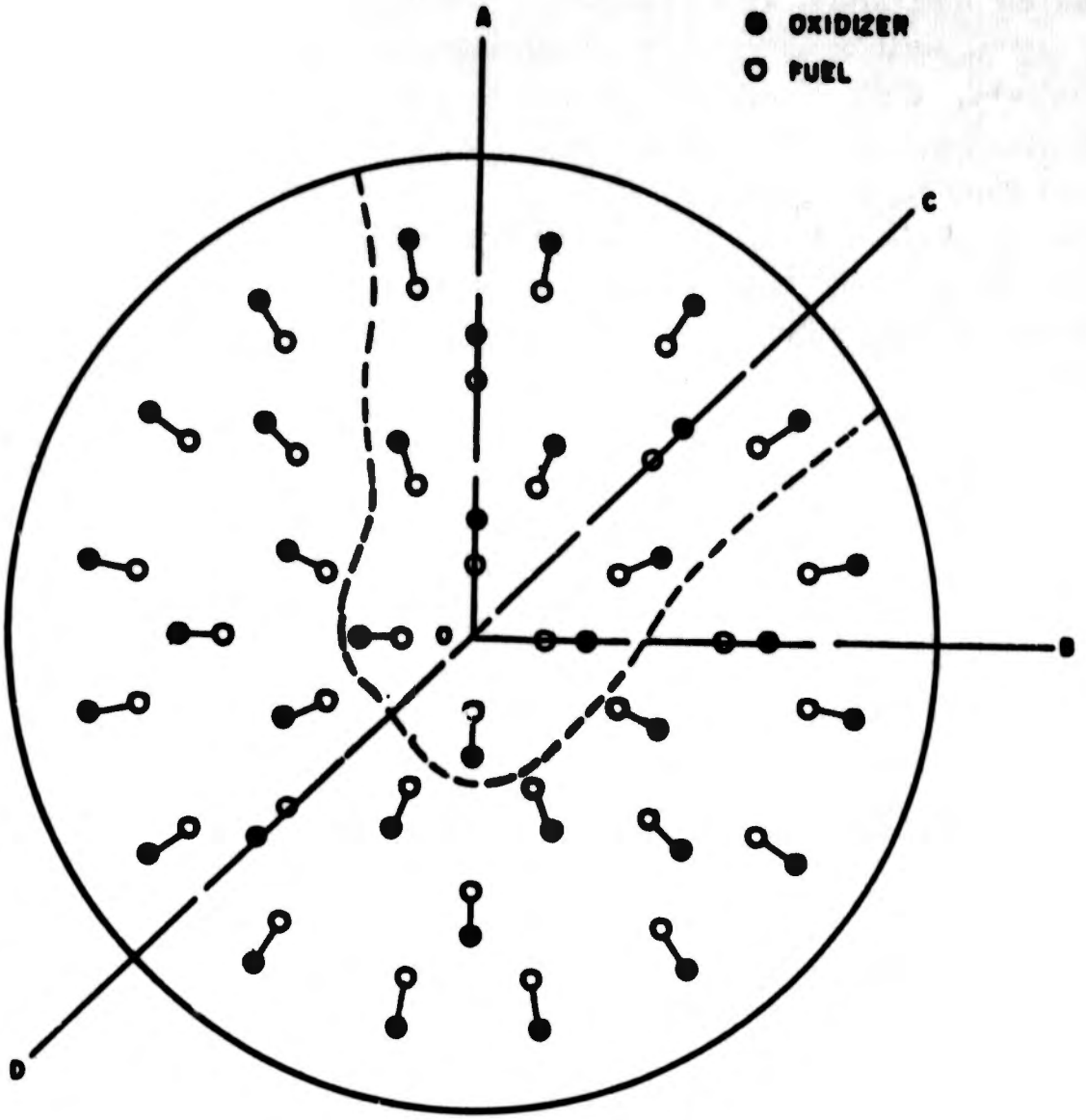

Figure 5. Example of Injector Face Pattern to Show Use of Symmetry Considerations in Defining Thrust Chamber Mesh System

must be defined outside of these surfaces to provide inflow equivalent to the outflow. In the example injector shown in Fig. 5 , specification of all elements within the dashed line surrounding AOC would be appropriate, although LISP also contains options for mirror-image or repeating-image "reflection" of fluxes if only elements within the sector under analysis are defined.

The transverse spray velocity components from some elements may result in spray impacting the combustion chamber wall or other solid surface, such as baffles installed on the injector for combustion stabilization. By proper selection of LISP input variables, such impingement upstream of z_0 on the chamber wall and/or radial baffles may be accumulated as abnormally high spray fluxes at surface mesh points. Both this accumulation at solid surfaces and the spray "reflections" at surfaces of symmetry are accomplished by defining mesh points outside of the sector under analysis and folding the calculated flows at those exterior mesh points into the appropriate surface or interior mesh points.

Considerably more details about selecting a sector for analysis, selecting the elements for definition, and setting up a mesh system have been given in earlier documents concerning the LISP computer program (Ref. 8 and 10). The version of LISP employed in PMDER is that of Ref. 8 , together with the simplified data input of Ref. 11 and improved computer plotting subroutines.

Mesh Point Fluxes

It is assumed that the propellant spray fluxes at each mesh point in plane z_0 are the linear sums of the fluxes produced by the individual injection elements. That is:

$$\hat{W}_f\,(r,\theta,z) = \sum_{i=1}^{N_{EL}} \hat{w}_{f,i}\,(r,\theta,z) \qquad (7)$$

and

$$\hat{W}_o\,(r,\theta,z) = \sum_{i=1}^{N_{EL}} \hat{w}_{o,i}\,(r,\theta,z) \qquad (8)$$

This assumption is justified if: (1) the individual injector elements have reproducible and predictable spray flux patterns which have been (or can be) measured and correlated; and, (2) spray patterns of individual elements are not altered grossly, between their injection sites and the plane z_0, by collisions between sprays from neighboring elements.

Concerning the first of these conditions, Rupe (Ref. 12) has observed experimentally that very reproducible sprays can be produced if quite long ($L/D > 50$) injection orifices are used. By roughening the orifices to force earlier attainment of fully developed turbulent jet velocity profiles in a shorter length, Rupe also obtained good spray flux reproducibility with $L/D \simeq 20$. For elements having even shorter orifices, the reproducibility becomes somewhat poorer but a substantial body of short orifice data has been satisfactorily correlated (Ref. 11). The method of correlation is discussed briefly in the next subsection.

The degree to which sprays from typical impinging-jet rocket injection elements conform to the second condition was discussed in Ref. 10. A propellant droplet from one injection element was estimated to have a mean free path in excess of 1 inch through the dense part of the spray of a neighboring element. It was concluded that, while collisions and interactions certainly occur, their affects will usually not be strong enough to invalidate the linear superposition assumption.

Elemental Flux Distributions

The mass flux distributions, $\hat{w}_{o,i}$, and $\hat{w}_{f,i}$, for the i^{th} individual element have been derived from measured single-element spray flux distributions determined in cold-flow experiments. Single-element flux patterns were fitted to the generalized expression:

$$\hat{w}_i\,(x,y,z) = \frac{\hat{w}_{001}}{z^2}\left\{\left[1 + C_1\left(\frac{y}{z}\right) + C_2\left(\frac{y}{z}\right)^2\right] + \left[C_3\left(\frac{x}{z}\right) + C_4\left(\frac{x}{z}\right)^2\right]\left[1 + C_5\left(\frac{y}{z}\right) + C_6\left(\frac{y}{z}\right)^2\right]\right\} e^{-a\left(\frac{x}{z}\right)^2 - b\left(\frac{y}{z}\right)^2} \qquad (9)$$

which is applied separately to each propellant from an element. The (x,y,z) coordinate system in Eq. 9 is referenced to the element's impingement point from which its spray is presumed to emanate, while the fluxes required in Eq. 7 and 8 must be referenced to the cylindrical coordinates of the chamber. The necessary transformations are performed internally by LISP.

The coefficients a, b, $\hat{w}_{001}$, and C_1 through C_6 are evaluated empirically by means of the cold-flow simulation test data. Briefly, the correlation method consists of:

1. Simplifying Eq. 9 to apply to a specific element type. This usually involves applying symmetry and continuity conditions to identify coefficients which must vanish or are functionally related to other coefficients.

2. Integrating the simplified elemental flux equation, and appropriate x and y moments of it, along the x and y axes or over the entire x,y-plane*

3. Performing the equivalent summations (numerical integrations) on the cold-flow distribution data to obtain empirical values of the integrals

4. Equating the appropriate expressions from steps 2 and 3 to form a system of algebraic equations in the unknown distribution correlation coefficients

5. Solving that set of equations (and, perhaps, starting over with a different set of integrals when a pathological case is encountered)

6. Repeating steps 1 through 5 for several different tests, with element design and operating conditions varied, and correlating the correlation coefficient values to the parameters varied. (Typically, varied parameters are orifice diameters, impingement angles, and impinging stream momentum ratios.)

---

*The form of Eq. 9 was chosen because it satisfies continuity, predicts the (observed) inverse square relationship between mass flux and distance downstream of the impingement point and because it is integrable over intervals like $0 \leq x \leq \infty$, $-\infty \leq y \leq \infty$, etc.

7. Coding a subroutine for the element type, so that the foregoing correlation and a method for extracting correlation coefficients from it become part of the LISP subprogram

More detailed information on this process, example calculations, and the currently available correlations may be found in Ref. 11 and 13.

There are several versions of LISP in existence. Two recent versions contain logic for approximate analyses of one or more gas/liquid injection systems and improved correlations for some liquid/liquid elements. One of these versions was developed for injector/chamber compatibility analyses and transfers mesh point flux data to a three-dimensional combustion analysis (Ref. 11). The other was developed for use in a DER computer program (Ref. 14) but it is not directly compatible with PMDER.

The version of LISP used in PMDER is strictly for analyzing liquid/liquid propellant injection. It considers an injector to be made up of one or more of the following element types:

Type 1. Unlike Doublets
Type 2. (Single) Like Doublets
Type 3. Like Doublet Pairs
Type 4. Triplets
Type 5. Pentads or 4-on-1 Elements
(Type 6. No Logic Provided)
(Type 7. Showerhead, but no correlations exist)
Type 8. Special callout by general spray flux equation
Type 9. Special callout by subprogram

LISP contains subroutines which provide spray flux distribution correlation coefficients for the first five element types. Some of the correlations were derived from quite narrow ranges of parametric variation; although the subroutines will return values so that LISP calculations may proceed, a user may occasionally be

startled by a vigorous error message warning him that the application is outside the correlated range.

Elements designated with a Type 8 callout are treated by LISP as if they were unlike doublets but the user must supply the correlation coefficients for Eq. 9 as input data. This feature permits having a cold-flow characterization made of the single element (or elements) to be incorporated into a prospective injector and then employing the correlated spray coefficients from the specific cold flow experiment in LISP. Such a procedure is useful not only for the situation where spray coefficients have not been determined previously for the intended elements, but it also permits accounting for factors such as short L/D orifices and manifold crossflows in LISP calculations by incorporating the effects in the single element cold-flow experiments. A Type 8 callout may also be used to lump together into a single effective source a number of elements near the center of a large injector.

The Type 9 callout is intended to be used for element designs whose mass flux profiles cannot be fitted by the general correlation equation. In that event, the user is expected to modify LISP to call a subroutine (which he will formulate and program) specifying the mass flux distribution produced by his specific element.

Element Injection Rates

LISP calculates injection rates for both propellants flowing through each element by means of a standard orifice equation:

$$\dot{w}_i = \frac{\sqrt{2g_c}}{12} C_{D_i} A_i \sqrt{\rho \Delta P} \qquad (10)$$

Injection velocities are then calculated from a simple one-dimensional continuity equation

$$u_i = \dot{w}_i / (\rho A_i) \qquad (11)$$

Element Spray Droplet Sizes

A very essential part of the combustion field initialization performed by LISP is the assignment of propellant spray droplet sizes. In the PMDER computer program, LISP computations are concerned only with a mass median diameter ($\bar{D}$) for each propellant's spray. Later, during PMSTC program block's initialization of stream tubes, the sprays are distributed into a discrete number of droplet size groups. The magnitudes of the $\bar{D}$'s frequently have a direct, strong influence on the steady-state propellant combustion efficiency computed by PMDER.

If an injector element is specified as being any of Type 1 through Type 5, LISP will calculate a mass median drop diameter for the propellant of each orifice of the element. These calculations for Types 4 and 5 elements are based upon the correlations of Dickerson et al. (Ref. 15) derived from hot wax experiments. Constants in the correlations have been modified to give characteristic diameters which make calculated c* efficiencies compatible with measured results for three injectors tested, analyzed, and reported in Ref. 10. With elements of Types 2 and 3, the mean drop diameters are based on the empirical correlation of Falk et al. (Ref. 16), modified to make c* efficiencies calculated by the STC computer program correlate with experimental data reported in Ref. 8. Drop diameters for Type 1 elements are based on empirical correlation of Zajac (Ref. 20). A correlation coefficient, $C_{\bar{D}}$, which is specified with input data has been added to permit the user to adjust the empirically derived drop sizes. Alternatively, the LISP user may assign his own estimation of drop diameter to the flow from each orifice of a given element. For elements defined as Types 8 or 9, the user always supplies his estimation of a characteristic drop size for each orifice of each element. The appropriate mean droplet diameter is the mass median diameter.

Spray Gasification

Partial propellant evaportation upstream of z_0 is calculated by a simplified, integrated evaporation expression

$$\hat{w}'(r,\theta,z_0) = \hat{w}(r,\theta,z_0)\left[1 - \frac{C_k,\Delta z}{\bar{D}^2 u_d}\right]^{3/2} \qquad (12)$$

where $\hat{w}'$ is the liquid spray flux actually arriving at the point (r,θ,z_0). The coefficient $C_{k'}$ is related to the evaporation coefficient k' used in the subsequent spray combustion analysis. However, because the liquid sprays are not fully atomized over the entire Δz distance, values of $C_{k'}$, including a convective Nusselt number, are usually assumed to be only about 1/5 to 1/4 of the stagnant values of k'. The propellant vapors said to be generated by this calculation are summed over all mesh points to yield a single overall vapor flow rate for each propellant. Use of such a simplified evaporation expression is, to some extent, justified by the relatively small percentage of evaporation in the spray formation zone.

LISP Output

Printed and computer-plotted output is provided by the LISP computer program, and a brief description of it follows. First, there is a tabulation of all input data, which permits both a full documentation of the computer run conditions for later analysis and a convenient method to check input for errors if unusual results are calculated. The table of input data is followed by a second table which cross references (by injector element) the calculated flow rates and drop sizes before evaporation to the read-in element coordinates.

The element reference table is followed by two tables referenced to the combustion zone mesh points. The third table lists the coordinates of the mesh points in the chamber slice at the collection plane z_0, together with the weight flux ($lbm/inch^2$ sec), the total collected mass (lbm/sec), the three mean droplet velocity components (ft/sec), and the mean drop diameters (inch) of each propellant at the mesh points. The total collected mass at a mesh point is defined as the weight flux times the associated area at the mesh point. The values in this third table are based upon cold flow conditions, i.e., no vaporization is assumed between elements and mesh point. The mesh points are listed in ascending order according to radial and angular coordinate.

The fourth table again lists the coordinates of the mesh points in the chamber slice in the plane z_0, together with the reduced weight fluxes and droplet diameters of the collected spray after evaporation. A mass-weighted average evaporation of the original spray flux to each mesh point is also listed in this table. At the bottom of the fourth table are listed the Rupe mixing factor, E_m, the mixing limited c* efficiency, and the overall percent vaporization of each propellant.

The LISP graphical output is exemplified in Fig. 6 through 10. Figure 6 shows the mesh system for the chamber slice analyzed and the element origin locations for all injection elements considered to contribute flux to that slice. Figure 7 is an example of the fuel and oxidizer mass flux profiles around the chamber slice at one fixed chamber radius. Figures 8 and 9 are the contour plots of fuel and oxidizer mass flux for the entire chamber cross section. A similar plot for total mass flux is not shown. Figure 10 is a contour plot of a modified fuel fraction function. The expression plotted is given at the top of the figure; it was chosen because it is bounded between zero and unity and has a value of 0.5 at the injection mixture ratio.

Computer Program Structure

The LISP computer program has been structured in a modular form to subdivide it into functional blocks and to keep the size of all subprograms within a reasonable size to aid in compiling. A simplified flow chart of LISP is shown in Fig. 11. Functional operations separated from the main control subprogram are the calculation of: flow parameters for each injector element, mean spray drop sizes, empirical coefficients for the spray flux distribution equation, spray flux parameters at each collection mesh point from each injector element, and spray flow parameter adjustments which account for boundary and symmetry conditions.

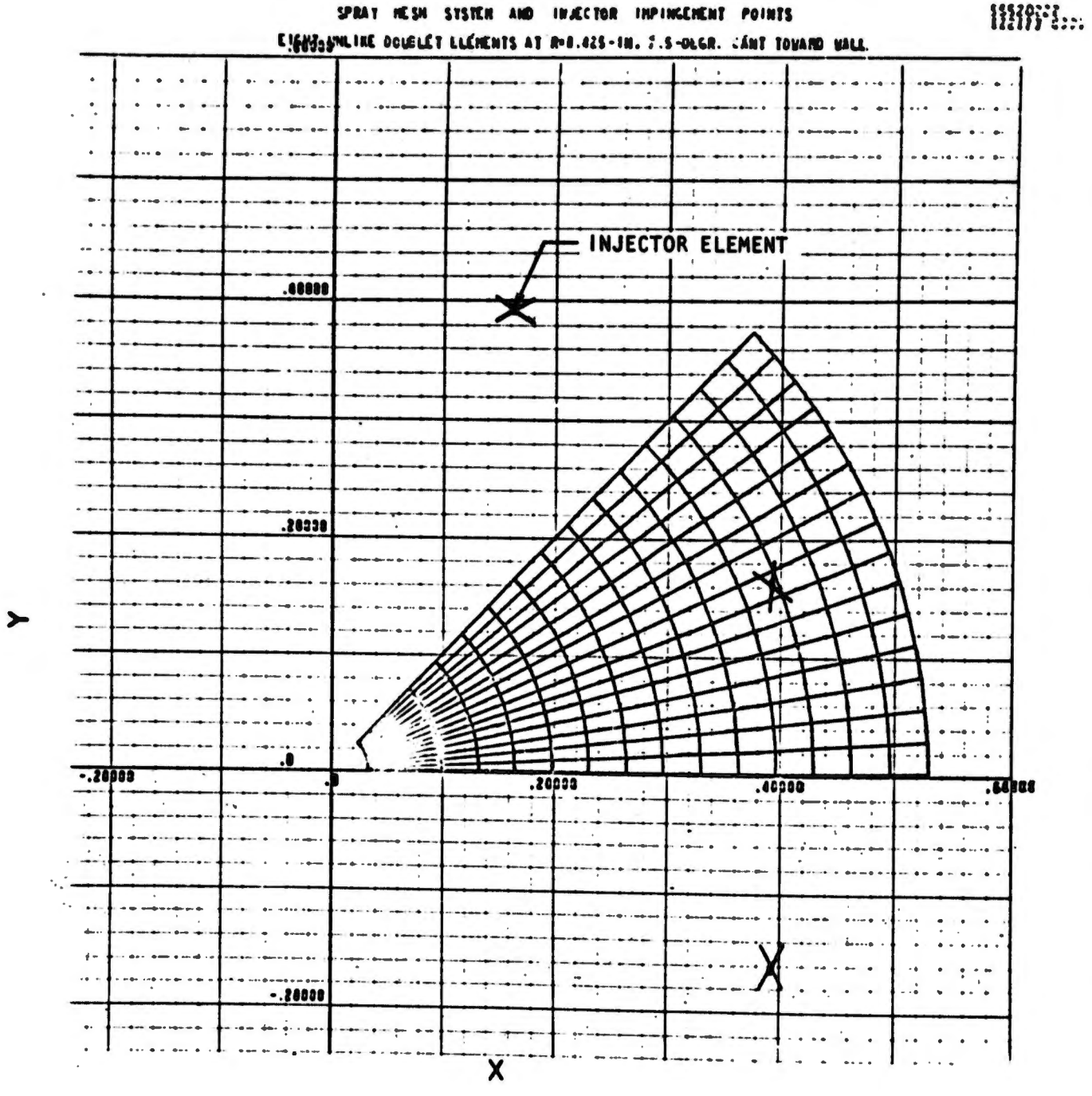

Figure 6. Sector of Injector Analyzed by LISP

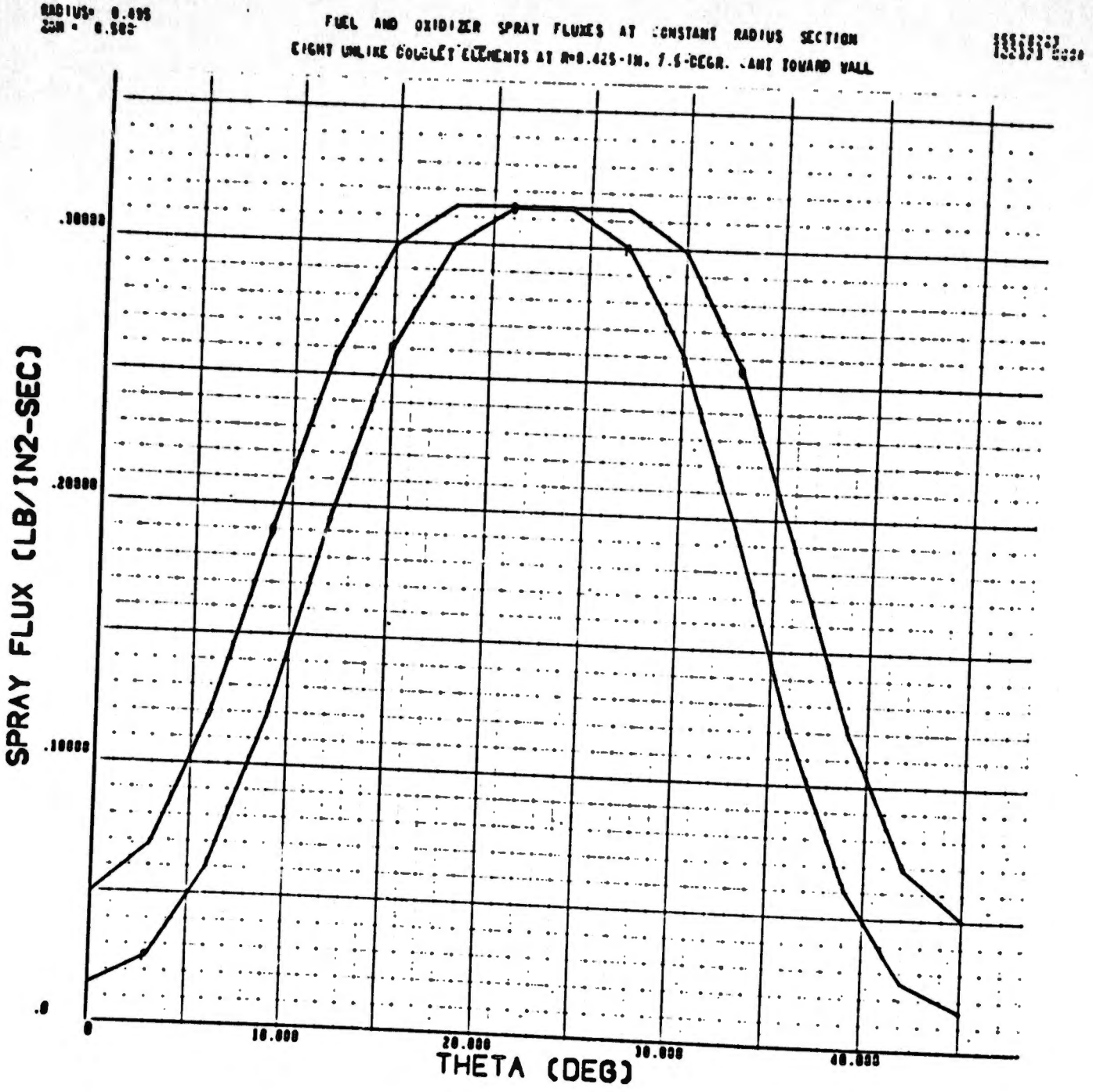

Figure 7. Fuel and Oxidizer Mass Flux Profiles Computed by LISP at a Given Chamber Radius

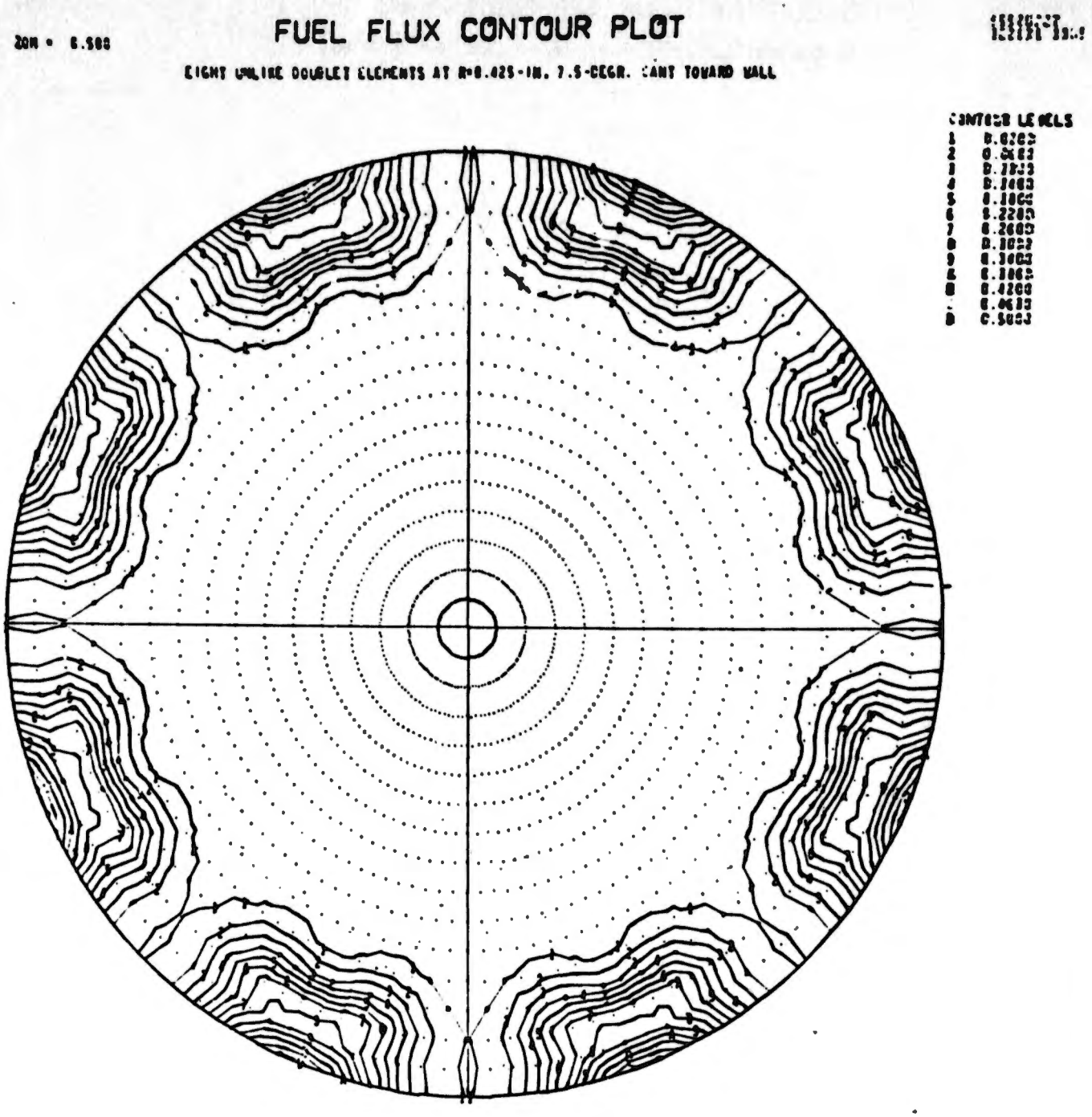

Figure 8. Contour Plot of Fuel Mass Flux Computed by LISP

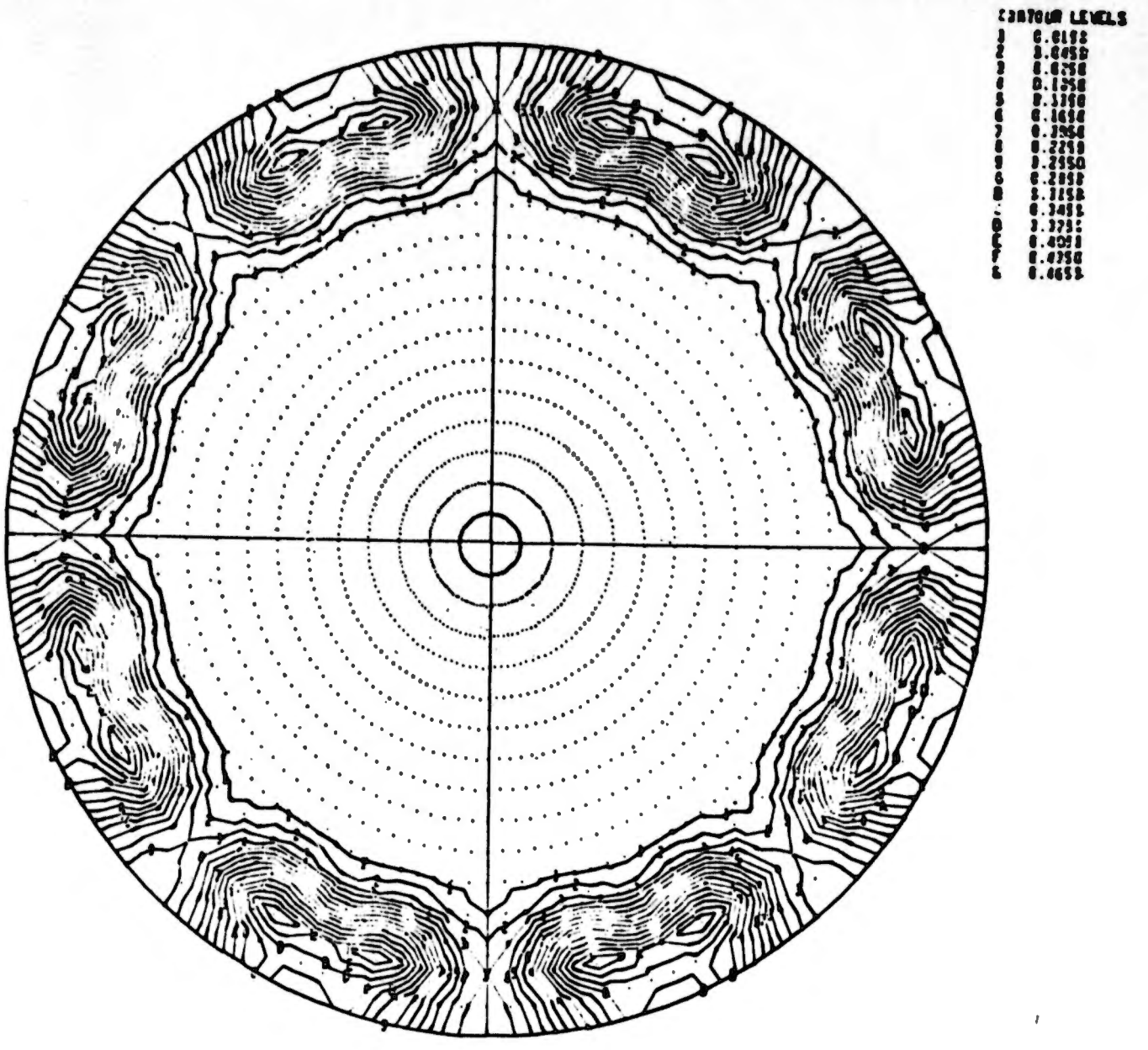

Figure 9. Contour Plot of Oxidizer Mass Flux Computer by LISP

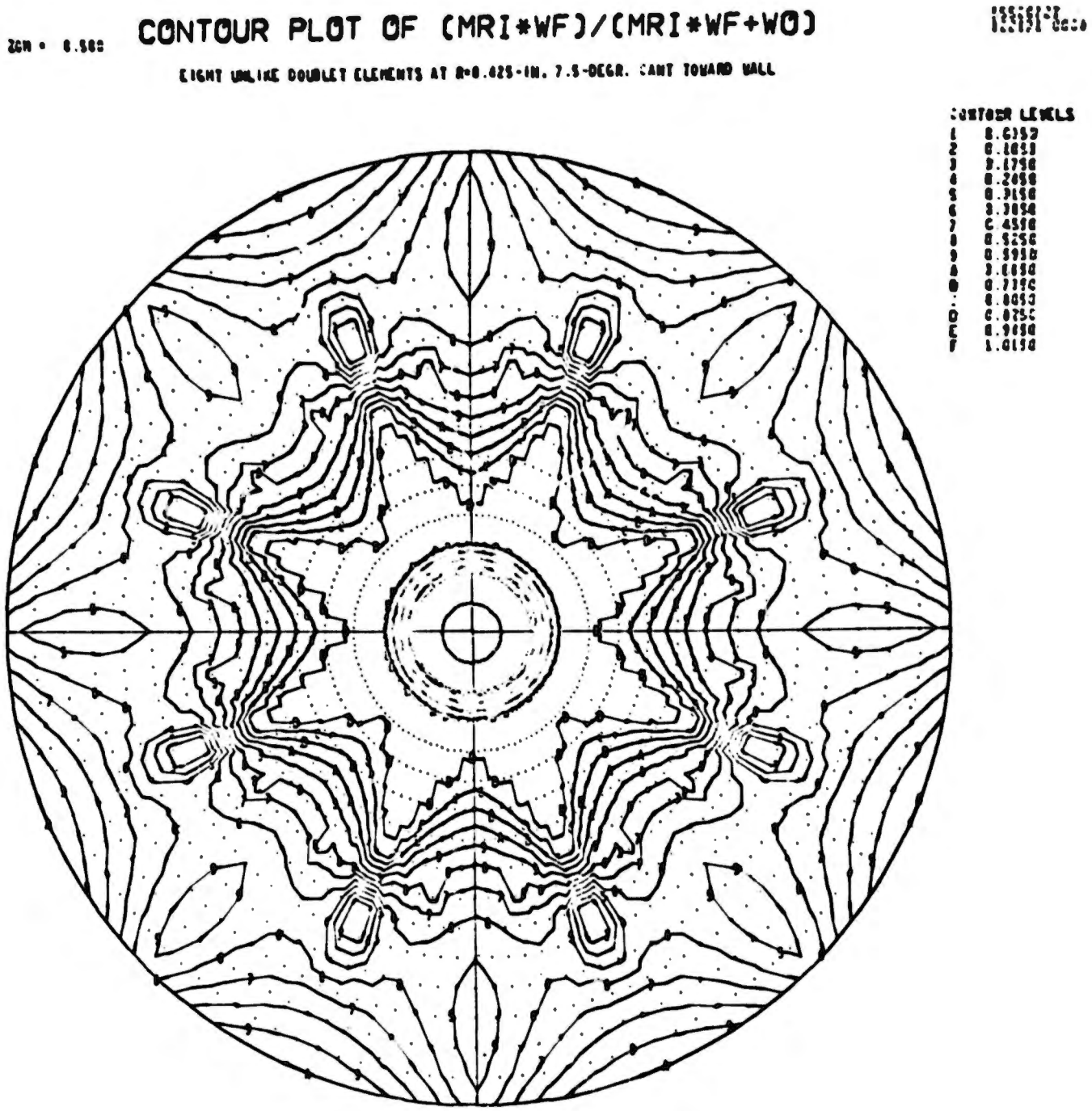

Figure 10. Contour Plot of Modified Fuel Fraction Computed by LISP

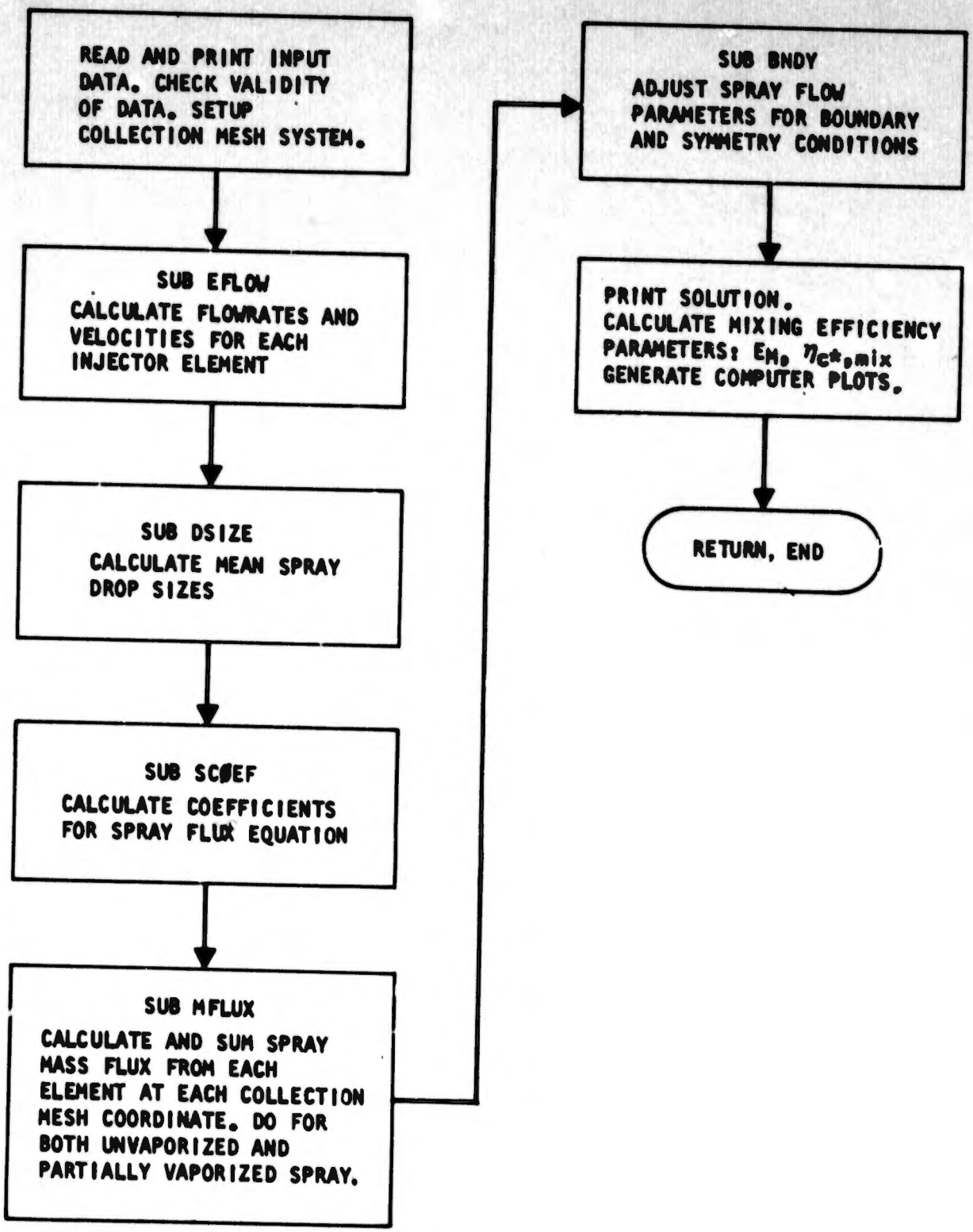

Figure 11. Simplified Flow Chart of LISP

COMBUSTION MODEL (PMSTC)

The PMSTC (Pulse Mode Stream Tube Combustion) computer subprogram block analyzes bipropellant liquid spray combustion from the LISP collection plane z_0 (where it is initialized) through the nozzle throat. Selected data computed by LISP are transferred (via scratch data unit) to the PMSTC subprogram block. There, by one of two alternate methods, propellant fluxes and flow areas of several mesh points are combined to form one of the stream tube flows to be analyzed by PMSTC. Model solutions for spray gasification and combustion are obtained numerically for several systems (one for each stream tube) of simultaneous ordinary differential and algebraic equations by starting from known conditions at the LISP collection plane and marching downstream in small axial steps.

Input to the PMSTC computer program consists of chamber wall profile, propellant properties, combustion gas properties and either (1) initial-plane gaseous flowrate and mixture ratio and spray flowrates, velocities, and droplet diameters for all spray size-groups entering each stream tube, or (2) data from LISP from which these variables can be calculated. Up to a total of 19 stream tubes can be initialized, with as many as 12 spray size-groups (fuel and oxidizer combined).

Stream Tube Initialization from LISP Data

Data transferred to PMSTC from LISP are: (1) propellant spray mass fluxes, mean droplet velocities, and mass median diameters at each mesh point; (2) mesh point coordinates; and (3) total initial plane flow and how much of it is gasified for each propellant. At this point, the gas mixture ratio is considered to be uniform (constant) across the r,θ,z_0 plane. Axisymmetric stream tube flows may be initialized from these data by means of the following options:

1. All mesh points along each circle (r = constant) of the LISP mesh points are combined into one stream tube. Gasified propellants are retained as transferred from LISP, with uniform mass flux and uniform mixture ratio. This initialization method may be appropriate for injectors that form essentially axisymmetric flows. When applied to injectors which produce angular gradients in local propellant mixture ratio, however, it can effect substantial mixture ratio averaging and result in overcalculation of combustion efficiency.

2. Stream tubes are formed by combining meshpoints of similar mixture ratio within specified annular zones. First, however, the gasified propellants are redistributed to provide a nearly uniform gas mass flux profile but a mixture ratio distribution similar to the spray mixture ratio distribution. The gas mass fluxes are initially approximated as being uniform:

$$\dot{w}_{g_{ij}} = (\dot{W}_{g,F} + \dot{W}_{g,O}) \frac{A_{ij}}{\sum_{i,j} A_{ij}} \tag{13}$$

Then the gas mixture ratio at each mesh point is said to be equal to the spray mixture ratio there:

$$c_{ij} = \frac{\dot{W}_{O_{i,j}}}{\dot{W}_{F_{ij}}} \tag{14}$$

In general, however, these two assumptions will not be compatible with conservation of propellant species flowrates, e.g.:

$$\dot{W}_{g,F} \neq \sum_{ij} \frac{\dot{w}_{g_{ij}}}{1 + c_{ij}} \tag{15}$$

Therefore, the fuel and oxidizer contributions to each mesh point's gas flow are scaled separately to preserve species continuity:

$$\dot{w}_{g,F_{ij}} = \frac{\dot{w}_{g_{ij}}}{1 + c_{ij}} \left[\frac{\dot{W}_{g,F}}{\sum_{ij} \frac{\dot{w}_{gij}}{1 + c_{ij}}} \right] \tag{16}$$

$$\dot{w}_{g,O_{ij}} = \frac{c_{ij}\dot{w}_{g_{ij}}}{1 + c_{ij}} \left[\frac{\dot{W}_{g,O}}{\sum_{ij} \frac{c_{ij}\dot{w}_{gij}}{1 + c_{ij}}} \right] \tag{17}$$

These definitions complete the specification of propellant flows at each mesh point.

Following distribution of the gases among the mesh points, a wall boundary layer stream tube is established by combining all the mesh points at the wall. If that stream tube does not contain more than one-twelfth of the total flow, the next inward circle of mesh points will also be combined into it, etc., until it does. Then the remaining LISP circles of mesh points are divided into a specified few (2 to 4, perhaps) circular or annular zones having roughly equal propellant flowrates.

Within each of these zones, the mesh point flows are accumulated into stream tubes according to their total propellant mixture ratios, rather than positions. The number of stream tubes per zone is specified and they are assigned roughly equal propellant flow rates. The lowest mixture ratio mesh points are combined into the first stream tube until its fraction of the zonal flowrate is reached, the next lowest mixture ratio mesh points are assigned to the second stream tube, etc. Finally, the resultant stream tubes are arbitrarily assigned radial positions within their respective zones, with the fuel-rich stream tubes lying inside of the oxidizer-rich ones.

This method preserves the angular averaging objected to before only at the wall and is accepted for a fraction of the flow in order to get a wall-bounding stream tube that is characteristic of the mean wall mixture ratio. For the remainder of the flow, the nonphysical combining of mesh points on the basis of mixture ratio has been found to effect only modest changes in calculated mixing efficiencies from those based on the full LISP distributions.

System of Equations

The system of equations for the i^{th} stream tube is:

Gas Phase. Continuity:

$$\frac{d}{ds}\left(\rho_i u_i A_{s_i}\right) = A_{s_i} \sum_{n,j} \left(\dot{m}_j^n\right)_i \tag{18}$$

Momentum:

$$\frac{d}{ds}\left(\rho_i u_i^2 A_{s_i}\right) = A_{s_i}\left[-g_c\left(\frac{dp}{ds} + \sum_{j,n}\left(F_j^n\right)_i\right) + \sum_{j,n}\left(\dot{m}_j^n\right)_i \left(u_{dj}^n\right)_i\right] \tag{19}$$

Adiabatic Energy Equation:

$$T_i = T_{o,i}\left[1 - \frac{\gamma_i - 1}{2}\left(\frac{u_i}{a_{o,i}}\right)^2\right] \tag{20}$$

where

$$T_{o,i} = T_o(c_i, M_i),\ \gamma_i = \gamma(c_i, M_i),\ M_{w,i} = M_w(c_i, M_i) \text{ and } a_{oi} = a_o(c_i, M_i)$$

are tabulated. These tabulated properties are not generated within this computer model, but must be obtained from separate calculations of equilibrium conditions for a wide range of mixture ratio values and at several Mach numbers from 0 to 1. The predecessor STC program was formulated assuming stagnation equilibrium throughout the chamber. For pulse-mode application, a switch to static equilibrium, especially at the throat, was considered necessary to obtain absolute values for thrust and flowrate. In order to be compatible with the previous formulation, static equilibrium values are input and pseudo-stagnation values are generated for internal use. The same relationship used for determining the pseudo-stagnation properties is inverted to back out the static properties; therefore, no loss in accuracy is incurred.

The local stream tube gas mixture ratio is obtained simply by integrating the evaporation rates to get gasified flowrates:

$$\dot{w}_{ji}(z) = \dot{w}_{ji}(z_0) + \int_{z'=z_0}^{z} A_i \sum_{n} (\dot{m}_j^n)_i \, dz' \tag{21}$$

Mixture Ratio:

$$c_i = \frac{\dot{w}_{oxid,i}(z)}{\dot{w}_{fuel,i}(z)} \tag{22}$$

State:

$$\rho_i = \frac{p \, M_{w,i}}{R \, T_i} \tag{23}$$

Spray Phase (n^{th} droplet size group of j^{th} propellant). Mass Continuity:

$$\frac{d}{ds}\left[\left(\rho_{d,j}^{\,n}\right)_i \left(u_{d,j}^{\,n}\right)_i \; A_{s_i}\right] = -A_{s_i}\left(\dot{m}_j^{\,n}\right)_i \tag{24}$$

Drop Number Continuity:

$$\frac{d}{ds}\left[\left(N_{d,j}^{\,n}\right)_i \left(u_{d,j}^{\,n}\right)_i A_{s_i}\right] = 0 \tag{25}$$

or, equivalently:

$$\left(\dot{N}_{d,j}^{\,n}\right)_i = \left(N_{d,j}^{\,n}\right)_i \left(u_{d,j}^{\,n}\right) A_{s_i} = \text{constant} \tag{26}$$

Momentum:

$$\frac{d}{ds}\left[\left(\rho_{d,j}^{\,n}\right)_i \left(u_{d,j}^{\,n}\right)_i^{\,2} A_{s_i}\right] = A_{s_i}\left[g_c \left(F_j^{\,n}\right)_i' - \left(\dot{m}_j^{\,n}\right)_i \left(u_{d,j}^{\,n}\right)_i\right] \tag{27}$$

The independent variable in these one-dimensional flow equations is the stream tube path length or flow direction, s_i. This variable is related to the cylindrical (r,z) coordinates of the stream tube through the differential expression

$$ds_i = \left(dz_i^{\,2} + d\bar{r}_i^{\,2}\right)^{1/2} \tag{28}$$

where $\bar{r}_i$ is the mean radius of the stream tube. For numerical stability in the solution, however, approximations are used that $ds_i = dz$ where the chamber wall is parallel to the axis and that

$$ds_i = dz\left\{\frac{\left[\bar{r}_i^{\,2} + (z_I - z)^2\right]^{1/2}}{|z_I - z|}\right\} \tag{29}$$

in the nozzle. The basis for Eq. 29 may be seen by examining the following schematic illustration of variables denoting local conical convergence of stream tubes.

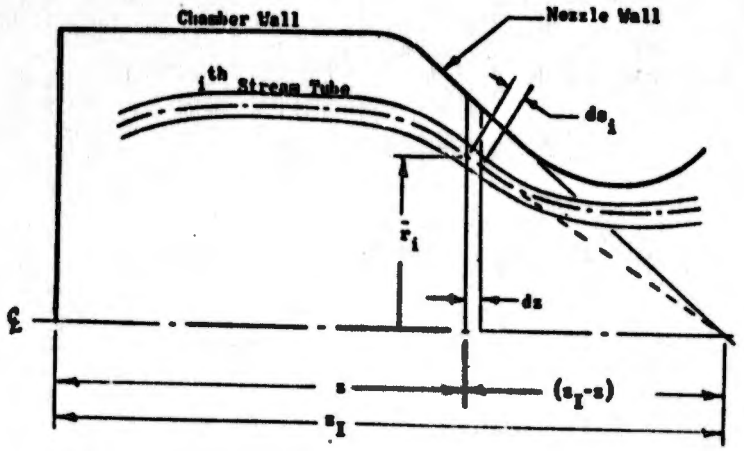

In this formulation, A_{s_i} appears as a dependent variable for which a solution is to be found. The gas phase equations are constrained, however, in terms of z-plane area:

$$\sum_i A_{z_i}(z) = A_c(z) \tag{30}$$

Therefore, the foregoing equations were modified for the computer program to permit direct solution for A_{z_i} by substituting:

$$A_{s_i} = A_{z_i} \frac{dz}{ds} \tag{31}$$

and neglecting the stream path curvature, i.e.: $\frac{d^2z}{ds^2} = 0.$

The sets of gas and liquid phase equations are coupled through mass and momentum exchange between phases. For droplet gasification, the simple evaporation coefficient model is utilized:

$$\dot{m}_j^n = N_j^n \left(\frac{\pi}{8}\right) P_{\ell_j}^n D_j^n Nu_j^n k'^n_{s_j} \tag{32}$$

where the evaporation coefficient is

$$k'^{n}_{s_j} = \frac{8}{\rho_{\ell_j}^{n}} \int_{T_d}^{T} \frac{k_g}{\Delta H_v + \int_{T_d}^{T} c_{p_v}\, dT}\, dT \tag{33}$$

and

$$Nu_j^{n} = 2 + 0.53\, Re_j^{n} \tag{34}$$

Drag forces on spray droplets are expressed by

$$F_{j_i}^{n} = \frac{\pi}{8 g_c} N_{d_j}^{n} \rho_i D_j^{n} C_{D_j}^{n} \left(u_i - u_{d_j}^{n} \right) \left| u_i - u_{d_j}^{n} \right| \tag{35}$$

with the drag coefficient specified as

$$C_{D_j}^{n} = 24\, (Re_j^{n})^{-0.84} \quad ; \; Re_j^{n} \leq 80$$

$$= 0.271\, (Re_j^{n})^{0.217} \quad ; \; Re_j^{n} > 80 \tag{36}$$

Performance Parameters. Two separate parameters are calculated which are indicative of the overall degree of propellant mixing. These are calculated once in LISP, based on the flowrates associated with the LISP mesh points, and once in PMSTC, based on the initial flowrates supplied to the stream tubes. One parameter is E_m, a mixing efficiency factor due to Rupe (Ref. 17) which expresses a mass-weighted average approach of local oxidizer mass fractions to the overall injected mass fraction:

$$E_m = 100 \left[1 - \sum_{i=1}^{n} \frac{\dot{w}_i (R - r_i)}{\dot{W} R} - \sum_{i=1}^{\bar{n}} \frac{\dot{w}_i \, (R - \bar{r}_i)}{\dot{W} \, (R-1)} \right] \tag{37}$$

where:

n = number of samples with $R > r$

$\bar{n}$ = number of samples with $R < r$

$\dot{w}$ = local propellant flowrate, lb_m/sec

$\dot{W}$ = total propellant flowrate, lb_m/sec

$r, \bar{r}$ = local oxidizer mass fractions, $\dot{w}_o/\dot{w}$

R = injection oxidizer mass fraction, $\dot{W}_o/\dot{W}$

The second parameter is a mixing c* efficiency, $\eta_{c^*,mix}$, which represents the maximum attainable c* efficiency corresponding to complete propellant gasification:

$$\bar{\eta}_{c^*,\,mix} = \frac{\sum_{i=1}^{n+\bar{n}} c^*(c_i)\dot{w}_i}{c^*(c_{inj})\dot{W}} \qquad (38)$$

where c_{inj} is the injection mixture ratio ($\dot{W}_o/\dot{W}_f$), c_i is local mixture ratio ($\dot{w}_{o_i}/\dot{w}_{f_i}$) and $\dot{w}_i$, $\dot{W}$, n, and $\bar{n}$ have the same meanings as above. Theoretical characteristic velocity is tabulated as a function of mixture ratio.

The stagnation pressure drop between the injector end and the throat is a critical parameter for satisfying the throat boundary condition on flow. The pressure in the PMSTC start plane is stagnated to obtain the injector end pressure, P_{IE}. In the single stream tube analysis, the nozzle stagnation pressure, P_{NS}, is calculated from the c* equation in a manner that makes it compatible with the equilibrium combustion properties:

$$P_{NS} = \frac{c^* \dot{W}_g}{A^* g_c} \qquad (39)$$

where c* is the theoretical value from the gas tables evaluated at the throat gas mixture ratio, $\dot{W}_g$ is the throat gas flowrate, and A* is the area required for sonic flow of $\dot{W}_g$ with Mach 1 equilibrium gas properties. The ratio of (P_{IE}/P_{NS}) is determined in the single stream tube analysis, and is used thereafter as an invariant ratio. Subsequently, it is used in the multiple stream tube analysis to calculate P_{NS} whenever the value of P_{IE} is altered:

$$P_{NS} = P_{IE} \quad (P_{IE}/P_{NS}) \qquad (40)$$

Other performance parameters are calculated in PMSTC as follows:

$$
\left.
\begin{aligned}
&1.\ \eta_{vap,f} = \frac{\text{(Sum fuel gas flowrate at throat)}}{\text{(Total fuel injection flow rate)}} \\
&2.\ \eta_{vap,o} = \frac{\text{(Sum oxidizer gas flowrate at throat)}}{\text{(Total oxidizer injection flowrate)}} \\
&3.\ \eta_{vap} = \frac{\text{(Sum gas flowrate at throat)}}{\text{(Total propellant injection flowrate)}} \\
&4.\ \eta_{c^*,MR} = c^*_{th}\,(MR_g)/c^*_{th}\,(MR_I) \\
&5.\ \eta_{c^*} = \eta_{c^*,mix}\,\eta_{vap}\eta_{enr}\eta_{c^*,MR} \\
&6.\ c^* = \eta_{c^*}\ c^*_{th}\,(MR_I) \\
&7.\ C_F = \eta_{C_{F,vac}} C_{F,vac,th} - P_a\varepsilon/P_{NS} \\
&8.\ \eta_{C_F} = C_F/(C_{F,vac,th} - P_a\varepsilon/P_{NS}) \\
&9.\ F = A_t P_{NS} C_F \\
&10.\ I_s = c^* C_F/g_c \\
&11.\ \eta_{I_s} = \eta_{c^*}\,\eta_{C_F}
\end{aligned}
\right\} \quad (41)
$$

Method of Solution

A simplified flow chart for the PMSTC computer program is presented in Fig. 12. The numerical integration scheme used to solve the system of equations for each stream tube is the simplest first-order Runge-Kutta (or Euler) method. Selected for its simplicity, minimal data storage requirements, low execution times, and numerical stability, the accuracy of this method is strongly dependent upon using sufficiently small step sizes. This limitation is reduced in importance by using backward differencing in writing finite-difference equations and by solving the

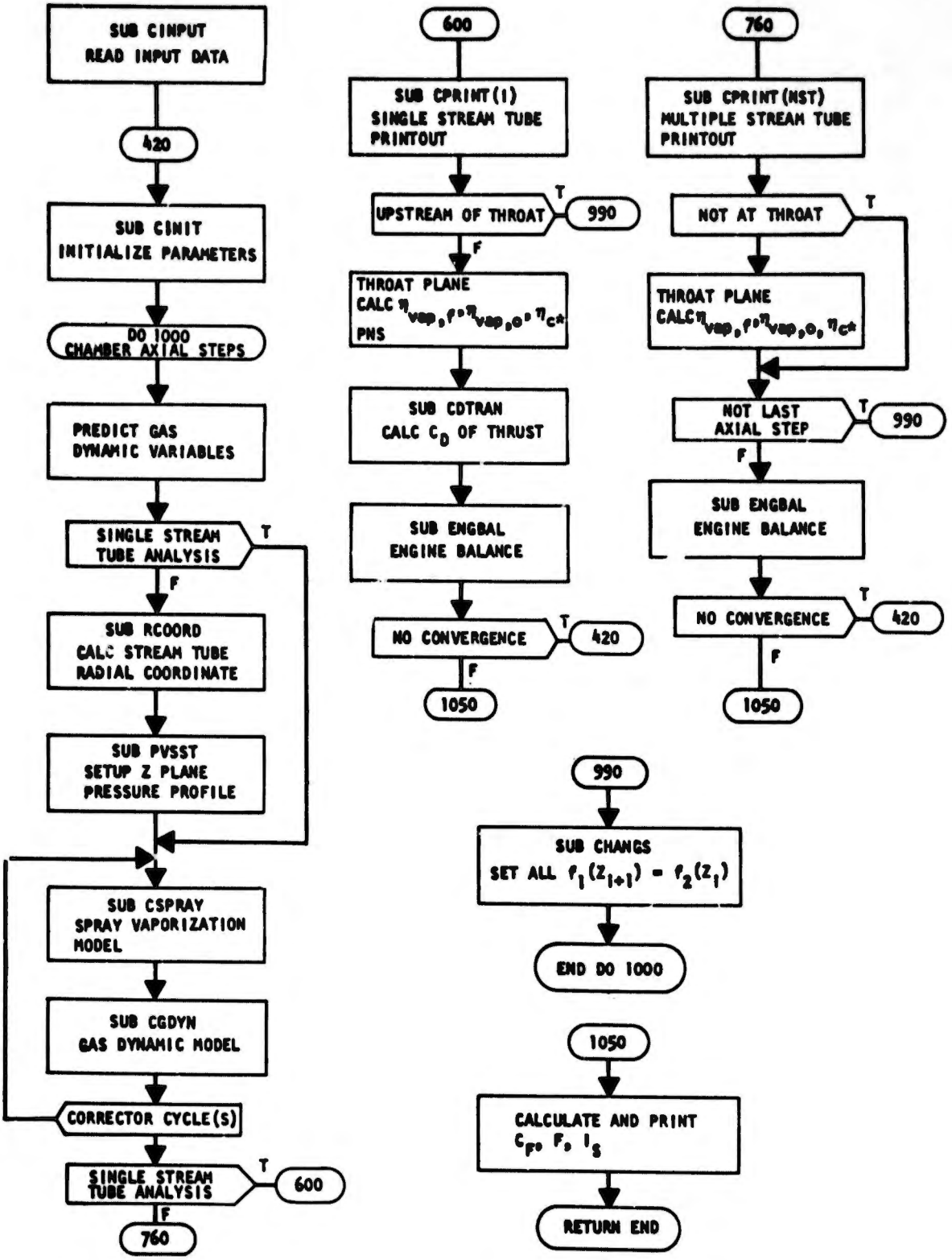

Figure 12. Simplified Flow Chart of PMSTC Subprogram

equations twice, using predicted values from the first, or predictor, solution as input data for a second, or corrector, solution.

The PMSTC program is first run in a single stream tube mode, i.e., a one-dimensional subsonic combustion analysis is made for the entire chamber using appropriate sums and averages of initial stream tube variables. This is conducted for several reasons: (1) to determine the stagnation pressure loss ratio, (P_{IE}/P_{NS}), (2) to minimize the number of passes required in the multiple stream tube analysis by improving the estimated values of $\eta_{vap,f}$ and $\eta_{vap,o}$, and (3) to provide a mean adiabatic expansion coefficient, $\bar{\gamma}$, for combustion gas flow in the convergent part of the exhaust nozzle.

The latter coefficient is given by:

$$\bar{\gamma} = \left(\frac{\ln \frac{\bar{p}^*}{\bar{p}_1}}{\ln \frac{\bar{\rho}^*}{\bar{\rho}_1}} \right) \tag{42}$$

where the subscript 1 refers to the beginning of nozzle convergence, the variables p^* and ρ^* are at sonic conditions and the over-bars refer to the one-dimensional flow analysis. It is used by the TRANS computer program (described in the next subsection) to calculate the coordinates of constant pressure surfaces (isobars) for transonic flow in the nozzle. TRANS isobars are generated and transferred to PMSTC in non-dimensional terms, so their use requires knowledge of the nozzle throat radius, R_T (an input parameter), and sonic flow pressure, p^*. An approximate value of p^* is estimated from the nozzle throat plane pressure of the preceding averaged, single stream tube analysis:

$$p^* = \bar{p}^* \; p(z_0)/\bar{p} \; (z_0) \tag{43}$$

Following PMSTC single stream analysis and TRANS analysis, the initial plane is reinitialized with its original input flowrates adjusted to agree with the latest ENGBAL flowrates. Then, PMSTC is run in a multiple stream tube mode. This analysis is the source of steady-state combustion and performance data which is used in the later pulse analyses.

As the multiple stream tube analysis proceeds, spray size group residual weight and residence time data are stored as functions of position in the chamber, for subsequent calculation of propellant spray depletion functions (subroutine CPM2).

One of the variables solved for is chamber pressure in each z-plane. Somewhere in the nozzle, the solution method is changed so that, rather than solving for pressure, absolute pressures are imposed upon the flow. These are obtained by multiplying the reduced pressures, p/p^*, of the TRANS isobars by p^*. The furthest upstream TRANS isobar may be planar or curved, depending upon the radius ratio at the nozzle and the shape of its convergent section. If it is curved, it is desirable to introduce a gradual transition from planar isobars to that first curved isobar which the solution encounters. Also, a gradual transition is desirable to smooth out any discontinuity in pressure levels between those solved for upstream and those imposed downstream of the transition. The gradual transition is provided by stopping the solution for pressure level at a position that is upstream of the nozzle throat by 1.3 times the axial distance that the furthest-upstream TRANS isobar intersects the nozzle wall, and using linear interpolation to obtain absolute pressures for the transition interval.

The imposition of absolute pressures overprescribes the problem and the solution then provides absolute values of stream tube areas which may or may not sum to the local nozzle flow area. Area continuity can only be satisfied by finding the appropriate combination of propellant flowrates and pressure level (p^*). This is accomplished only for the minimum flow area (irrespective of whether it is precisely at the throat position) by comparing it with the geometric throat area. The areas must agree within some input tolerance, along with compatibility of engine balance variables, to satisfy the throat boundary conditions. Otherwise, the multiple stream tube analysis is reperformed with adjusted values of initial flowrates and P_{IE}. When the deviations are only slightly too large, computer time is saved by redoing only the nozzle analysis.

Transonic Nozzle Flow (TRANS)

A transonic flow analysis section was adapted from the reference TDK computer program (Ref. 9), as modified (Ref. 18) to utilize an elliptic coordinate transformation solution method (Ref. 19). This section was removed from the TDK program and modified so that it would generate a family of isobaric lines throughout the transonic flow regime and provide a computer-plotted graph of that family. The necessary input data are obtained from the averaged, single stream tube solution of STC, so this TRANS subprogram block gives a homogeneous flow solution. For homogeneous flow, TRANS solutions are stable with radius ratios as small as 5/8. As input data, TRANS needs values only of the nozzle throat radius, R_R, and a mean expansion coefficient, $\bar{\gamma}$. Isobaric coordinates are calculated in terms of axial distance, X, from the throat plane and radial distance, R, from the nozzle axis; both dimensions are normalized to the throat radius. Multiple isobars are generated, one at a time, by starting downstream of the throat and marching upstream with equal intervals, $\Delta\alpha$, in the angle between the nozzle axis and a line tangent to the nozzle wall at the isobar/wall intersection point. The program is structured such that that intersection point for the fifth isobar is at the throat; this isobar later becomes the TDK start-line. Four isobar/wall intersection points lie downstream of the throat ($\alpha > 0$) and the remainder lie upstream of the throat ($\alpha < 0$). The angular interval between isobars is given by:

$$\Delta\alpha = -\left(1 + \frac{2}{R_r}\right) \tag{44}$$

Generation of isobars continues until either: (1) there are twenty of them, or (2) an isobar exhibits significant reverse, or upstream curvature. In the latter case, that last upstream-curving isobar is replaced with a planar surface.

Subroutine CDTRAN calculates a nozzle discharge coefficient using the 3rd order equation given in Ref. 19:

$$C_{ND} = 1 - \frac{\bar{\gamma} + 1}{(1+R_T)2}\left[\frac{1}{96} - \frac{(8\bar{\gamma} - 27)}{2304(1+R_T)} + \frac{(754\ \gamma^2 - 757\ \bar{\gamma} + 3633)}{276{,}408(1+R_T)2}\right] \tag{45}$$

Spray Depletion Functions (CPM1 and CPM2)

For selected axial steps in the multiple stream tube analysis, subroutine CPM1 is called to store, on a secondary computer storage device, spray weight flowrates and residence times for all droplet size groups. Only selected axial steps are used to keep the number of core storage locations used within a reasonable limit. At each axial increment, up to 456 values must be stored, requiring 136,800 values if data were saved at all 300 axial stations. Therefore, axial stations are selected to limit the maximum number of them to 36 as shown below:

Axial Station	Selection Interval	Cumulative Number
1 through 6	1	6
8 through 20	2	13
25 through 50	5	19
60 through 140	10	28
160 through 300	20	36

Upon completion of the multiple steam tube combustion analysis, subroutine CPM2 generates two time-dependent functions, one for fuel and another for oxidizer, from the axial-dependent data recorded by subroutine CPM1. The time scale is set up ranging from zero up to the maximum droplet residence time and is subdivided into 50 equally spaced time values. Residual fuel and oxidizer spray mass flowrates are evaluated by interpolating at each of these times in the tables generated by CPM1, summing over all drop group sizes in every stream tube. The spray flowrate arrays are then reduced to fractions of injected flowrates.

The steady-state combustion analysis starts at an axial plane downstream of the impingement plane and with some of the propellant already vaporized. Therefore,

the initial portions of the fuel and oxidizer spray depletion functions must be generated by some other means. The method used is to fit a quadratic curve between point (0,1), i.e., no depletion at time zero, and the first point of the calculated function such that the curve is tangent to the calculated function. One restraint limits the curve fit to values less than or equal to unity. In order to obtain meaningful mixture ratios at the onset of combustion, the curve fit is also restricted to values no greater than a linear fit through the (0,1) point with a slope equal to 0.02 times the slope at the first point of the calculated function. An example of the fuel and oxidizer spray depletion functions is shown in the computer generated plot in Fig. 13.

PMSTC Data Output

PMSTC data output consists of tabular printout, punched cards and computer-generated figures. Input data are written out immediately as they are read in. Input data transferred from LISP are not printed out. Instead, the stream tube initialization data are tabulated and simultaneously punched out in cards.

Based on the stream tube initialization data, a table is printed out of stream tube total flowrates and overall mixture ratios. This table is followed by values of the Rupe mixing efficiency factor, E_m, and a mixing c* efficiency. The latter represents an upper limit for multiple stream tube c* efficiency, since it corresponds to complete evaporation and burning of sprays within all stream tubes.

Subroutine AVAR sets up the array of chamber areas and writes out a table of chamber geometry information. Similarly, subroutine KPRIME computes and writes out tables of evaporation coefficients.

Single stream tube analysis is preceded by writing out a one-page table of input total flows and averaged spray and gas parameters. During single stream tube analysis, data are written out as they are generated. At each z-plane to be printed, complete gas and propellant spray group data are given. Additionally, the percentages of propellants evaporated and burned are listed.

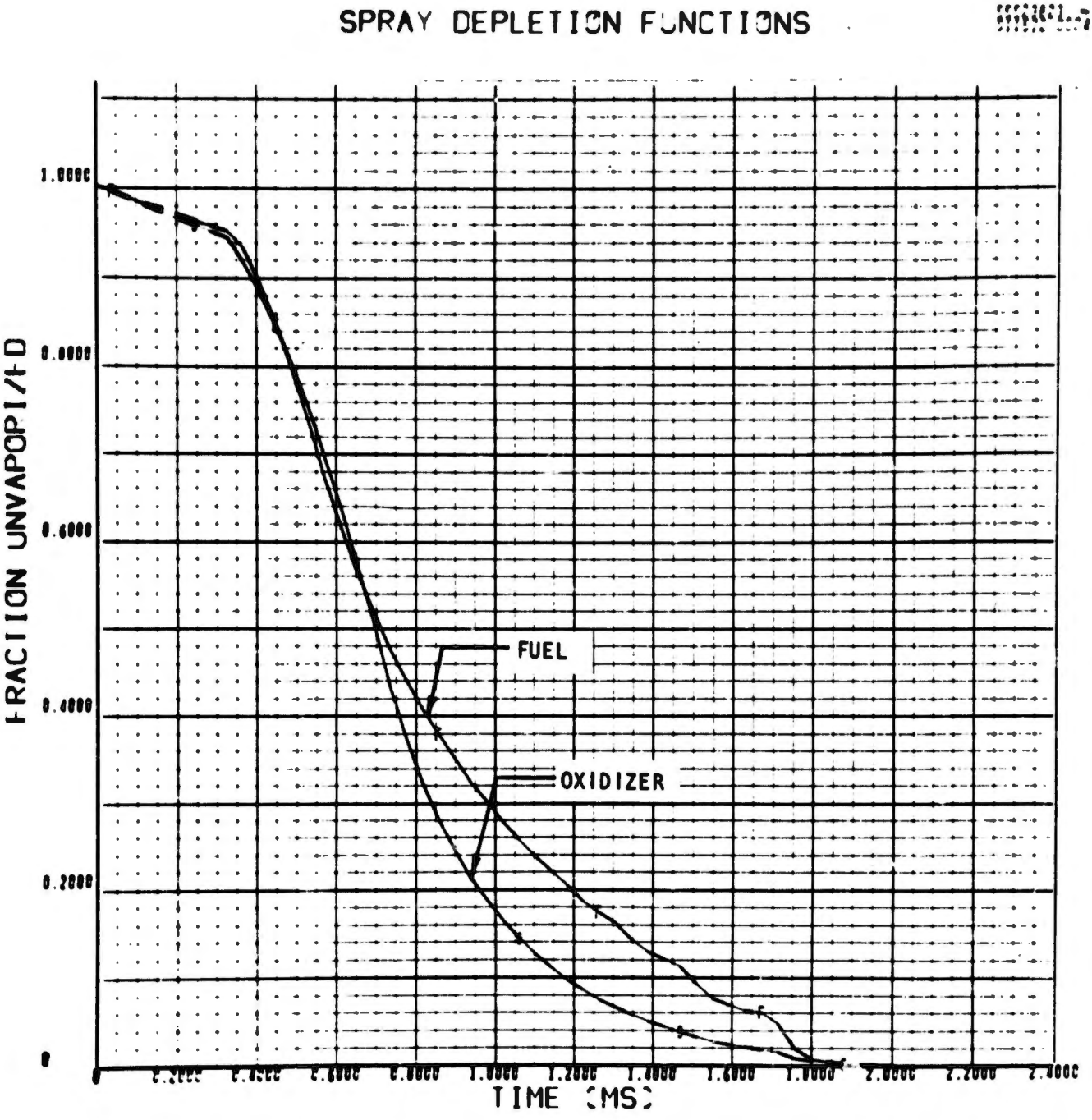

Figure 13. Example of Spray Depletion Functions Computed by PMSTC Subprogram for N_2O_4/MMH

An engine balance summary printout appears immediately following the throat plane printout of every single stream tube analysis. If reiteration through LISP analysis is required, an entire LISP printout may also appear here.

When the foregoing analysis has converged on its solution, the input value of nozzle radius ratio and calculated value of mean nozzle expansion coefficient, $\bar{Y}$, are used by TRANS to generate transonic flow region isobars. The reduced coordinates and flow directions for each of 20 points along each isobar are written out, beginning with the furthest downstream isobar and progressing upstream. Additionally, for the $\alpha=0$ isobar, the absolute coordinates are written out for 40 points. Finally, a value is printed out for the nozzle discharge coefficient, C_{ND}.

TRANS also generates a CRT plot of the isobars' coordinates. Examples are shown in Fig. 14 for two throat radius ratios.

Multiple stream tube input data are re-initialized and some additional data are written out to more completely define the initial-plane conditions. At each prescribed z-plane for printing multiple stream tube results, complete definitive data for combustion gases and propellant sprays are written out. Local chamber area and contraction ratio are given; additionally, percentages of the propellants evaporated and burned are listed.

At the throat position and intermittently downstream, diagnostic-type printouts containing data concerning dividing streamline intersections with the fifth, $\alpha=0$, isobar are inserted between the regular z-plane printouts. A summary table of these data is given near the end of the multiple stream tube printout. Finally, a long summary table is given of the stream tubes' outer radii at each z-plane. This is terminated with the minimum value of the sum of stream tube areas and the ratio of that value to throat area ratio. The magnitude of this latter value's deviation from unity and compatibility of ENGBAL variables determine whether or not all, or a portion, of PMSTC's multiple stream tube analysis will be repeated. If so, it is readily apparent in the printout.

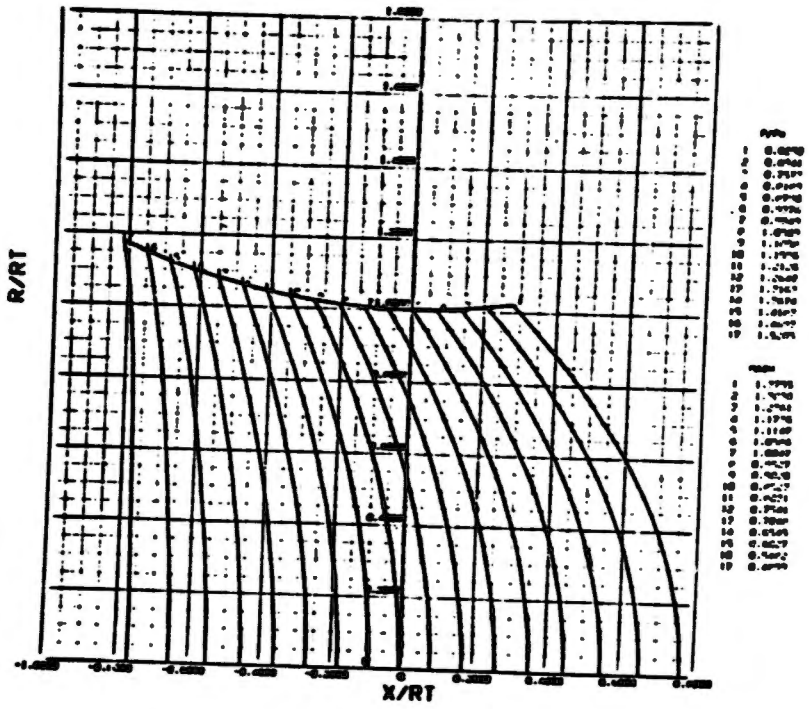

a) Radius Ratio = 2.00

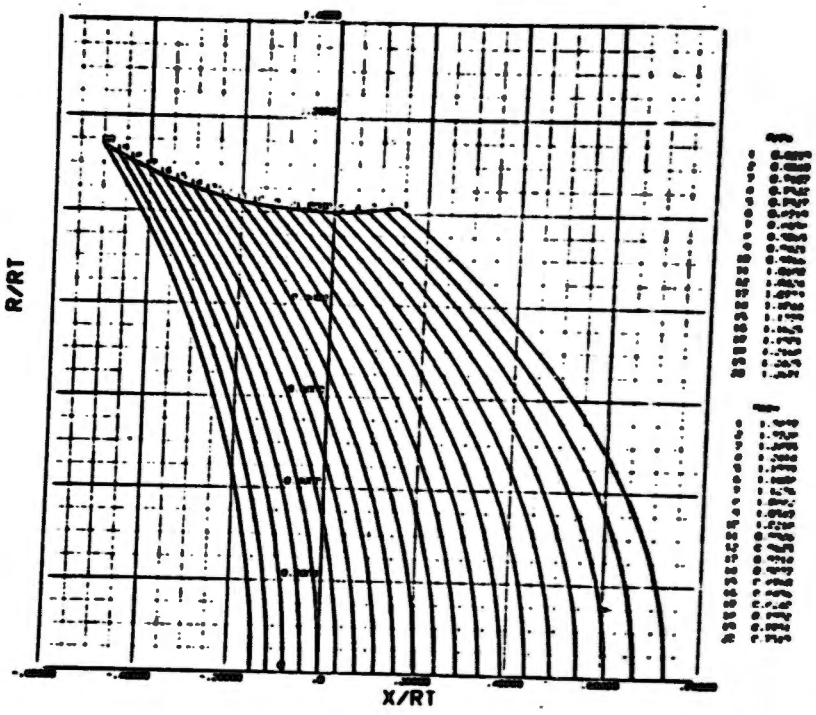

b) Radius Ratio = 1.00

Figure 14. Nozzle Pressure Distributions Calculated by the TRANS Computer Program

One (or more) computer-plotted graphs accompany the printout discussed above, showing the outer radii of the stream tubes along the entire chamber length, as illustrated in Fig. 15. One of these graphs is plotted for each iteration through the multiple stream tube analysis.

Following the last pass through the multiple stream tube analysis, a table is printed which lists the data punched by PMSTC for subsequent use in running the TDK computer subprogram block.

Punched card output is generated for those STC-TDK interface data, as well as for the earlier stream tube initialization data.

Supersonic Nozzle Expansion (TDK)

The TDK computer program block of the PMDER computer program is a shortened and somewhat modified version of the reference TDK program (Ref. 9). The basic approach was to initialize the TDK start-line via data calculated by PMSTC, supplementing those data with TDK computations as required, and to retain the multiple axisymmetric stream tube nature of the solution by utilizing TDK's long-form option. To the extent possible, modification of the reference program was held to a minimum.

Initialization from PMSTC Data. Coordinates and flow direction at 40 points along the isobaric TDK initial-line, computed by TRANS, are transferred to TDK. In the PMSTC analysis, the intersections of dividing-stream-lines (between neighboring stream tubes) with the TDK initial-line are found and their coordinates are transferred to TDK. Also transferred to TDK are the gas mixture ratio and velocity at the intersection of each stream tube with the initial-line. The initial-line pressure and a mean vaporization efficiency complete the specification of data from PMSTC.

The composition of the combustion gases of each stream tube must be specified at the initial line. The simplified tabular specification of combustion product properties as functions of mixture ratio and Mach number essentially provides

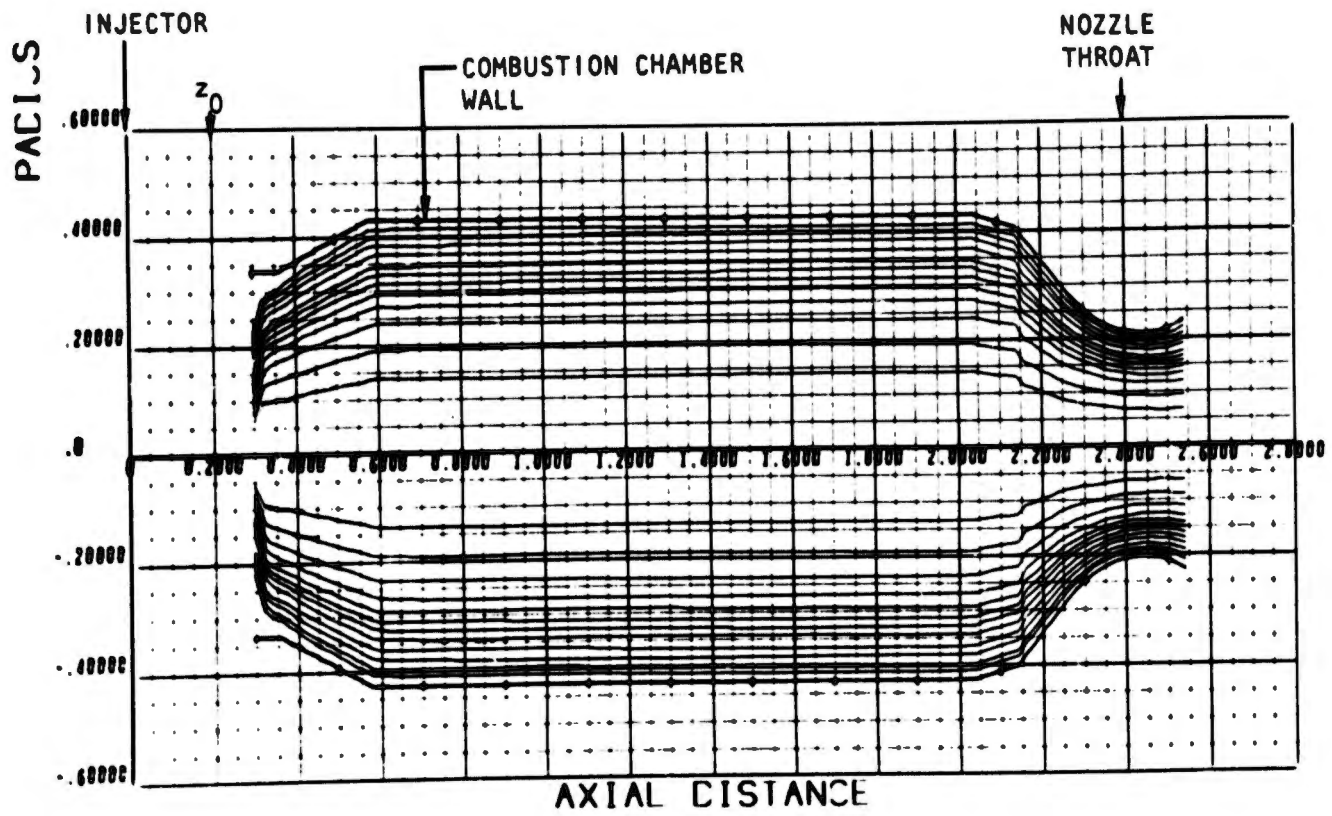

Figure 15. Example of Computer-Plotted Dividing Stream Lines From STC Program Block

local static equilibrium expansion. Species concentrations are not included in that specification because they are not needed for PMSTC computations. Therefore, the equilibrium analysis section of TDK is used to obtain equilibrium initial line conditions for each stream tube, based on the specified mixture ratio, flow velocity, and pressure. In addition to gas composition, the molecular weight, temperature, and density are derived from the equilibrium solution of TDK.

TDK Program Modifications. A large part of the reference TDK program is identical to the reference ODK (one-dimensional kinetic) computer program. That section of TDK has been modified for PMDER program usage by:

1. Solving for equilibrium conditions only at the initial-line position in the flow, rather than at chamber stagnation, throat position, and an expansion point (this avoids generation of unneeded data)

2. Performing that initial line equilibrium solution repetitively, once for each stream tube

3. Bypassing the one-dimensional kinetic nozzle flow analysis

The transonic flow analysis section of the reference TDK program has been replaced completely. Transonic flow is no longer analyzed here; the functions now performed by this section are distribution of 49 discrete initial line points among the stream tubes and assignment of appropriate flow properties to those points. Two points, having identical coordinates but different properties, are required to define each dividing stream line between stream tubes. This limits to 24, the number of stream tubes which can be initialized. If there are n_t stream tubes, there are $49-2n_t$ extra points which are assigned as interior points of the widest stream tubes. The foregoing equilibrium flow properties for each stream tube are then assigned to all initial line points associated with that streamtube.

The section of TDK which calculates the supersonic, kinetic expansion in the nozzle downstream of the initial-line has been modified to account for the reduction

in specific impulse due to incomplete combustion, i.e., unevaporated propellants passing through the nozzle throat. In the reference program, specific impulse is calculated at any given point in the solution by dividing a local integrated value of thrust by the total gaseous flowrate, obtained by integrating ρu over the initial-line. In the modified version, that total gaseous flowrate has been replaced by a total propellant flowrate.

If condensed species are found to exist at any point along the TDK initial-line, the reference TDK computer program terminates the analysis and does not perform the supersonic expansion calculations. Because one or more stream tubes may be at mixture ratios which produce some condensed combustion products, the DER version of TDK was modified to bypass this termination control. The mass of the condensed species is neglected and the mass fractions of the attendant gaseous species are normalized so that their sum is unity.

TDK Data Output. Extensive tables of TDK data are printed out. A series of tables, one for each stream tube, details the results of the start-line equilibrium computations. The flow properties at each start-line point are tabulated, as are the coordinates of a series of points along the nozzle wall. The major data printout is a massive table of calculated combustion gas chemical composition and physical properties along selected left-running characteristics in the method of characteristics solution of TDK. To illustrate the physical nature of this TDK output, coordinates of the start-line, dividing streamlines, and left-running characteristics for an eight-stream-tube flow are shown in Fig. 16.

Performance data are also printed in this last TDK printout table. When a left-running characteristic intersects the nozzle wall, values of specific impulse and thrust coefficient are printed for that local expansion ratio.

TDK will also punch out a table of data concerning the flow along the nozzle wall, by input option, for subsequent input data to the reference TBL computer program, which calculates wall boundary layer losses. However, the PMSTC subprogram block does not punch out similar data for the flow upstream of the nozzle throat, nor has a logical structure been provided for recomputing nozzle performance with the DER version of TDK with inputs modified to reflect the TBL results. Exercising this option is not recommended.

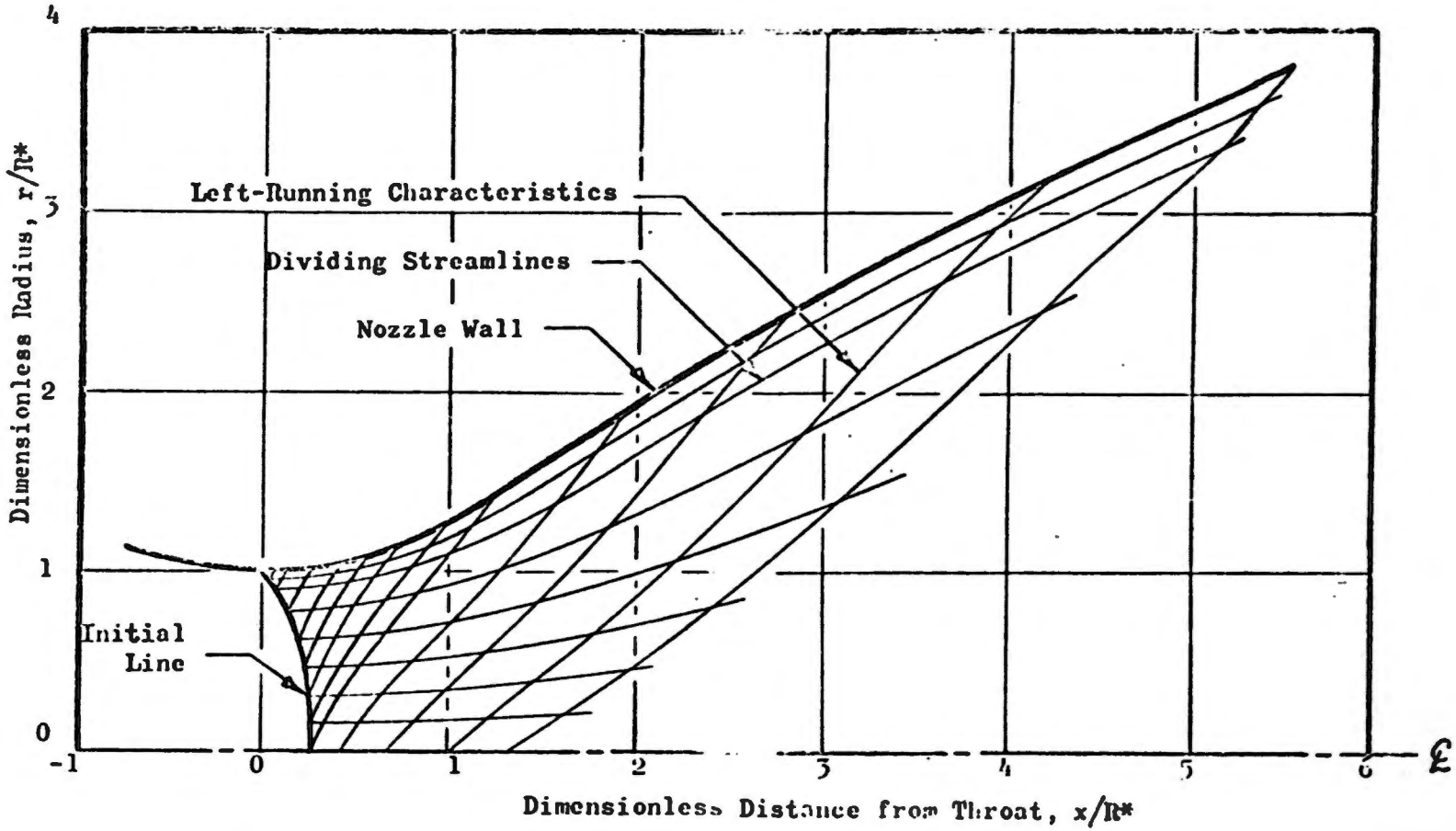

Figure 16. Manually Plotted Coordinates of Dividing-Stream-Lines and Left-Running-Characteristics From TDK Subprogram Block

PULSE CHARACTERIZATION MODEL (PULSE)

In analyzing the characteristics of an individual pulse, it is advantageous to consider the pulse as comprising three time periods: (1) a start transient period; (2) a mainstage, or essentially steady-state, period; and (3) a decay transient period. Accurate evaluation of performance parameters during each of these periods consequently forms the basis for characterizing the entire pulse. The three periods and their relationships to several pulse events are indicted schematically in Fig. 17, for a single pulse, as an aid to the following discussion.

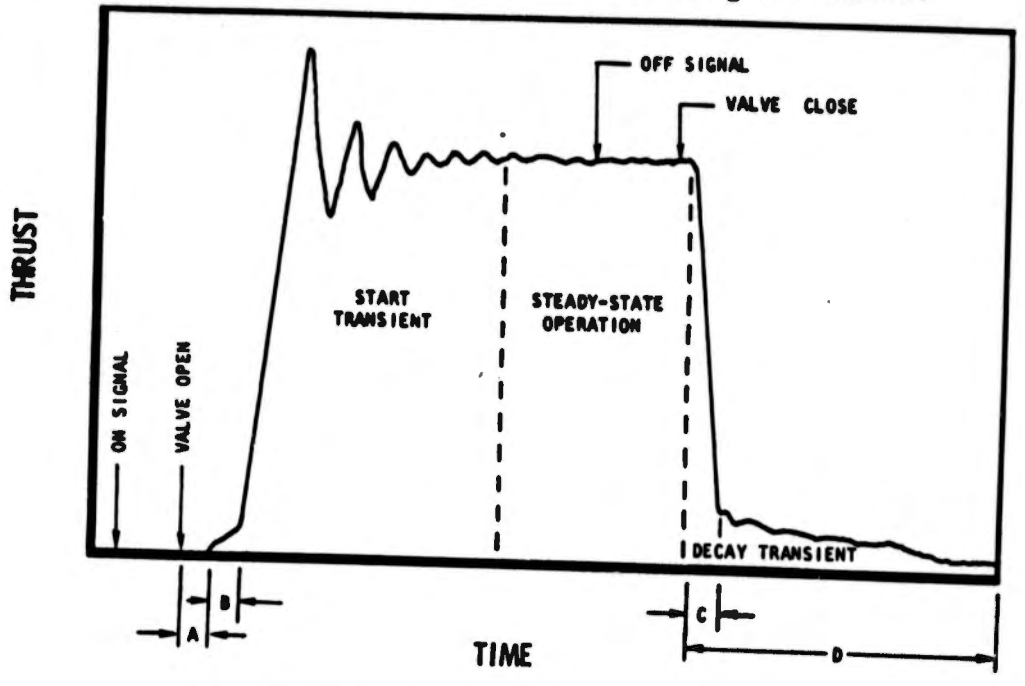

A MANIFOLD FILLING AND INITIAL IMPINGEMENT
B PROPELLANT VAPORIZATION AND IGNITION
C BLOW DOWN
D MANIFOLD BOIL-OFF
ON SIGNAL TO VALVE OPEN = COIL ENERGIZE + VALVE TRAVEL
OFF SIGNAL TO VALVE CLOSE = DE-ENERGIZE + VALVE TRAVEL

Figure 17. Typical Pulse Thrust Trace Characteristics

The characteristics of the start transient period depend upon the conditions existing in the propellant supply systems and in the combustion chamber at its initiation and upon the duration of the period. More propellant will be inefficiently exhausted as vapors and unreacted spray under vacuum start conditions, for example, than if the feed system contains residual propellants and the chamber is still

partially pressurized with hot combustion gases from a prior pulse. In that latter case, losses during chamber pressurization and ignition delay phases would be minimized or avoided. In general, smaller losses will be experienced if the start transient is kept as short as possible, particularly if the period is marked by substantially off-nominal mixture ratio burning.

Similarly, performance losses associated with the decay transient depend upon the off-time between pulses and upon the relative boiloff rates of the propellants. An individual pulse's decay transient losses will be larger as one propellant boils off at a different time or at a faster rate than the other propellant.

Conversely, steady-state performance parameters (except for those which are time integrals, such as total impulse) are essentially independent of the duration of steady-state operation. A given pulse, however, may exhibit only a pseudo-steady-state period because the combustor walls have not yet been heated to their steady-state temperature distribution. In formulating the Pulse Mode Performance Model, therefore, it is assumed that each pulse's "steady-state" performance is the true steady-state performance corrected by a gas heat loss factor.

These relationships led to the fundamental concept that each pulse in an engine operating duty cycle can be synthesized from performance data for steady-state and for start and decay transients of a modest number of "standard" width pulses, in which steady-state operation is very brief. Subprogram block PULSE analyzes specified sequences of standard-width pulses as illustrated in Fig. 18 with variation of pulse-to-pulse off-time (τ_n) within each sequence and variation of assumed mean wall temperature from sequence-to-sequence, and sets up tables of parametric pulse performance data. The tabular data are stored and used later by subprogram block DCYCLE in analyzing an engine duty cycle.

Figure 19 is a simplified flow chart for the PULSE subprogram. Subroutine PULSE is primarily an executive and service routine for the subprogram block of the same name. It performs and calls upon other subroutines to perform service functions,

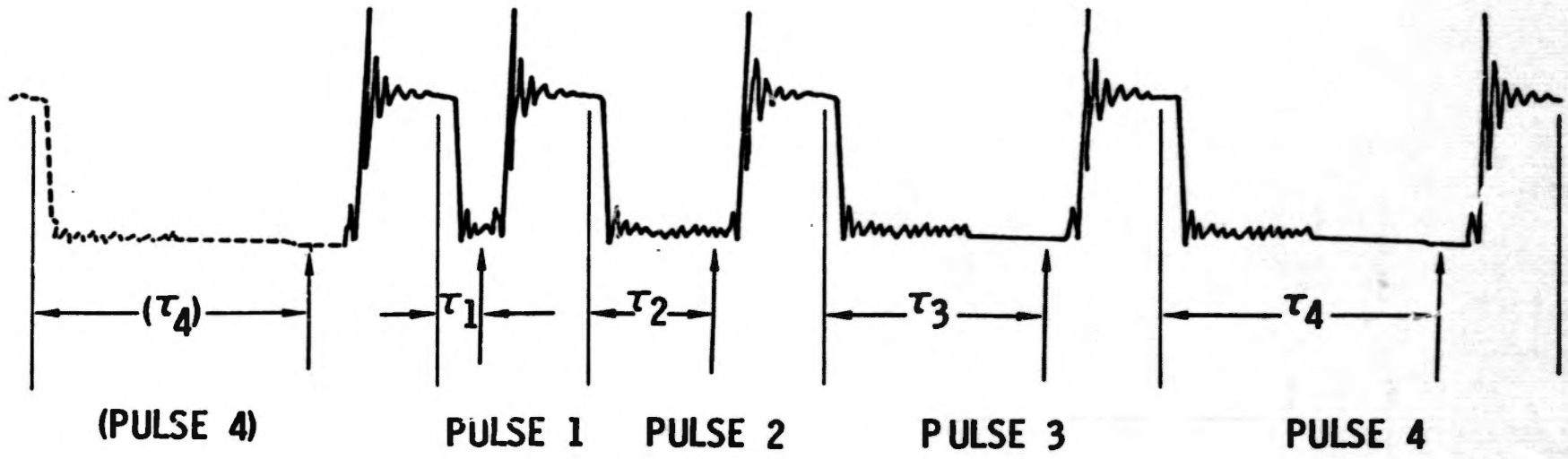

Figure 18. Illustration of Analysis Concept for a Sequence of Standard-Width Pulses

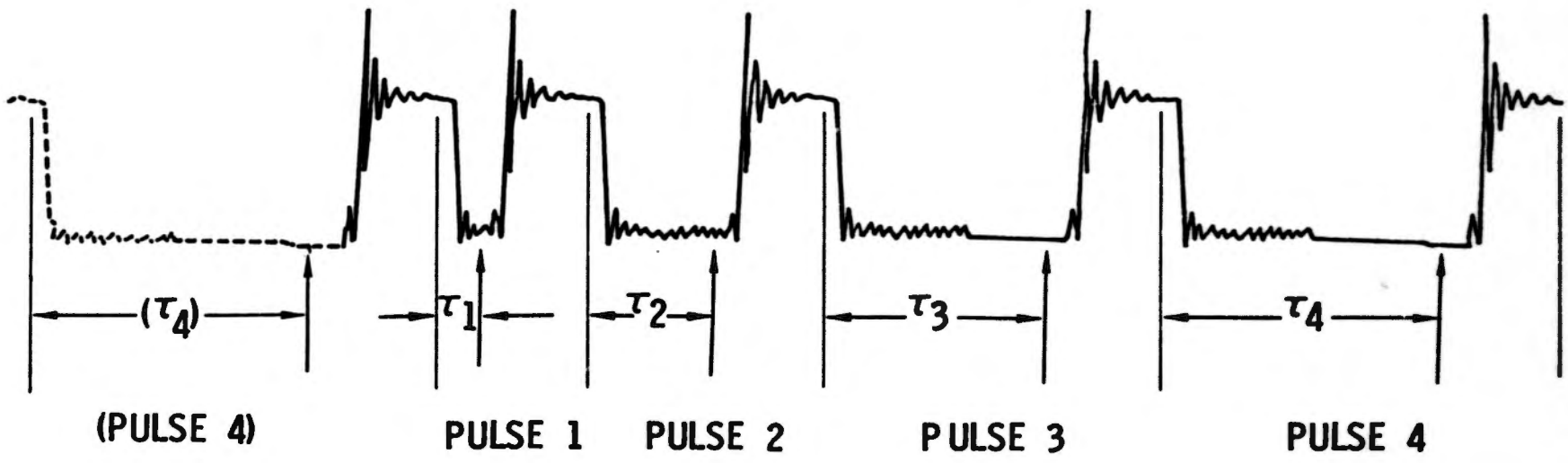

Figure 18. Illustration of Analysis Concept for a Sequence of Standard-Width Pulses

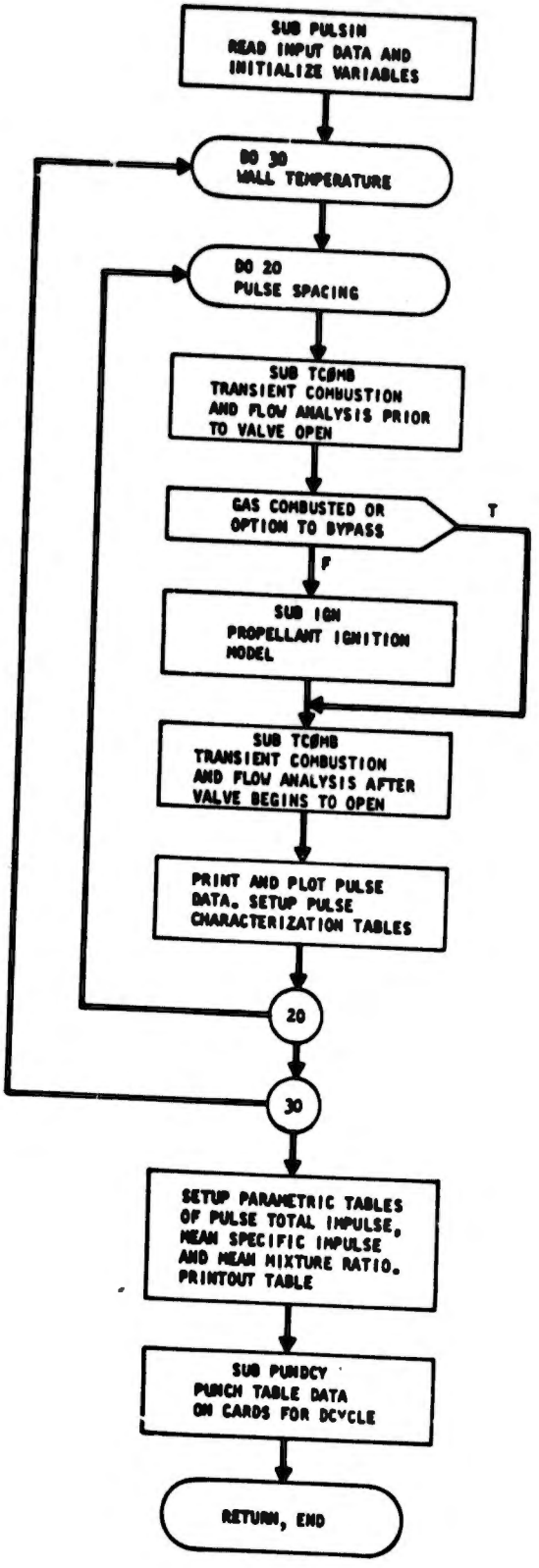

Figure 19. Simplified Flow Chart of PULSE Subprogram

e.g., reading data, initializing variables, printing and plotting data, and structuring, storing, printing, and punching parametric performance tables. Subroutine TCØMB (Transient Combustion) is called upon to perform the actual pulse analyses.

TRANSIENT PERFORMANCE (TCØMB)

The transient performance model, TCØMB, simulates transient behavior of a propellant feed system, propellant ignition process, spray vaporization, and combustion chamber performance. A few of the basic functions of the model are shown conceptually in the block flow chart in Fig. 20. Transient analysis for a series of pulses is conducted step-wise in time.

Only the start and decay transients are of interest in the TCØMB analysis. Pulse width is minimized for computational efficiency, and is kept constant to provide a common basis for comparison between pulses. The standard pulse width should be selected long enough such that the start transient approaches steady-state operation.

A fairly detailed block flow chart of TCØMB is presented in Fig. 21 and will be referred to in subsequent sections. TCØMB is entered twice during a pulse, once at the first time step, and again after an ignition analysis by IGN (if it is not bypassed). Initialization of TCØMB parameters is done internally and according to various entry conditions. Simulated time is advanced one increment. Spray ensembles are set up in GASGEN and quantity of gas generated from ensembles is summed. Continuing in TCØMB, nozzle flow is calculated, and the net accumulation of gases in the chamber resulting from the gas generation and nozzle exhaust rates is solved. Bulk chamber combustion properties are determined from equilibrium combustion tables. Thrust is calculated and integrated to obtain total impulse. Finally, the feed system flow is solved in subprogram FEEDS before cycling back to increment time. These processes are discussed in detail in subsequent sections.

Before describing the formulation of the major features of TCØMB, a brief phenomenological description of the various transient pulse phases is provided as background for discussing the model assumptions and simplifications.

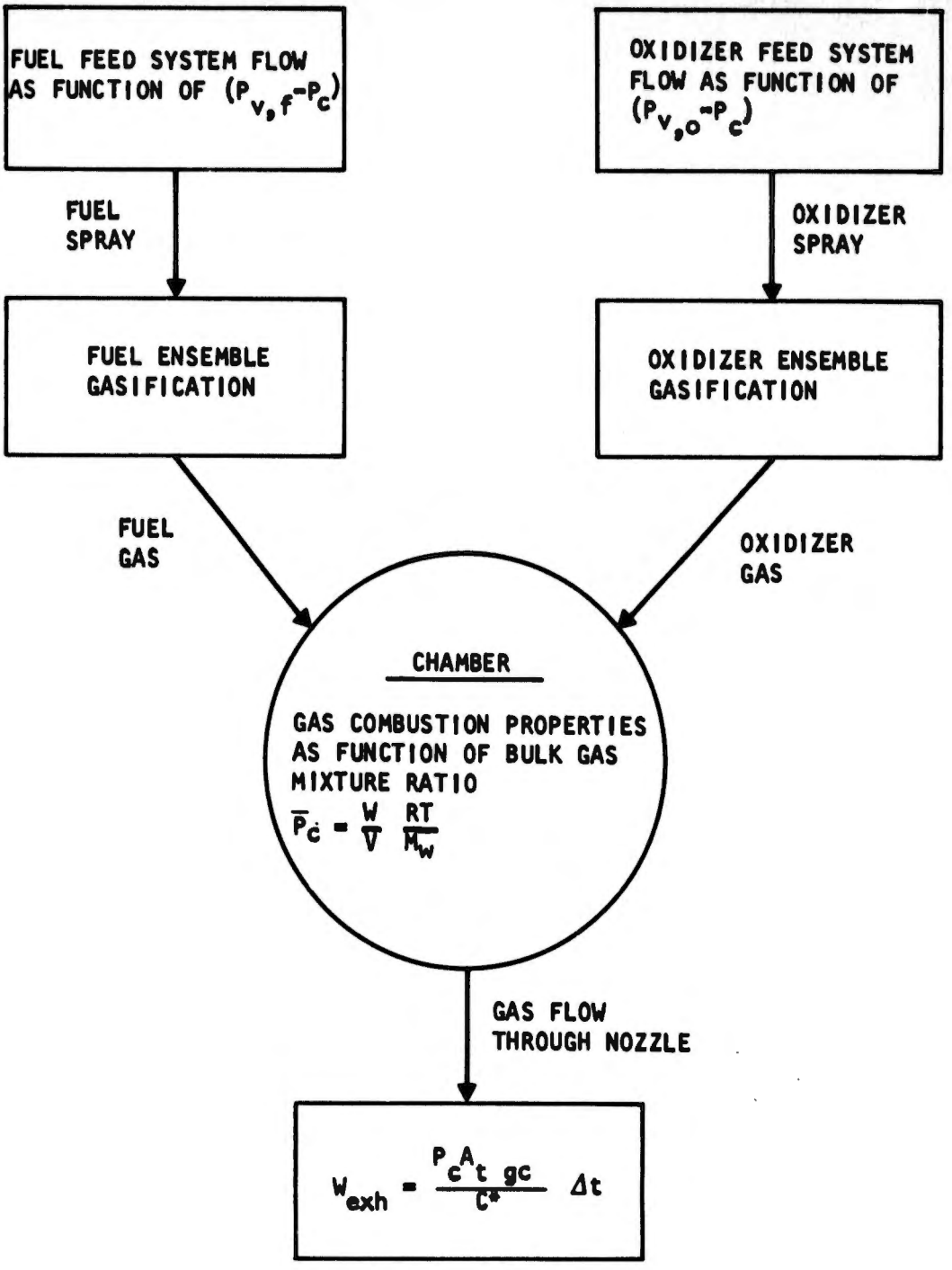

Figure 20. Conceptual Flow Chart of TCØMB

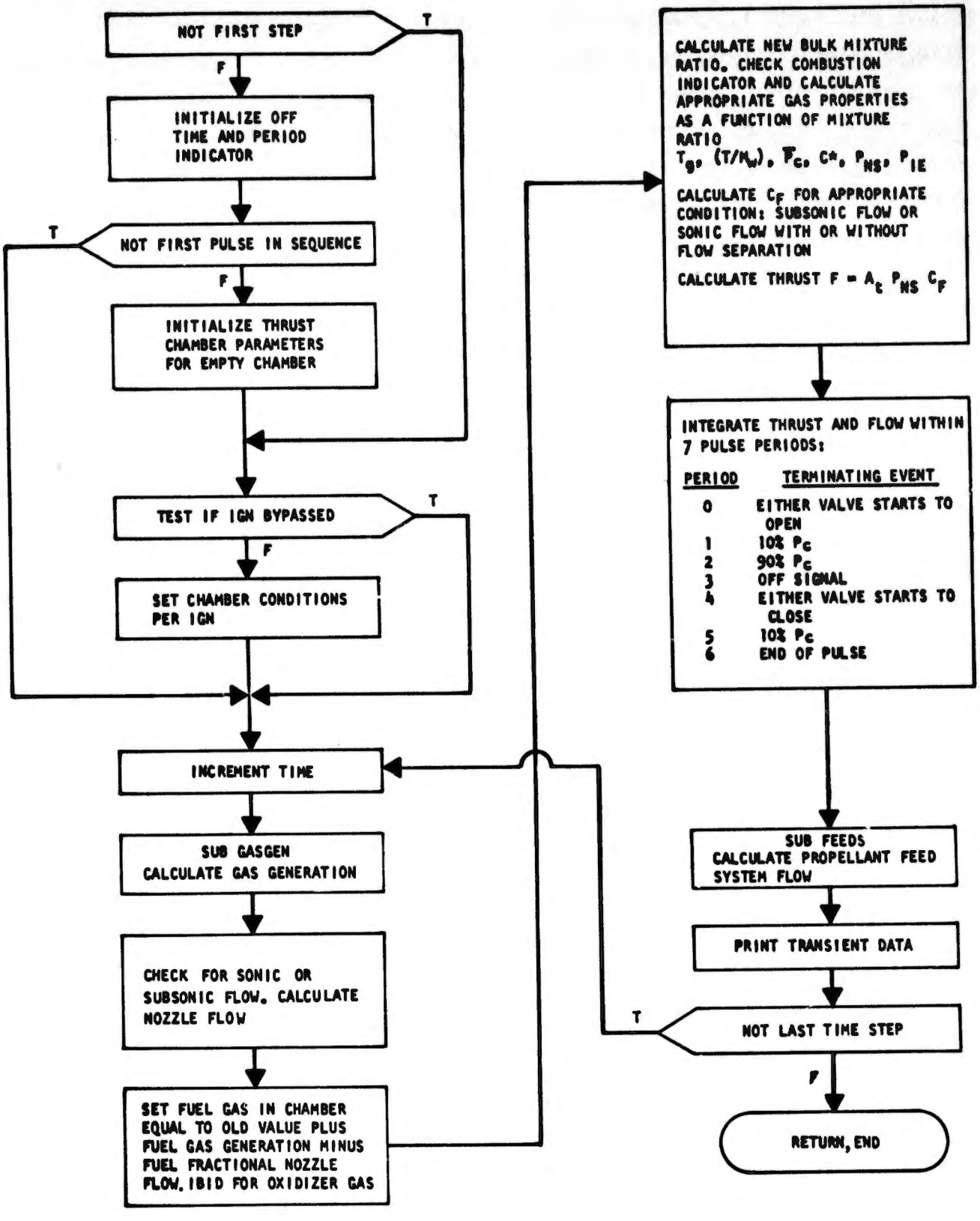

Figure 21. Simplified Flow Chart of TCØMB

Description of Pulse Transient Phases

Feed System Priming. Under space ambient conditions, propellant lines and manifolds downstream of shutoff valves are initially evacuated. Upon opening a propellant valve, propellant will rush into the manifold system. The initial liquid to enter the manifold will briefly exhibit the same behavior here as when liquid is initially injected into the chamber a few microseconds later: i.e., there will be flash vaporization with its disruptive fragmentation of liquid elements, rapid gasification of small droplets accompanied by subcooling, even to the freezing point, and rapid expansion of the vapors to fill the manifold. These vapors are free to escape through the injector into the combustion chamber and they do so. The injector restricts the vapor flow considerably, however, so the manifold, having a rather limited volume, is rapidly pressurized. Depending upon the valve opening rate, the manifold pressure might get as high as the propellant vapor pressure at its storage temperature before it is essentially liquid filled.

Liquid passing through the valve a short time later will thus encounter a modest backpressure so that, though a lot of bubble formation and frothing may still occur, the disruptive forces are not nearly as violent as they were for the earliest liquid through the valve. As the manifold fills with this two-phase flow, its pressure will rise abruptly and the two-phase mixture will become more and more dense as vapor bubbles are recondensed and the mixture will rapidly approach a flow of liquid at nearly storage conditions. In the meantime, injection of the frothy, two-phase flow has commenced but is soon replaced by a wholly liquid flow. There may be flow separation and flash vaporization within the injection orifices for a time, until the chamber pressure rises enough to prevent their occurrence.

Ignition Delay. Following initial propellant injection into a space-evacuated rocket combustion chamber, there is a measurable time lag before ignition occurs. Several processes which transpire during that time determine its duration and the characteristics of the actual ignition and the combustion which follows. The liquid propellants are atomized, first by flash vaporization, and later by hydraulic forces such as occur in splash-plate or liquid-stream impingement, liquid sheet disintegration, etc. The liquid sprays tend to evaporate, forming

vapors which both pressurize the chamber and escape unreacted from it, and perhaps condense on cold combustor walls. Nearly adiabatic vaporization tends to chill the residual spray droplets, which may even freeze and escape largely unevaporated from the combustor.

To achieve ignition, there must be a combustible mixture of vapors in the combustor, at least a portion of which is heated past its minimum ignition temperature. If an ignition source is provided, local heating may suffice, whereas, with hypergolic propellants, ignition may involve global heating of all the vapors by more or less gradual accumulation of energy from preignition vapor- and liquid-phase reactions. Once ignition occurs, it is usually propagated rapidly throughout the combustor and sustained.

Chamber Pressurization by Combustion. The same processes continue to take place after ignition as were occurring before ignition, but their rates and relative importance are greatly changed. Spray elements are now surrounded by hot gases, which raises their evaporation rates and their bulk temperatures, and convection becomes a dominant effect. Rapid oxidation reactions supplant the slower, less energetic preignition reactions. Condensation rates fall off rapidly. Chamber pressure rises rapidly and, as a result, the propellant injection rates are gradually lowered. Propellant atomization is altered; coarser sprays are produced as flash vaporization ceases and surface disruption, by gasification within the liquid, is replaced by shear forces stripping spray from the surface.

Because liquid inertia introduces a time lag between a time-varying injection (ΔP) and the resultant time-varying injection rate, and because at ignition the chamber generally contains more propellant sprays than it does during steady-state combustion, a pressure spike substantially higher than steady-state chamber pressure is sometimes produced. An oscillatory pressure, with decaying amplitude, may then precede the steady-state portion of the pulse. Its transient nature causes this period to be considered as part of the start transient.

Decay Transient. Upon closure of the propellant valves, injection manifold pressures quickly fall to the steady-state chamber pressure and injection ceases. The chamber pressure and thrust do not begin to decay immediately, however, because the spatially distributed sprays continue to burn at their precutoff rates. When their gas generation rates begin to diminish, chamber pressure begins to decay. Complete consumption of the stored sprays generally takes from one to several milliseconds; then the pressure falls precipitously as the combustion gases escape from the chamber.

The early part of the decay transient thus resembles the blowdown of a gas vessel. Eventually, however, chamber pressure falls below the vapor pressure of the propellants, whereupon the propellants will begin to boil in the manifolds, arresting the falling pressures there. Then, with manifold pressures higher than the decaying chamber pressure, the injection of propellants recommences. After a short delay time (during which injection, flash vaporization, atomization, and droplet vaporization transpire), combustion gas generation is resumed, slowing the rate of chamber pressure decay. This boiloff and pressure decay process is continued, frequently with a great deal of transient surging, until the manifolds are completely emptied, the sprays are all evaporated, and the chamber gases have been exhausted (or until the propellant valves are opened again to begin another pulse). The process is accelerated by soakback of heat from the combustor walls into the propellants.

Feed System Model

Three subprograms constitute the feed system models; each contains parallel logic for oxidizer and fuel systems. Subroutine FEEDS calculates delay times from the propellant flow control valve energize (and de-energize) signals to commencement of valve travel, calculates valve open areas as functions of time, and calls upon subroutines FLØW or BØIL to compute the feed system propellant dynamics. Subroutine FLØW is called if either propellant valve has nonzero open area; it computes feed system priming and flow phenomena. Subroutine BØIL is called if either valve is fully closed and calculates boiloff of residual propellants left in the feed systems, downstream of the valves when they are closed.

Each propellant feed system is considered to consist of a flow control valve, a short line segment, a small manifold, and one or more injection orifices (Fig. 22). Dynamics of feed system components upstream of the valves are not analyzed; propellants are supplied to the valves at constant pressures and temperatures. These supply parameters are input as known values. The components analyzed are presumed to be physically short so that acoustic (pressure) wave travel times are very small relative to the times over which hydraulic flowrate changes occur. Thus, wave motion in the feed system is not analyzed; the only pressures considered are the (constant) valve supply pressure and the time-varying injection-end chamber pressure.

Valve Dynamics: Subroutine FEEDS. Two distinct periods comprise the actuation of typical solenoid valves used for propellant flow control: valve coil energization, and valve travel. Of these events, coil energize time is usually the longest, by far. Normal variations in spacecraft supply voltages and coil temperatures can cause significant variations in coil energize time. The approach programmed in subroutine FEEDS permits accounting explicitly for the voltage effect. Linear variations of valve energize and deenergize times are given, respectively, by

$$t_e = t_{on} + (C_o)_e + (C_1)_e V_v \tag{46}$$

$$t_{de} = t_{off} + (C_o)_{de} + (C_1)_{de} V_v \tag{47}$$

The coefficients C_o and C_1 are supplied as input variables, one set for each propellant. They may be varied from one run to the next to obtain an implicit evaluation of coil temperature effects, but it would be more practical to expand the program.

Valve opening and closing rates are accounted for by providing input tabular functions of open-area fraction versus elapsed travel time. Any form of general dependence on important static variables can thus be built into the tables.

Priming and Flow Dynamics: Subroutine FLØW. In constrast to the rather violent, two-phase, feed-system priming phenomena described earlier, the formulations for subroutine FLØW considers priming to occur as an orderly hydraulic progression,

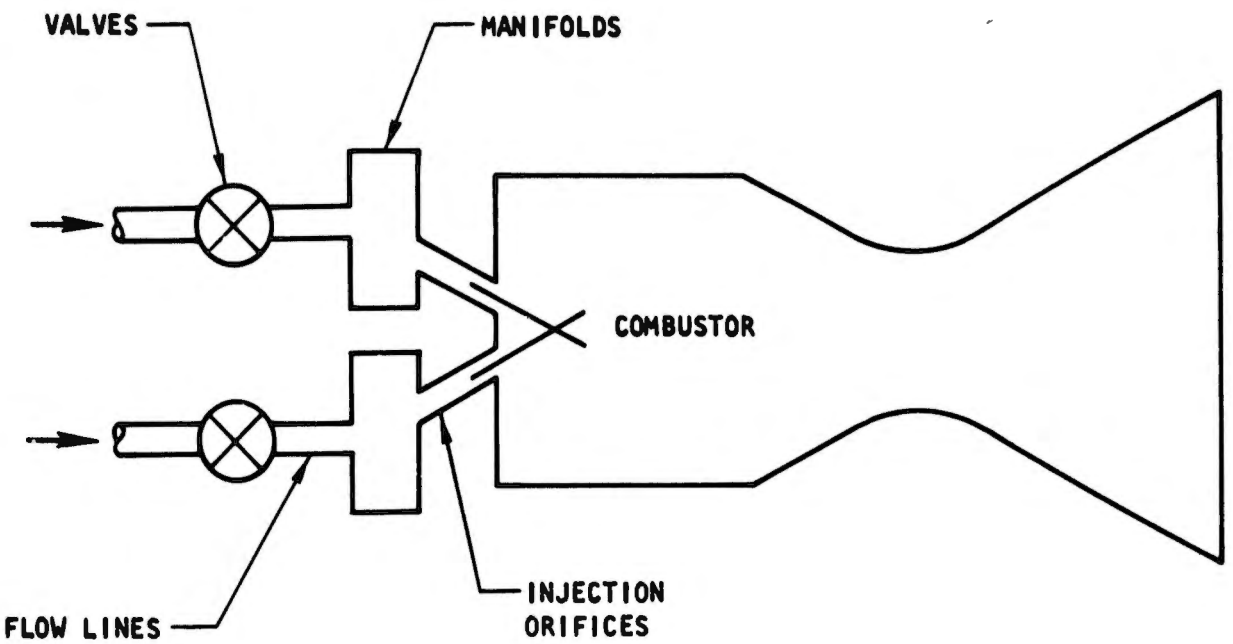

Figure 22. Schematic Representation of Propellant Feed Systems

filling the feed system components sequentially, proceeding from the valve through the injection orifices. Propellant injection into the combustion chamber is presumed not to occur until the feed system components are full, and then to start impulsively as single-phase, liquid injection. At the instant that the valve begins to open, the system may be void of propellant, may be partially filled, or may be completely filled, depending upon what has transpired before the particular valve actuation. In any event, a partially filled system is divided into a liquid phase, occupying volume as close as possible to the valve, and a void volume as close as possible to the injection sites. This treatment makes it possible to formulate a single solution for the feed system flow dynamics; certain component terms simply drop out if the component does not contain fluid. The formulation is also valid if the flow is reversed, i.e., chamber pressure is higher than valve supply pressure and the system is emptied by forcing liquid back through the valve.*

A single dynamic flow equation is used which relates system pressure drop (valve supply to chamber) to fluid dynamic pressure drops, component entrance losses due to area reductions, and component friction losses. The equation is written in terms of volumetric flowrate, $\dot{q}$ (in.^{3}/sec).

$$P_V - P_{IE} = \frac{\rho}{(144)^2 g_c} \left[\frac{d\dot{q}}{dt} \sum_i \left(\frac{\ell_i}{A_i} \right) + \frac{\dot{q}^2}{2} \sum_i \frac{K_i}{A_i^2} \left[1 - \left(A_i / A_{ei} \right)^2 \right] + \frac{\dot{q}|\dot{q}|}{2} \sum_i \frac{R_{fi} \ell_i}{A_i^2 L_i} \right] \tag{48}$$

where the summations are over the i specific components: valve, line, manifold, and injection orifices. Each component is analyzed in terms of its cross-sectional flow area, A_i, its geometric length, L_i, and its fluid column length, ℓ_i, which may vary with time. The dynamic and friction loss terms obviously vanish if a component contains no fluid ($\ell_i = 0$); the entrance loss term is also omitted for any component which is completely devoid of liquid. An entrance loss term is

*Backflow through a valve is limited to the weight of propellant contained in its feed system at the instant that backflow began.

included only if the component's cross-sectional area, A_i, is smaller than that of the next component upstream, A_{ei}, and if $\dot{q} > 0$. The flow control valve is assumed to have zero length and volume and so contributes only an entrance loss term, and then only if it is not fully open.

Equation 48 is solved numerically in subroutine FLØW by making the first-order finite difference approximation that

$$\frac{d\dot{q}}{dt} \approx \frac{\dot{q}_2 - \dot{q}_1}{\Delta t} \tag{49}$$

across a short time interval, $\Delta t = t_2 - t_1$, by defining

$$\dot{q} = (\dot{q}_1 + \dot{q}_2)/2 \tag{50}$$

and making the forward difference approximations that the initial values $P_{IE}(t_1)$, $A_v(t_1)$ and $\ell_i(t_1)$ apply across the time interval. Then Eq. 48 reduces to a quadratic equation which is solved explicitly for $\dot{q}_2$.

To exemplify the various features and capabilities of the FLØW subroutine, data describing the feed system design of the Rocketdyne SE-9 engine and its NTO/MMH propellants were used. The valve flow areas were increased linearly from fully closed to fully open in 3 milliseconds. A linear ramp increase of chamber pressure was arbitrarily imposed which rose to pressures substantially higher than both valve supply pressures and was then followed by a linear ramp decay. The timing was selected to provide examples, in a single computer run, of several aspects of FLØW behavior, viz., initial feed system filling, initial overshoot of injection velocity, asymptotic approach to a steady flowrate, decay of the flow with decreasing ΔP, flow stoppage after P_{IE} becomes greater than P_v, backflow of chamber gases into the feed system (and of liquid through the valve), and resumption of injection after P_c again falls below P_v. Each of these aspects may be identified by inspection of Fig. 23 , a plot of the computed results. Additionally, the backflow limit during extraordinarily long periods of $P_c > P_v$ may be seen in

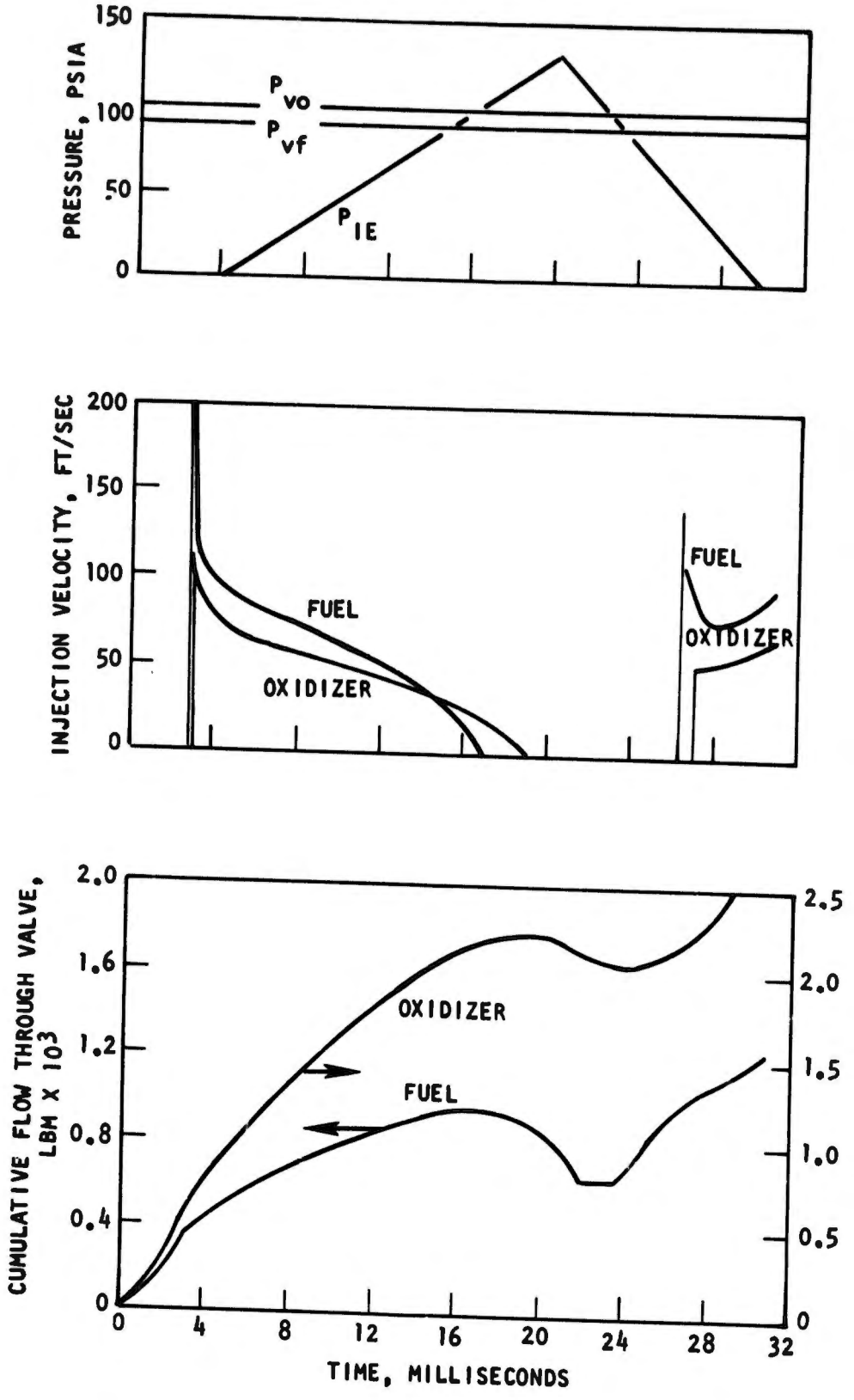

Figure 23. Propellant Flow Parameters Calculated by Subroutine FLØW for NTØ/MMH Propellants in SE-9 Engine With an Imposed P_c Transient

the curve for cumulative fuel flow through its valve: all of the liquid in the feed system was permitted to flow back through the valve, but chamber gases were checked.

Propellant Boiloff: Subroutine BØIL. Propellant boiloff from the feed systems is analyzed by subroutine BØIL, which calculates, as functions of time, the residual propellant weight (W_m), its temperature (T_m), vapor pressure (P_m), liquid, vapor, and mean densities (ρ_ℓ, ρ_v, and ρ_m, respectively), and the fraction (X_v) of the feed system volume (V_{fs}) occupied by propellant vapors. Simultaneously, spray combustion and chamber exhaustion are being analyzed by TCØMB, resulting in a solution for the chamber backpressure into which the boiling propellants must flow.

The residual feed system propellants are assumed to be homogeneous, varying only in time (i.e., heat soakback is uniformly distributed). When injection occurs, it is that homogeneous fluid which is injected. Two injection mechanisms are considered. If $X_v = 0$, $P_m \leq P_{IE}$ and $d\rho_\ell/dt < 0$, liquid expansion forces some liquid out

$$\dot{w}_{inj} = -\frac{dW_m}{dt} = -V_{fs}\frac{d\rho_\ell}{dt} \tag{51}$$

If $P_m > P_{IE}$, an orifice equation provides the injection rate

$$\dot{w}_{inj} = \frac{dW_m}{dt} = C_D A_{inj}\left[2 g_c \rho_m (P_m - P_{IE})\right]^{1/2} \tag{52}$$

The mean density is given by $\rho_m = W_m/V_{fs}$ and also by

$$\rho_m = X_v \rho_v + (1 - X_v)\rho_\ell \tag{53}$$

where

$$\rho_v = \frac{P_m M_w}{R T_m} \tag{54}$$

and $\rho_\ell = \rho(T_m)$ is tabulated as a function of temperature. Propellant vapor pressure is also tabulated as a function of temperature, $P_m = P_v(T_m)$. A differential

equation relates changes in propellant temperature and volume fraction filled by vapor to the heat soakback rate:

$$W_m \left[c_{p\ell} \frac{dT_m}{dt} + \lambda_v \frac{dX_v}{dt} \right] = \dot{Q}_{SB} \tag{55}$$

The temperature of the feed system body is assumed to be a function of the mean chamber wall temperature. Finally, the heat soakback rate is proportional to the wall-to-propellant temperature difference, and the heat transfer coefficient is a function of the quality

$$\dot{Q}_{SB} = \dot{Q}_{SB,SS} * (1-0.95X_v) * \left(\frac{T_{FS} - T_m}{T_{FS,SS} - T_v} \right) \tag{56}$$

$$\text{with } T_{FS} = T_{amb} + (T_W - T_{amb})\ (T_{FS,SS} - T_{amb})/(T_{W,SS} - T_{amb})$$

where $Q_{SB,SS}$ is the user-supplied steady-state heat soakback rate when the propellant is at its valve supply temperature, T_v.

The foregoing system of equations is solved in subroutine BØIL by recasting Eq. 55 to the form $dT_m/dt = f(T_m,t)$ and considering all other unknown variables to be functions of T_m and time. Subroutine BØIL consists of a fourth-order Runge-Kutta solution for T_m and subsequent solutions for the other unknowns.

Paralleling the example given above of the computed results of the flow, boiloff of N_2O_4 and monomethylhydrazine from their SE-9 engine feed systems is illustrated in Fig. 24. The systems were assumed to be full of liquids at the instant of simultaneous valve closure and, for simplicity, the chamber pressure was assumed to be zero at that time and thereafter. Constant values of heat soakback into each feed system were set at 10 Btu/sec.

NTO was seen to boiloff considerably faster than MMH, which still had approximately one-quarter of the initial fluid in the feed system after 10 milliseconds. Until the oxidizer was over half gone, the heat soakback went predominantly into providing heat of vaporization. Eventually, as the residual mass decayed, this heat caused the fluid temperature and feed system pressure to increase abruptly. Because the fuel is less volatile, the computed behavior of MMH was less dramatic than that of NTO.

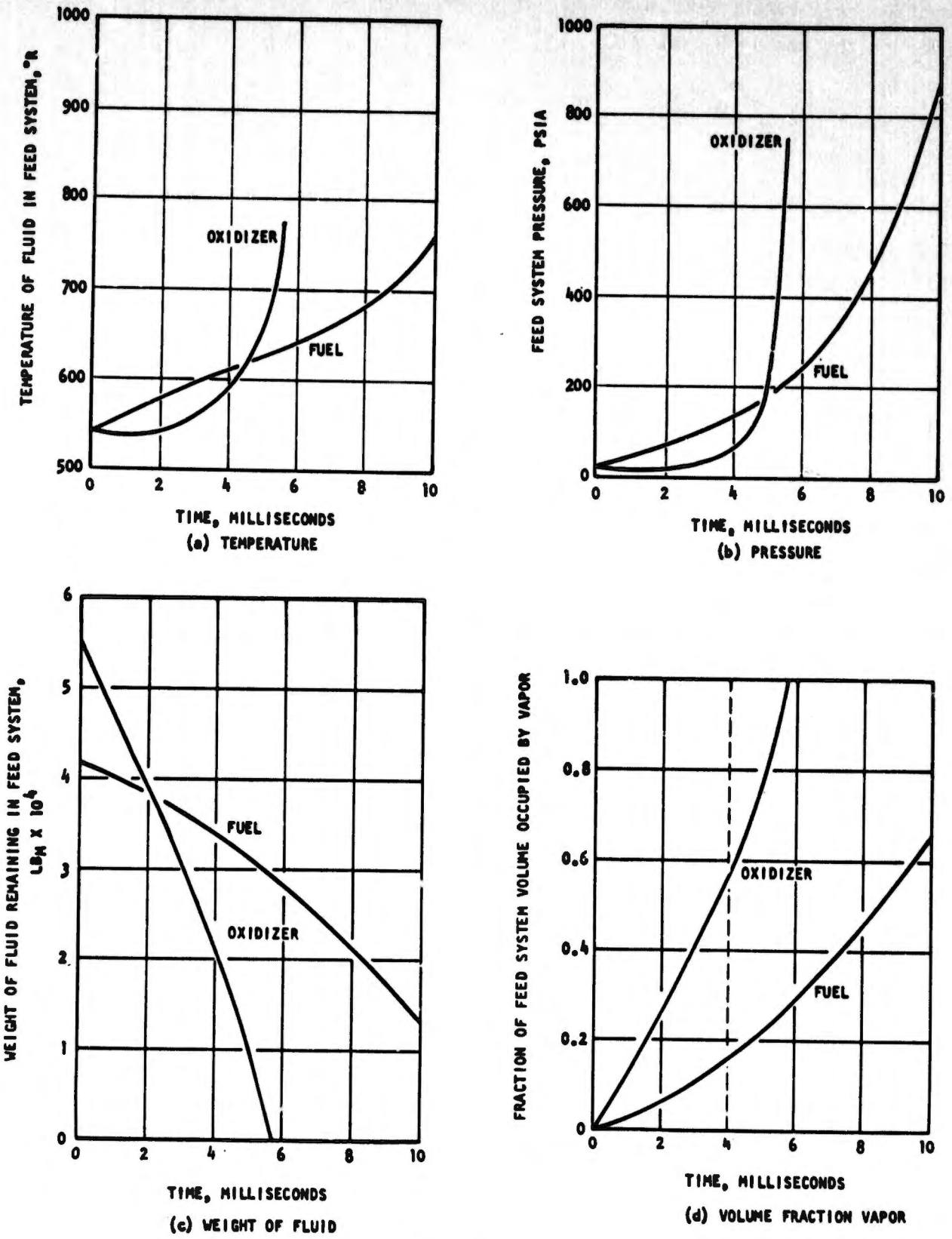

Figure 24. Propellant Boiloff From SE-9 Engine Feed Systems Calculated by Subroutine BØIL

To a large degree, the boiloff rates are controlled by the heat soakback rates. In other computer runs, with lower heat soakback rates, the oxidizer was calculated to be cooled below the freezing point. Boiloff and injection are not stopped when this condition is reached; rather, the temperature is held at the freezing point and vaporization is limited to that due to the heat soakback rate.

Ignition

As stated in the Technical Approach section, it was planned from the inception of the pulse mode performance model that the preignition flow, vaporization, and chemical processes would be analyzed by an adapted version of Seamans' hypergolic ignition model (Ref. 3). A substantial amount of work was directed toward extending that model, by removing some of its limitations, and adapting it to the pulse mode problem. The resultant computer subprogram block, IGN, was operated under Seamans' published example case conditions and came close to reproducing his results.

However, when typical pulse mode operating conditions (which have higher flows and more nearly simultaneous valve actuations than in Seamans' case) were input, severe numerical problems were encountered which invariably caused run termination before ignition was achieved. Although some exploratory modifications were tried, the causes of the problem were not fully identified nor were the ranges of conditions mapped for which IGN will predict ignition. The behavior of the computed results, as the program progressed, suggested that conditions were changing too rapidly for the numerical solution method employed. Attempts to evaluate this possibility, by using somewhat reduced time intervals, were not successful. Large reductions in step size are impractical because spray ensembles are generated every time step, which both increase execution times drastically and tend to fill the assigned spray storage locations with incompletely evaporated, etc., droplet ensembles that should still be analyzed. (When the storage is filled, the oldest ensembles are simply annihilated in order to make room for the new ensembles being injected; continuity is no longer maintained.) It appeared, therefore, that substantial modification of the solution method, and perhaps of the model formulation,

would be required to assure operability of IGN under pulse mode conditions. Since the previous modifications and evaluation of IGN had already exceeded the projected effort for this task, no additional work was undertaken on IGN, and a constant ignition time delay option was provided in subroutine TCØMB. The development of IGN, whose use is not recommended, is described and discussed in Appendix III.

The constant ignition delay time, τ_{ign}, is an input data parameter. Its use, which is recommended, is moderately complicated and proceeds as follows (in subroutine GASGEN). A logical variable, CØMB, is initialized as being "false," meaning that there is not yet combustion. While CØMB is false, a set of combustion criteria are examined at each time step to see if it should be made "true," i.e., ignition has occurred and combustion is to proceed. The first criterion is that ensembles of both propellants had to have been impinging a time τ_{ign} earlier. Two other criteria must be satisfied over that entire ignition time-delay period, viz., the chamber pressure must exceed the ambient pressure by 0.002 psi or more, and the gas mixture ratio must be such that, were the gases burned, the combustion gas temperature would exceed 650 R. Failure to satisfy either of these latter criteria, during the post-impingement ignition time-delay period, causes all knowledge about earlier propellant impingement to be "forgotten," and the whole ignition problem is reinitiated, beginning with the propellant ensembles then being injected. The pressure and gas temperature criteria are not checked while waiting for impingement to occur.

This degree of complexity was introduced so that the same logic could be used to compute reignition if gas temperature or pressure fell low enough so that combustion could not be sustained, e.g., during oscillatory combustion or during the decay transient period.

Spray Ensemble Generation and Gasification Model (GASGEN)

Transient combustion is assumed to be rate-limited by spray vaporization (gasification), and it is simulated analytically with a spray ensemble gasification model, subroutine GASGEN. Two spray ensembles, one fuel and the other oxidizer, are

generated directly from the feed system outputs during each time step that propellants are injected. A propellant weight flowrate injected in a given Δt is stored in the computer as a value in each of two different variable arrays: ensemble initial weight, and ensemble current weight. Values in that second array are diminished, during succeeding time steps, to account for the gasification of the ensemble. The fraction of an ensemble original weight remaining after a given chamber residence time is determined from the spray depletion function of that propellant generated in the PMSTC steady-state combustion analysis. Depletion is begun only after passage of an ensemble impingement delay time. The absolute time of ensemble impingement is defined as its injection time plus its injection-to-impingement travel time, traveling at its initial injection velocity. When the fraction remaining of an ensemble original weight drops below the steady-state vaporization inefficiency for that propellant, the ensemble is simply annihilated (as if it had passed through the nozzle throat) without contributing further to performance.

Calculation of spray gasification is thus seen to require three parameters for each ensemble: initial spray weight, current spray weight, and impingement time. Total gas generation for a propellant in a given time step is obtained by calculating and summing the spray weight reductions for all ensembles of that propellant currently residing in the chamber. Fuel and oxidizer gasifications are computed separately.

The ensemble model requires considerable computer core storage to maintain information on ensembles generated at a rate of two (one fuel and one oxidizer) for each computational time step. A total of six parameters per time step must be saved. Therefore, a dynamics storage allocation system was developed to efficiently reuse storage locations of ensembles which have been fully depleted. This allocation procedure progressively reuses storage space occupied by the oldest ensembles. However, with this procedure it is possible for the arrays to become saturated if the ensemble residence time (including impingement travel time) exceeds 500 times the computational time increment. If this situation occurs, a warning message (diagnostic) is written out, and the ensemble is vaporized to accommodate a new ensemble. To help prevent saturation of the storage space, a lower limit is placed on injection velocity to prevent excessive impingement delay times.

A block flow chart of the GASGEN computer model is shown in Fig. 25. This subprogram is called from the transient combustion model TCØMB, at each time step except during any time period that the ignition model, IGN, is invoked. In addition to performing the functions already stated, the GASGEN computer model contains instructions for initializing parameters and indicators for several types of starting conditions: first time step of computer run, first time step of pulse sequence, and first time step following ignition analysis with IGN. It also contains the logic for determining ignition with a constant time delay, which was discussed in an earlier section.

Combustion Chamber Analysis (TCØMB)

The combustion chamber resembles an accumulator with combustion gases being supplied by the ensemble gasification model and being exhausted through the nozzle throat. The chamber is considered as a lumped volume with unspecified spatial dimensions. Combustion gases residing in the chamber at any instant are assumed to be homogeneous, and gas properties are evaluated at the instantaneous bulk mixture ratio. Volume of liquid propellant within the chamber is neglected.

In the steady-state analysis, three chamber pressures are calculated for use in the transient analysis:

1. The static injector end pressure, P_{IE}
2. The mean stagnation pressure at the nozzle throat plane, P_{NS}
3. The bulk chamber pressure, $\bar{P}_c$, calculated by:

$$\bar{P}_c = \frac{W_g}{V_c} \frac{RT}{M_w} \tag{57}$$

The steady-state ratios of $(P_{NS}/\bar{P}_c)$ and (P_{IE}/P_{NS}) are assumed to hold constant during transient combustion.

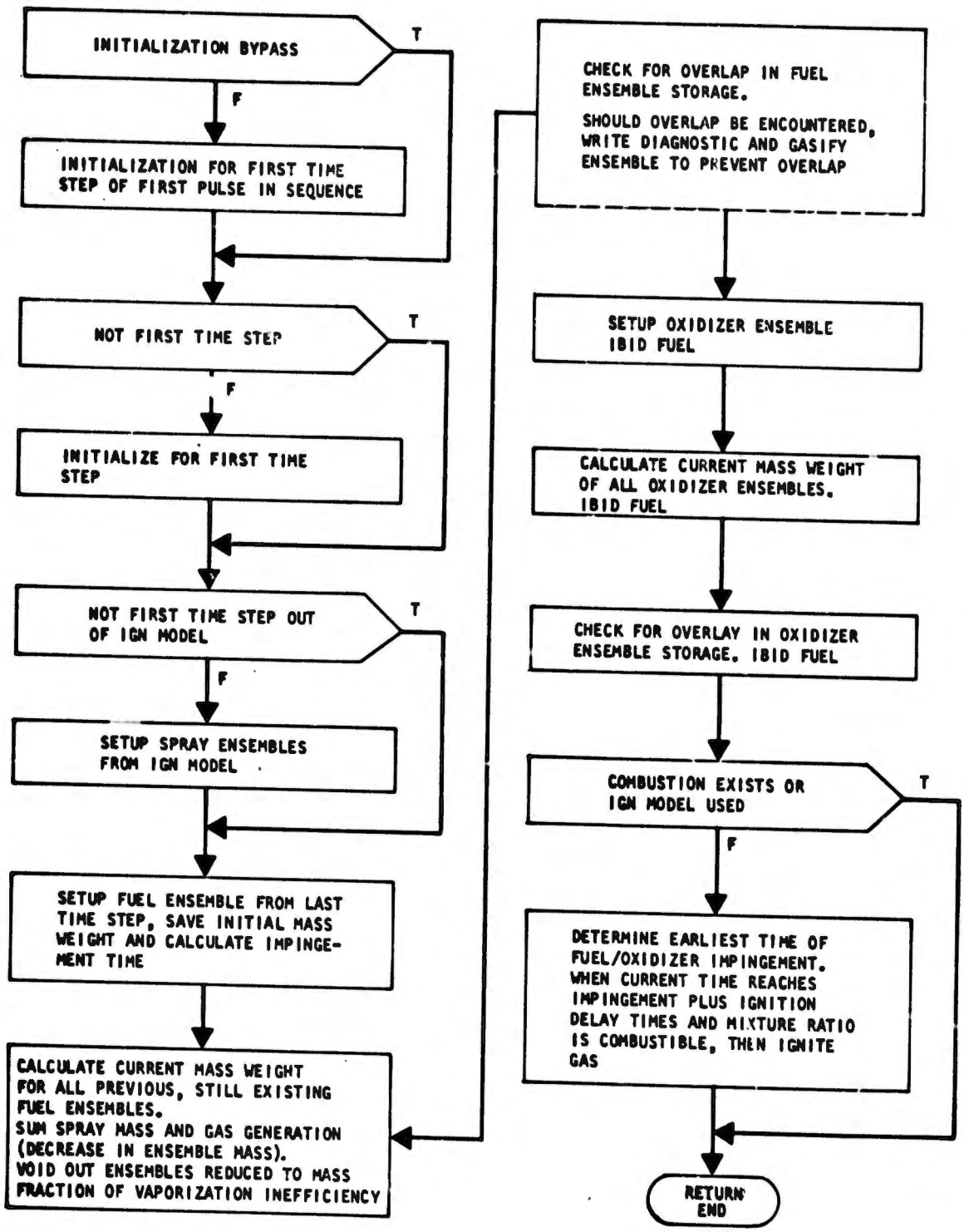

Figure 25. Simplified Flow Chart for GASGEN Subroutine

The gas generation and exhaust rate are calculated with the following equations:

$$\dot{w}_{gen} = \frac{1}{\Delta t} \sum_{ens} w_{ens}(t_1) - w_{ens}(t_2) \tag{58}$$

$$\dot{w}_{exh} = \frac{P_{NS} A_t g_c}{\eta_{c^*_1} c^*} \tag{59}$$

The factor $\eta_{c^*_1}$ is the product of the c* mixing efficiency, compliment of heat loss (or energy) factor, and the ratio of theoretical c* at throat gas mixture ratio to that at the injected mixture ratio, i.e., all steady-state combustion chamber efficiencies except the fuel and oxidizer vaporization efficiencies. Vaporization efficiencies are directly accounted for in the ensemble gasification model.

The time-varying gas mass accumulation in the combustion chamber is obtained by integrating the mass flowrate entering by means of gasification and the mass flowrate exhausted through the nozzle throat. The instantaneous value of accumulated chamber gas, W(t), and equilibrium gas properties evaluated at the bulk mixture ratio are used in determining the time-varying bulk chamber pressure

$$\bar{P}_c(t) = \frac{W(t)}{V_c} \frac{T}{M_w}(t) R \tag{60}$$

Gas flowrate through the nozzle throat, w_{exh}, may be either subsonic or supersonic depending on the ambient-to-nozzle stagnation pressure ratio. The pressure ratio dividing the two flow regimes is $[2/(\gamma+1)]^{\gamma/(\gamma-1)}$ Under vacuum conditions, only supersonic flow exists because the pressure ratio is always zero. Under non-vacuum conditions, the extent of subsonic flow is generally very brief and its effect on overall pulse performance is very small. Therefore, the pressure ratio criteria and subsonic flow equation have been simplified in the computer program by assuming a constant gas γ of 1.3. This establishes the pressure ratio criteria at 0.547. For pressure ratios greater than 0.547, subsonic flowrate is calculated by

$$\dot{w}_{exh} = A_t P_{NS} \frac{2\gamma M_w g_c}{(\gamma-1) RT} \left\{ \left[R_p^{2/\gamma} - R_p^{(\gamma-1)/\gamma} \right] \right\}^{1/2} \tag{61}$$

where R_p is the ambient-to-nozzle stagnation pressure ratio. The computer coding of this equation assumes $\gamma = 1.3$.

Supersonic flow is calculated by the c* equation:

$$\dot{w}_{exh} = A_t \, P_{NS} \, g_c/c^* \tag{62}$$

The nozzle thrust coefficient, C_F, also has subsonic and supersonic regimes. For subsonic flow, the equation

$$C_F = \left\{ \frac{2\gamma^2}{\gamma-1} \left(\frac{2}{\gamma+1}\right)^{\left(\frac{\gamma+1}{\gamma-1}\right)} \left[1 - R_p^{\left(\frac{\gamma-1}{\gamma}\right)} \right] \right\}^{1/2} \tag{63}$$

has been coded using $\gamma = 1.3$.

Supersonic C_F calculation is complicated by the possibility of nozzle flow separation upstream of the exit. The ambient-to-nozzle wall exit pressure ratio, (P_{amb}/P_{exit}), is used as an indicator to test for separation. Nozzle stagnation-to-nozzle exit wall pressure ratios, (P_{NS}/P_{exit}) have been calculated (assuming $\gamma = 1.3$) and tabulated in the computer model over a wide range of nozzle expansion area ratios, ε. Interpolation in this table is used to obtain the pressure ratio for the specific nozzle ε. Then the pressure ratio for separation criterion is calculated.

$$(P_{amb}/P_{exit}) = (P_{NS}/P_{exit}) \times (P_{amb}/P_{NS}) \tag{64}$$

Flow separation is assumed to occur if $(P_{amb}/P_{exit}) > 3$; and C_F is calculated

$$C_F = \eta_{C_F} \left\{ \frac{2\gamma^2}{\gamma-1} \left(\frac{2}{\gamma+1}\right)^{\frac{\gamma+1}{\gamma-1}} \left[1 - (P_w/P_{NS})^{\frac{\gamma-1}{\gamma}} \right] \right\}^{1/2} + (P_w/P_{NS}) \, \varepsilon_s - \left(\frac{P_{amb}}{P_{NS}}\right) \varepsilon_s \tag{65}$$

Where $(P_w/P_{NS}) = P_{amb}/(3 \, P_{NS})$, η_{C_F} is the vacuum C_F efficiency and ε_s is obtained by interpolating from the built-in tables of (P_{NS}/P_{exit}) and ε.

For the more general case, (P_{amb}/P_{exit}) is less than 3, and no wall separation occurs. Then

$$C_F = \eta_{C_F} C_{F,th}(MR_g, \epsilon) - P_{amb}\, \epsilon / P_{NS} \tag{66}$$

where $C_{F,th}(MR_g, \epsilon)$ is the theoretical vacuum C_F evaluated from input tables at the gas mixture ratio and nozzle ϵ.

Finally, instantaneous thrust, F, is calculated using the following equation:

$$F = A_t\, P_{NS}\, C_F \tag{67}$$

PARAMETRIC PULSE PERFORMANCE

Pulses are simulated with the transient performance model under various operating conditions in order to set up parametric tables which are sufficiently broad to permit determining, by interpolation on operating parameters, the performance of a specific pulse without the need for detailed combustion analysis. The pulse characterization model, PULSE, is the control program for performing the parametric analysis and setting up the parametric tables.

Pulse Subdivision

The standard width pulse simulated in TCOMB is subdivided into two periods (Fig.26): start transient, and decay transient. In a sequence of pulses, the start transient begins with an electrical "on" signal to the propellant valves and ends as soon as either valve begins to close. Then the decay transient commences and continues until the "on" signal for the next pulse. This subdivision is applied to the thrust transient to characterize start and decay total impulses separately. Flow consumption of a propellant attributed to a pulse is assumed to be the integrated flowrate through the valve during that pulse, and it is not adjusted for residual propellant in the feed system before or after the pulse. All propellant flows through the valves are attributed to the start transient period.

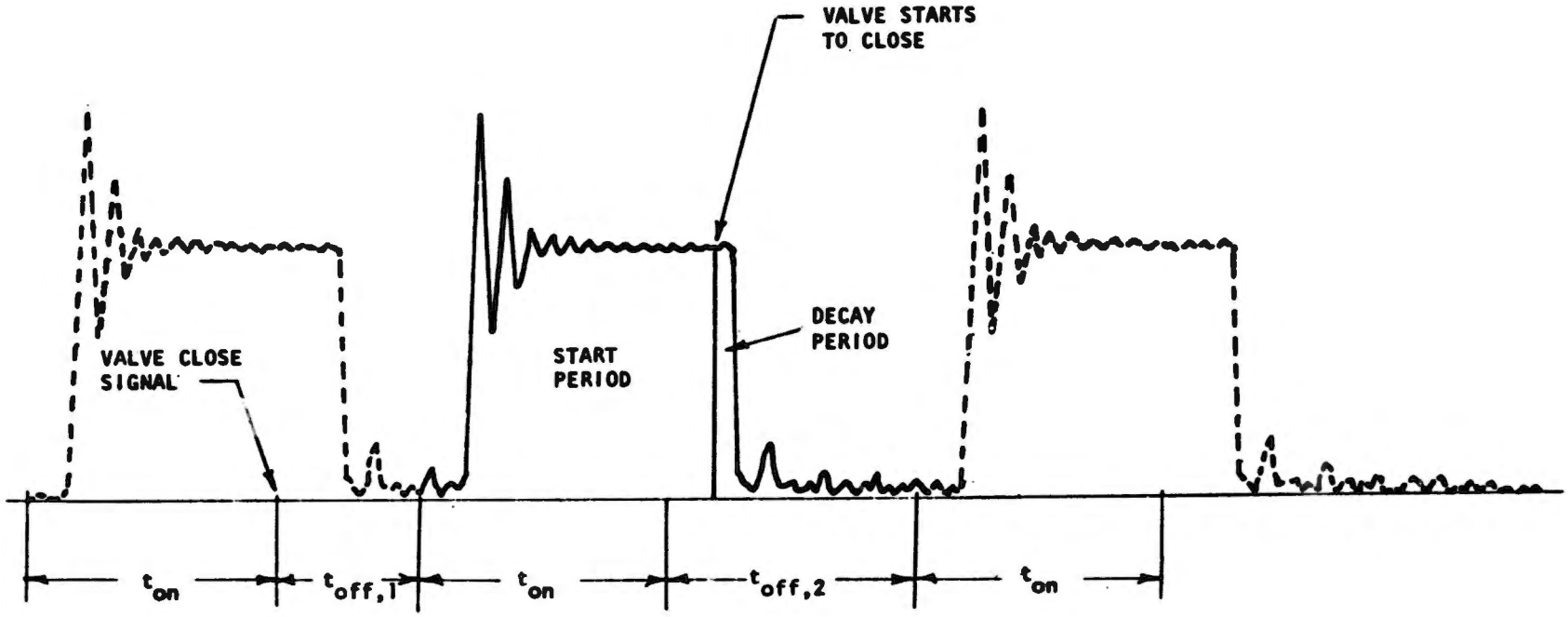

Figure 26. Standard Width Pulse Time Periods

The start and decay transient subdivision is used in determining overall pulse performance, such as pulse total impulse and mean pulse specific impulse. Other pulse characteristic parameters are needed, which require further subdivision of the standard width pulse. Included are parameters such as response times for pressure rise and decay, and total impulse for pressure rise, decay, and tailoff.

In order to determine the required pulse characteristics, the pulse is subdivided into seven periods in TCØMB as listed on Fig. 21. Each period begins when its preceding period ends and continues until a specific event occurs. Period 0 is the time interval from the electrical "on" signal until either valve starts to open; then, program control returns to subprogram PULSE. The next period, period 1, begins when TCØMB is reentered following the ignition analysis by IGN or immediately if IGN is by passed. Period 1 ends when 10 percent of steady-state chamber pressure is attained, and period 2 ends when 90 percent is attained. Period 3 runs until the electrical "off" signal occurs. Period 4 ends coincident with the end of the start transient at the time either valve begins to close. A decay in pressure to 10 percent of steady-state pressure marks the end of period 5. Period 6 runs to the end of the pulse or to the "on" signal for the next pulse.

Predominant Operating Parameters

Although many operating parameters affect pulse performance variations, only the ones which affect the start and decay transient are considered here. The start transient performance and repeatability are primarily affected by residual feed system propellants, valve opening rates and lags, and the chamber gas condition. Decay transient performance is influenced mainly through the boiloff of residual feed system propellants, and boil-off rate is dependent on heat soakback rate from the chamber wall to the feed system. The primary operating parameter on both start and decay transients is considered to be the "off" time, or spacing, between pulses. A typical sequence of pulses with "off" time as a parameter (τ_n) is shown in Fig. 18. The range of "off" times should extend from the shortest spacing anticipated in the duty cycle up to a spacing sufficient for all the propellant in the feed system to boil off. A sufficient number of "off" times should be included to permit reasonable accuracy for interpolating between values.

The second most important parameter was considered to be the chamber wall bulk temperature, through its effect on heat soakback to the residual propellants in the feed systems. Therefore, multiple pulse sequences, or trains, of pulses having identical, standard pulse on-times and systematically varied pulse off-times (like that illustrated in Fig. 18) are simulated at different wall temperatures.

Parametric Tables

The standard width pulse is divided into a start period and a decay period with the beginning of valve closure as the dividing time. Performance parameters are computed in TCØMB for both of these pulse periods plus several response characteristics. These are tabulated in PULSE as functions of off-time either preceding ($t_{off,1}$) or following ($t_{off,2}$) a pulse (see Fig. 25A) and of chamber wall temperature (T_w). These parameters for standard width pulses, along with their independent variables, are listed below:

Performance Parameter	Independent Variables	
1. Fuel flow	$t_{off,1}$	T_w
2. Oxidizer flow	$t_{off,1}$	
3. Total impulse during start period	$t_{off,1}$	
4. Total impulse during decay period	$t_{off,2}$	
5. Rise time, on to 90% P_c	$t_{off,1}$	
6. Rise total impulse	$t_{off,1}$	
7. Rise time, 10 to 90% P_c	$t_{off,1}$	
8. Drop time, off to 10% P_c	$t_{off,2}$	
9. Drop total impulse	$t_{off,2}$	
10. Pressure overshoot	$t_{off,1}$	
11. Tail-off total impulse*	$t_{off,2}$	
12. Integral of P_c for start period	$t_{off,1}$	
13. Integral of P_c for decay period	$t_{off,2}$	

A typical pulse performance summary page printed by PULSE is shown in Table I. Operational and steady-state parameters occupy about the upper two-thirds of the pulse summary page and the pulse performance parameters are found below. By comparing the foregoing list of parameters with Table I, all except items 4, 12, and 13 may be seen to occur in the printout.

*Integrating from the time that chamber pressure has fallen to 10% of steady-state P_c until the on-time of the next pulse.

TABLE I. TYPICAL PULSE PRINTOUT OF PERFORMANCE DATA FOR A STANDARD-WIDTH PULSE

PULSE PERFORMANCE
STANDARD PULSE SEQUENCE

TIME AT CN-SIGNAL	MSEC	0.0	FUEL INLET PRESSURE	PSIA	197.80
DURATION (ON-SIG TO OFF-SIG)	MSEC	40.0	OXID INLET PRESSURE	PSIA	195.65
			FUEL INLET TEMPERATURE	R	530.0
STEADY-STATE			OXID INLET TEMPERATURE	R	530.0
CHAMBER PRESSURE	PSIA	9.1655E 01	THROAT AREA	SQ IN	1.3461E-01
THRUST	LBF	2.1836E 01	NOZZLE EXIT AREA	SQ IN	5.3952E 00
C-STAR	FT/SEC	5124.5	NOZZLE EXIT PRESSURE	PSIA	0.0
EFFICIENCY	PCT	89.92	OFF-PERIOD PRECEDING PULSE	MSEC	0.0
THRUST COEFFICIENT		1.7692	OFF-PERIOD FOLLOWING PULSE	MSEC	15.0
EFFICIENCY	PCT	94.33	CHAMBER WALL TEMP AT OFF-SIGNAL (RCII-OFF PARAMETER)	R	630.0
SPECIFIC IMPULSE	LBF-SEC/LBM	281.78			
EFFICIENCY	PCT	84.92			
FUEL VALVE			OXID VALVE		
APPLIED VOLTAGE	VOLTS	25.05	APPLIED VOLTAGE	VOLTS	25.05
COIL ENERGIZE TIME	MSEC	7.285	COIL ENERGIZE TIME	MSEC	7.580
LEAD (OR LAG) TIME	MSEC	0.295	LEAD (OR LAG) TIME	MSEC	-0.295
OPENING TRAVEL TIME	MSEC	1.000	OPENING TRAVEL TIME	MSEC	1.000
CN-SIGNAL TO FULL OPEN	MSEC	8.285	CN-SIGNAL TO FULL OPEN	MSEC	8.580
COIL DE-ENERGIZE TIME	MSEC	4.009	COIL DE-ENERGIZE TIME	MSEC	3.997
CLOSING TRAVEL TIME	MSEC	1.000	CLOSING TRAVEL TIME	MSEC	1.000
TOTAL FUEL FLOW	LBM	1.3222E-03	TOTAL OXID FLOW	LBM	2.1624E-03
TRANSIENT CHARACTERISTICS			OVERALL PERFORMANCE		
RISE (CN-SIG TO 90 PCT) TIME	MSEC	11.712	TOTAL IMPULSE	LBF-SEC	7.3944E-01
RISE TOTAL IMPULSE	LBF-SEC	4.9462E-03	TOTAL PROPELLANT FLOW	LBM	3.4851E-03
RISE (10 TO 90 PCT) TIME	MSEC	0.491	MEAN MIXTURE RATIO (O/F)		1.636
DROP (OFF-SIG TO 10 PCT) TIME	MSEC	9.200	MEAN SPECIFIC IMPULSE	LBF-SEC/LBM	226.53
DROP TOTAL IMPULSE	LBF-SEC	1.5264E-01	SPECIFIC IMPULSE EFFICIENCY	PCT	68.195
PRESSURE OVERSHOOT	PCT	40.143	PULSING TO S-S EFFICIENCY	PCT	80.349
TAIL-OFF TOTAL IMPULSE	LBF-SEC	5.7866E-03	MEAN C-STAR	FT/SEC	4146.5
			MEAN CHAMBER WALL TEMP	R	360.0

In the sequence of pulses simulated in TCØMB, the off-time preceding each pulse is different from the off-time following it. In addition to the parameters listed above, pulses are essentially restructured in PULSE to provide pulse performance data as if pulses were spaced with equal off-times preceding and following each one. This is accomplished by combining the start transient period of a standard pulse in the foregoing analysis with the decay period of its immediately preceding pulse. Referring to Fig. 18, this process denotes a series of time periods denoted as "Pulse 1," "Pulse 2," etc. The idea is to tabulate performance parameters for a sequence of equally-spaced pulses, e.g., a sequence of "Pulse 2" pulses as shown below:

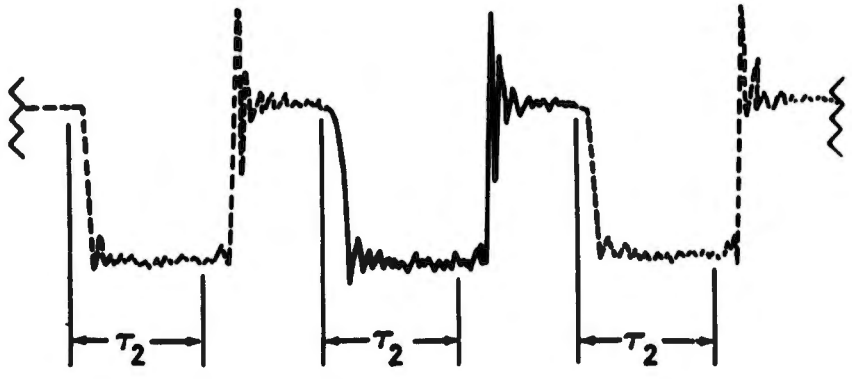

As also indicated on Fig. 18, the start period of the first standard pulse in a sequence is combined with the decay period of the last standard pulse to form the longest spacing for equally-spaced pulses tabulated by PULSE; it is assumed to be long enough that its use for all longer pulse spacings will be valid. Since the first standard pulse had complete vacuum start conditions, any residual propellants left after the decay period of the last standard pulse is deducted from the propellant consumption of the first pulse in structuring the maximum-spacing, equally spaced performance.

Tables are constructed and printed out of pulse total impulse, mean specific impulse, mean mixture ratio, and fuel and oxidizer flows for these equally spaced pulses as functions of pulse spacing (equal off-time before and after pulse) and chamber wall temperature.

Computer-plotted CRT graphs of chamber pressure, thrust, fuel and oxidizer flowrates, and a mixture ratio function are generated for the entire combined start and decay periods of each of the standard pulses analyzed by PULSE. Plots for one pulse, i.e., the second one in a sequence, are reproduced in Fig. 27. Note that all parameters are normalized to their steady-state values.

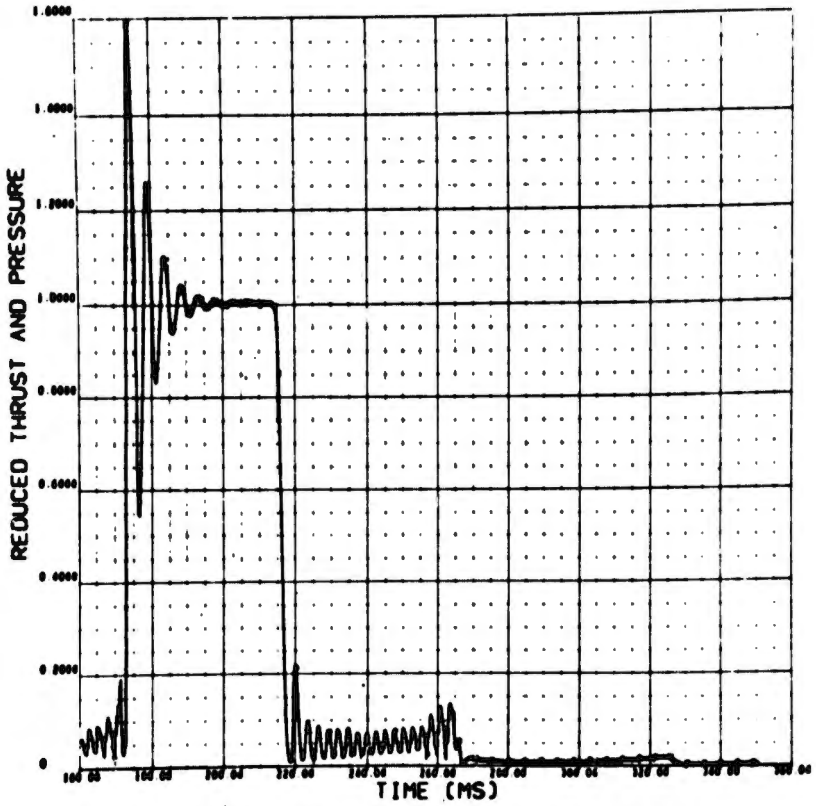

(a) Thrust and Chamber Pressure

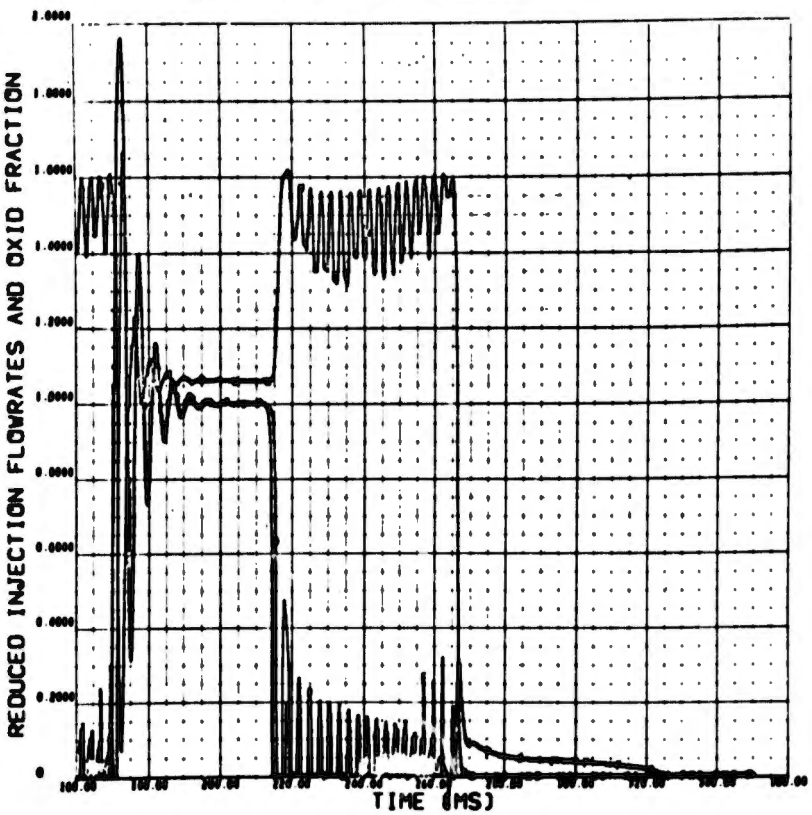

(b) Propellant Flowrates and Oxidizer Fractions

Figure 27. Example of Computer-Plotted Standard-Width Pulse Data (Normalized to Steady State)

DUTY CYCLE MODEL (DCYCLE)

A pulse-mode duty cycle (or mission) is analyzed in subprogram DCYCLE by synthesizing performance of individual pulses from the tables of transient performance set up in PULSE and the steady-state performance generated in PMDER. The bulk of the duty cycle analysis is performed in subroutine SYNTHE, with DCYCLE functioning essentially as a control program. A simplified flow chart of DCYCLE is shown in Fig. 28.

DUTY CYCLE SPECIFICATION

The duty cycle is prescribed by the program user by specifying an electrical on-time of each pulse along with the off-time between it and the next pulse. Pulses are specified sequentially in time, and a repetition of the same on/off time pattern may be specified. Parameters used for synthesizing pulse performance are: (1) electrical on-time, (2) electrical off-time preceding a pulse, (3) electrical off-time following a pulse, and (4) mean chamber wall temperature. The latter parameter is calculated from pulse to pulse, starting at the ambient temperature and heating and cooling at user prescribed exponential rates during pulse on and off times, respectively.

CHAMBER WALL TEMPERATURE

Values of chamber wall temperature during duty cycle operation are approximated to modify performance in order to account for variations in (1) the rate of heat soakback to the propellant feed system during boiloff and (2) energy loss caused by heat transfer from the combustion gases to the chamber wall. Wall temperature is assumed to rise exponentially during pulse on-time and decay exponentially during pulse off-time. The following equations are used:

Heating

$$T_w\,(t_1 + \Delta t) = T_w(t_1) + \left[T_{w,ss} - T_w(t_1)\right]\left(1-e^{-\lambda_h \Delta t}\right) \qquad (68)$$

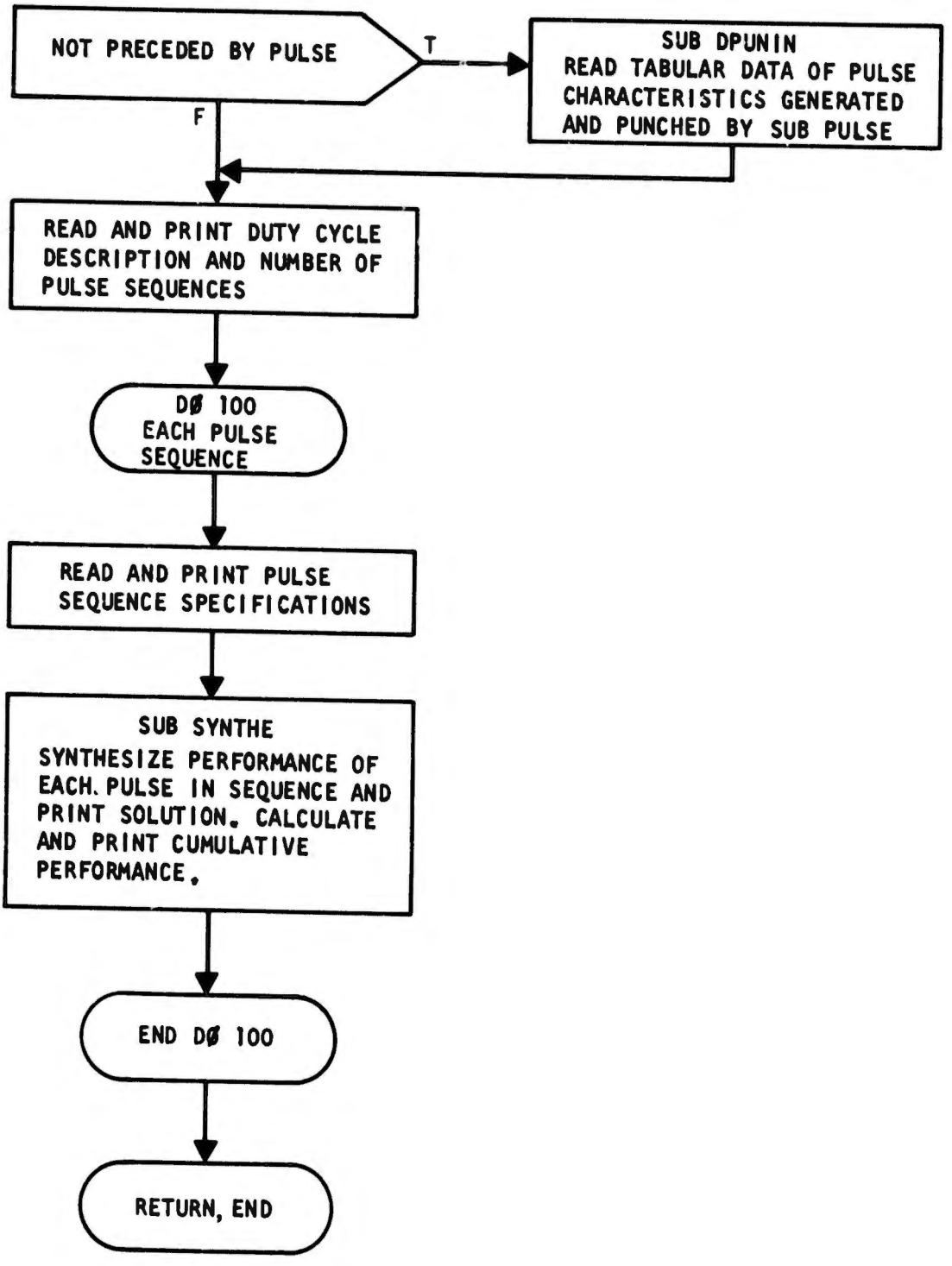

Figure 28. Simplified Flow Chart of DCYCLE

Cooling

$$T_w(t_1 + \Delta t) = T_w(t_1) - \left[T_w(t_1) - T_{w,o}\right]\left(1-e^{-\lambda_c \Delta t}\right) \qquad (69)$$

where

$T_{w,ss}$ and $T_{w,o}$ are the steady-state and ambient wall temperatures, respectively, and λ_h and λ_c are the heating and cooling exponential constants, respectively.

The exponential coefficients, λ_h and λ_c, must be determined either from test data or with a heat transfer analysis and supplied to the program as input data.

The means by which the heat soakback rate is accounted for is through wall temperature as an independent variable in parametric tables of transient performance generated in PULSE. The heat soakback rate affects the feed system boil-off phenomenon which is an integral part of the pulse decay transient.

THRUST CORRELATING FACTOR

An adjustment factor, η_T, is calculated and applied to pulse total impulse in the duty cycle analysis. It is a function of the time-varying chamber wall temperature, T_w, and an input specified thrust correlation coefficient, C_T. This coefficient was adjusted in the evaluation runs to a value specific to each engine to obtain agreement between predicted and experimental pulse efficiency as a function of off-time between pulses. The adjustment factor is calculated as follows*:

$$\eta_T = \left[\frac{1}{C_1(1+C_2)} + \frac{C_2\, T_w}{C_1\, T_g\, (1+C_2)}\right]^{1/2}$$

where

$$C_1 = (\eta_{ENR}\, C_T)^2$$

and

$$C_2 = \frac{1 - C_1^{\,2}}{C_1^{\,2} - \frac{T_{w,ss}}{T_g}}$$

*During the final writing of this report, the derivation of this expression was found to be in error. If the expression were to be changed to the intended relationships, correlation of pulse efficiency variation with off-time could probably be improved.

PULSE SYNTHESIS (SYNTHE)

Pulse synthesis is performed in subroutine SYNTHE. Because pulses are frequently fired in sequencesof equally spaced, constant width pulses, duty cycle input specifications were set up to accept data in this manner to minimize input. Each pulse sequence specification requires the number of pulses, pulse width, off-time between pulses, and off-time following the last pulse. The off-time preceding the first pulse is set equal to the off-time following the preceding sequence, or equal to the longest pulse in the table for the first sequence in the duty cycle. Pulses may be specified individually by setting the number of pulses equal to 1.

Subroutine SYNTHE performs the duty cycle analysis by repetitive-pulse sequences for efficiency of computation. Figure 29 shows a simplified flow chart of SYNTHE. Pulses are analyzed sequentially in time. The off-times preceding and following the pulse are determined. The chamber wall temperature at the beginning of the pulse is known from the end of the previous pulse. Chamber wall temperatures at the mid-time of the pulse, off-time, and end of the pulse are calculated. The energy loss correction factor is then calculated using the wall temperature at the mid-time of the pulse. Start transient performance of the pulse is obtained by double interpolations in the applicable tables with the off-time preceding the pulse and the wall temperature at the on-signal of the pulse as the independent parameters. The shutdown performance of a pulse is obtained by double interpolation in the applicable tables with the off-time following the pulse and the wall temperature at the off-signal of the pulse as the parameters. Steady-state performance is inserted between the start and shutdown periods for a duration equal to the difference in its on-time and the standard on-time used in generating the parametric tables. Figure 30 is a visual representation of the construction of the pulse.

Fuel and oxidizer flows and total impulse for each pulse are accumulated from pulse-to-pulse in SYNTHE. These cumulative values along with the cumulative mean specific impulse and mixture ratio are printed at the end of each pulse analysis. The overall duty cycle performance (or requirements) are in the final cumulative parameters following the last pulse of the duty cycle, exemplified in Table II.

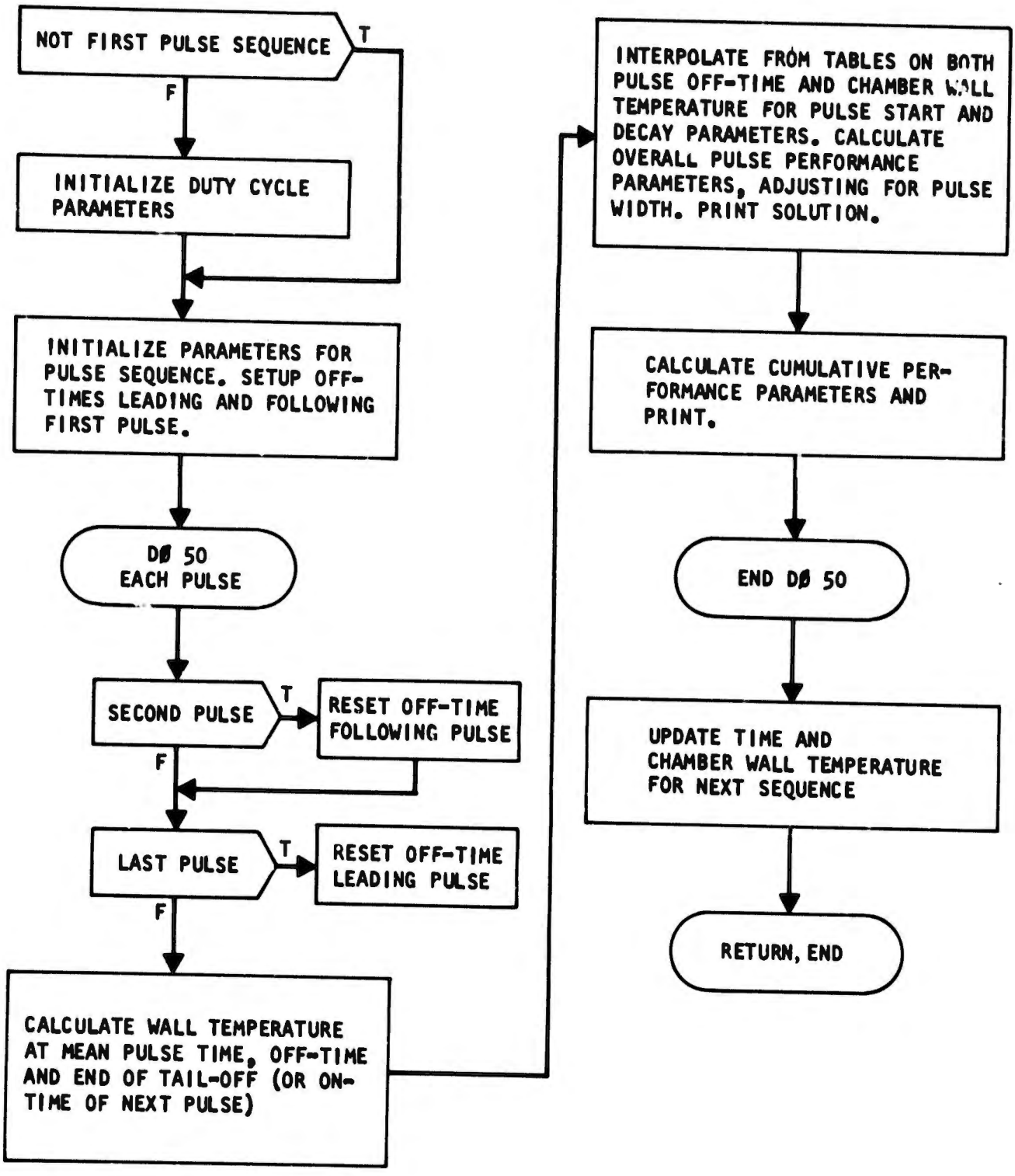

Figure 29. Simplified Flow Chart of SYNTHE

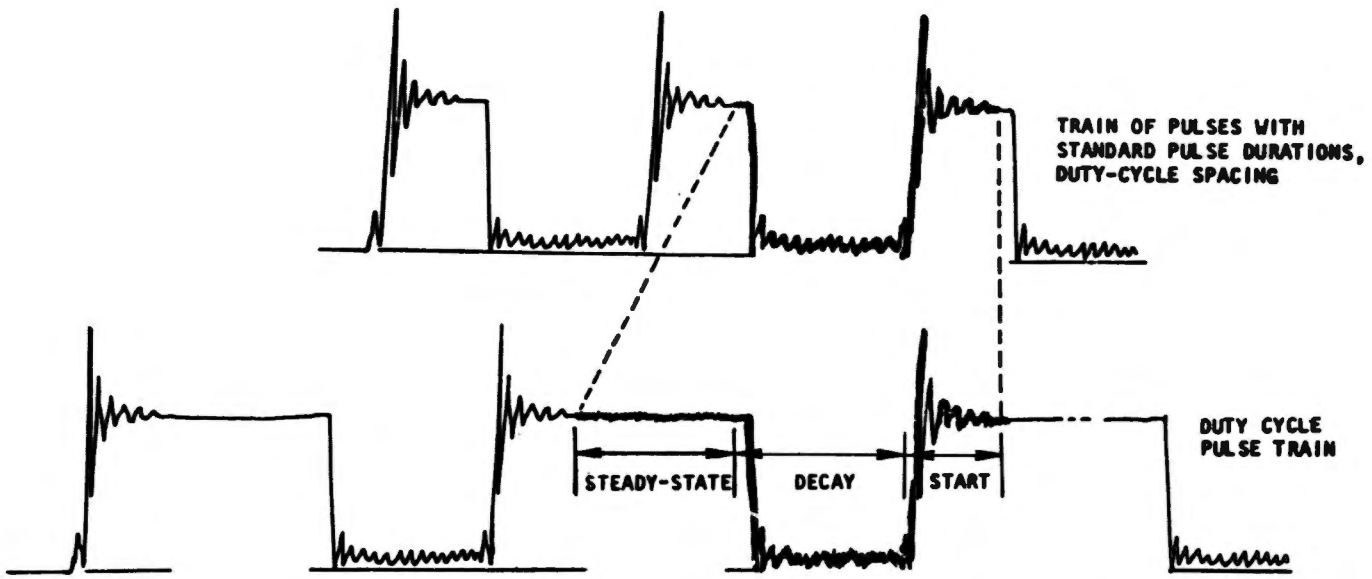

Figure 30. Construction of a Duty Cycle Pulse from Steady-State and Standard-Width Pulse Data

TABLE II. TYPCIAL DCYCLE PRINTOUT FOR A PULSE IN A DUTY CYCLE

PULSE PERFORMANCE
DUTY CYCLE SEQUENCE 1
PULSE NO. 15

TIME AT ON-SIGNAL	MSEC	4650.780	FUEL INLET PRESSURE	PSIA	197.80
DURATION (ON-SIG TO OFF-SIG)	MSEC	16.2	OXID INLET PRESSURE	PSIA	195.90
STEADY-STATE			FUEL INLET TEMPERATURE	R	530.0
CHAMBER PRESSURE	PSIA	9.1690E 01	OXID INLET TEMPERATURE	R	530.0
THRUST	LBF	2.1836E 01	THROAT AREA	SQ IN	1.3461E-01
C-STAR	FT/SEC	5124.5	NOZZLE EXIT AREA	SQ IN	5.3900E 00
EFFICIENCY	PCT	80.92	NOZZLE EXIT PRESSURE	PSIA	0.0
THRUST COEFFICIENT		1.7692	OFF-PERIOD PRECEDING PULSE	MSEC	316.0
EFFICIENCY	PCT	94.33	OFF-PERIOD FOLLOWING PULSE	MSEC	316.0
SPECIFIC IMPULSE	LBF-SEC/LBM	281.78	CHAMBER WALL TEMP AT OFF-SIGNAL (BOIL-OFF PARAMETER)	R	726.
EFFICIENCY	PCT	84.82			

FUEL VALVE			OXID VALVE		
APPLIED VOLTAGE	VOLTS	25.05	APPLIED VOLTAGE	VOLTS	25.05
COIL ENERGIZE TIME	MSEC	7.285	COIL ENERGIZE TIME	MSEC	7.580
LEAD (OR LAG) TIME	MSEC	0.295	LEAD (OR LAG) TIME	MSEC	-0.295
OPENING TRAVEL TIME	MSEC	1.000	OPENING TRAVEL TIME	MSEC	1.000
ON-SIGNAL TO FULL OPEN	MSEC	8.285	ON-SIGNAL TO FULL OPEN	MSEC	8.580
COIL DE-ENERGIZE TIME	MSEC	4.005	COIL DE-ENERGIZE TIME	MSEC	3.997
CLOSING TRAVEL TIME	MSEC	1.000	CLOSING TRAVEL TIME	MSEC	1.000
TOTAL FUEL FLOW	LBM	4.1678E-04	TOTAL OXID FLOW	LBM	6.8004E-04

TRANSIENT CHARACTERISTICS			OVERALL PERFORMANCE		
RISE (ON-SIG TO 90 PCT) TIME	MSEC	11.726	TOTAL IMPULSE	LBF-SEC	2.2273E-01
RISE TOTAL IMPULSE	LBF-SEC	1.6440E-03	TOTAL PROPELLANT FLOW	LBM	1.0968E-03
RISE (10 TO 90 PCT) TIME	MSEC	0.596	MEAN MIXTURE RATIO (O/F)		1.632
DROP (OFF-SIG TO 10 PCT) TIME	MSEC	11.557	MEAN SPECIFIC IMPULSE	LBF-SEC/LBM	203.07
DROP TOTAL IMPULSE	LBF-SEC	1.4555E-01	SPECIFIC IMPULSE EFFICIENCY	PCT	61.125
PRESSURE OVERSHOOT	PCT	473.664	PULSING TO S-S EFFICIENCY	PCT	72.066
TAIL-OFF TOTAL IMPULSE	LBF-SEC	1.5676E-02	MEAN C-STAR	FT/SEC	5088.2
			MEAN CHAMBER WALL TEMP	R	719.

CUM PERFORMANCE SUMWF= 6.117E-03 SUMDC= 1.001E-02 SUMTI= 3.262E 00 SIMEAN= 2.023E 02 XMRMN= 1.636E 00

MODEL EVALUATION

EVALUATION PROCEDURE

Evaluation of PMPM was accomplished through performance analysis of two rocket engine models. One of these was the Rocketdyne RS1402 and the second was the Marquardt R-1E. Both of these engines are well-suited for pulse-mode operation, although the RS1402 was originally designed for steady-state operation (and thus has larger dribble volume than does the R-1E). Considerable test data were available from each of them, especially the RS1402. The thrust chamber design characteristics of these engines are summarized in Table III.

Operational capability of the computer program, executing with numerous options and over ranges of operating conditions, was tested and demonstrated after some debugging. The computer program has been applied sufficiently to demonstrate its operational status.

A series of calculations was made during which the values of the input parameters were varied to determine their individual effects on predicted performance. This parametric analysis provided the basis for (1) determining which parameters were most critical (had the greatest effect), (2) selecting values for input variables which are not well known, and (3) guiding the subsequent adjustment of input variables to improve the agreement between predicted and measured test results.

EFFECTS OF VARYING CRITICAL INPUT PARAMETERS

SPRAY SPREADING DISTANCE

In the LISP model of PMDER, propellant spray distributions, mean drop sizes, and initial vaporization are calculated. Fuel and oxidizer sprays are each assumed to spread out from an impingement point in rays until they reach a prescribed chamber cross-section plane, the "collection" plane. Mass and mixture ratio distributions for the spray depend on the choice of this distance, Z_{OM}.

TABLE III. THRUST CHAMBER DESIGN

	RS1402	R-1E
Propellant		
Fuel	MMH	MMH
Oxidizer	NTO	NTO
Feed System Dribble Volume		
Fuel, $in.^3$	0.01633	0.00174
Oxidizer, $in.^3$	0.00851	0.00240
Injector		
Number of Elements	1	1
Element Type	Unlike Doublet	Unlike Doublet
Orifice Diameter		
Fuel, in.	0.0372	0.039
Oxidizer, in.	0.0420	0.046
Orifice Angle With Chamber Axis		
Fuel, degrees	45	45
Oxidizer, degrees	35	45
Free Stream Distance		
Fuel, in.	0.094	0.050
Oxidizer, in.	0.076	0.050
Combustion Chamber and Nozzle		
Chamber Diameter, in.	0.676	0.860
Throat Diameter, in.	0.424	0.414
Chamber Length to Throat, in.	2.10	2.44
Throat Entrance Radius of Curvature, in.	0.318	0.25
Nozzle Expansion Profile	80% Bell	-
Expansion Area Ratio	9 + 22-deg Scarf	40
Method of Wall Cooling	Heat Sink + Radiation	Radiation

Most previous applications of the LISP model have pertained to multiple element injectors, where the amount of mixing between spray fans was the primary consideration which affected the selection of a "collection" plane distance. However, with single element injectors, as used in this evaluation, the shape of the spray mixture ratio distribution is insensitive to distance until the spray flow is constrained by the wall.

It seems reasonable to expect some of the spray to impinge on the wall before sufficient gas is generated to turn the spray paths axially. A range of "collection" plane distances, Z_{OM}, from 0.3 to 0.9 inches were run with LISP; the resultant effects on spray mixing performance efficiency, $\eta_{c^*,mix}$, before any evaporation occurs, are shown in Table IV. Corresponding computer generated contour plots of mass and mixture ratio distributions are shown in Fig.31 and 32.

The overall mixing performance efficiency, $\eta_{c^*,mix}$, is also shown in Table 4. To calculate this parameter ($\eta_{c^*,mix}$), the gas at the collection plane must be combined with the sprays. Gas mixture ratio distribution calculated in PMSTC differs from the spray mixture ratio distributions and, therefore, because the gas generation varies with distance, the overall propellant mixing performance efficiency varies with distance even when the spray pattern is not constrained by the wall.

A "collection" plane distance, Z_{OM}, of 0.5 inches was selected for both the RS1402 and R-1E evaluation cases. Several factors were considered in making this selection: (1) only a moderate amount of spray was constrained by the chamber wall (the contour plots, Fig. 31 and 32, show that only the third out of 14 or 15 contours reached the outer radial mesh zone); (2) the difference between spray and overall propellant mixing performance efficiencies was small or insignificant; (3) the percentage of propellant vaporized at the beginning of the streamtubes is within the 5 to 15 percent range which has been used during most previous applications for correlating predicted performance with test data.

TABLE IV. CALCULATED VARIATION OF PROPELLANT MIXING PERFORMANCE EFFICIENCY WITH "COLLECTION" PLANE DISTANCE

Z_{OM}, inches	Unevaporated Spray $\eta_{c^*_{mix}}$	η_{vap} at Z_{OM}	Resultant $\eta_{c^*_{mix}}$
RS1402			
0.3	0.9741	0.0547	0.9722
0.5	0.9743	0.0944	0.9748
0.7	0.9762	0.1323	0.9828
0.9	0.9796	0.1678	0.9856
R-1E Thrustor			
0.4	0.9327	0.0589	0.9333
0.5	0.9370	0.0738	0.9406
0.7	0.9547	0.1013	0.9659
0.9	0.9668	0.1271	-

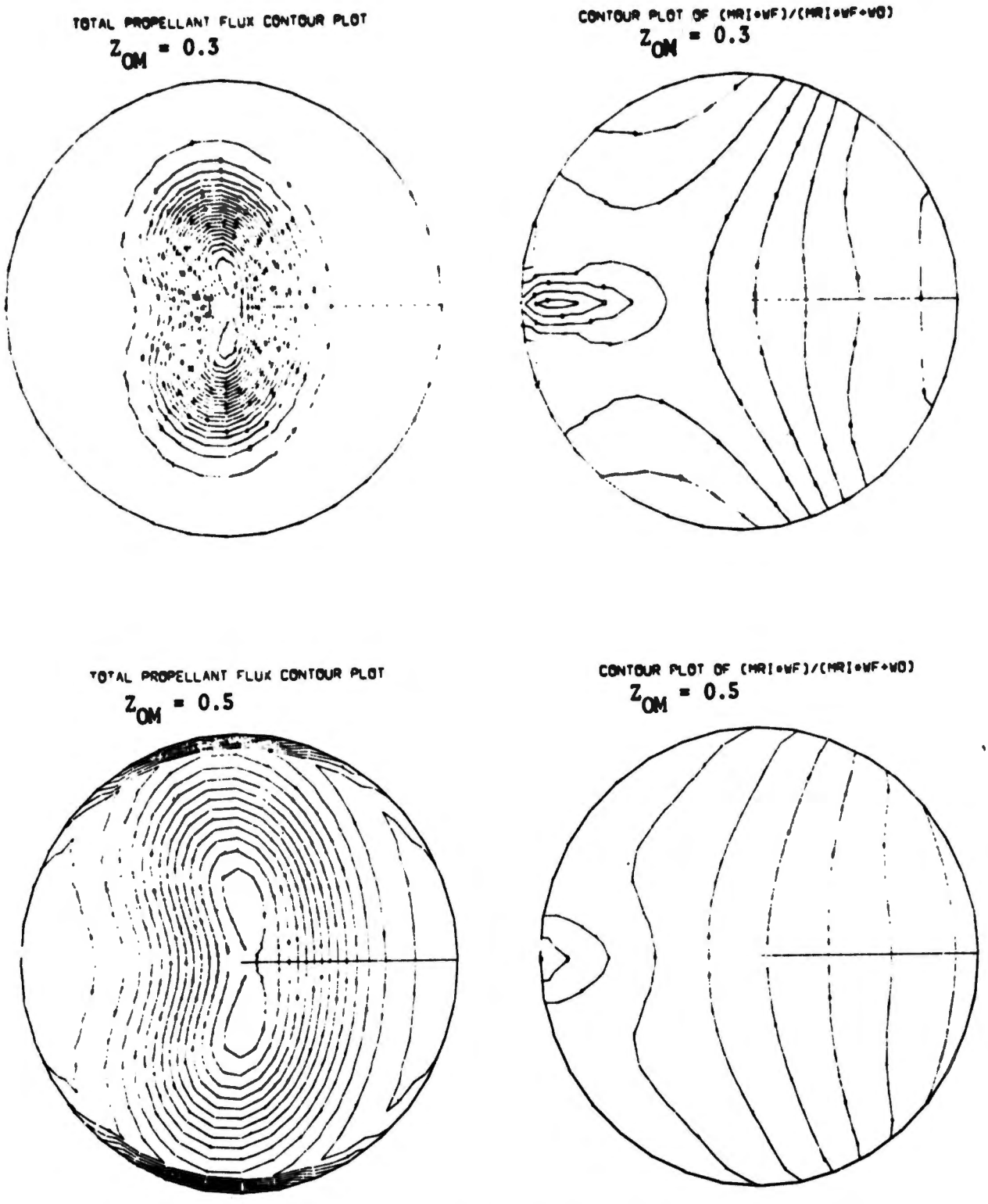

Figure 31. Propellant Spray Mass Flux and Mixing Contour Plots Generated by LISP Model for RS1402

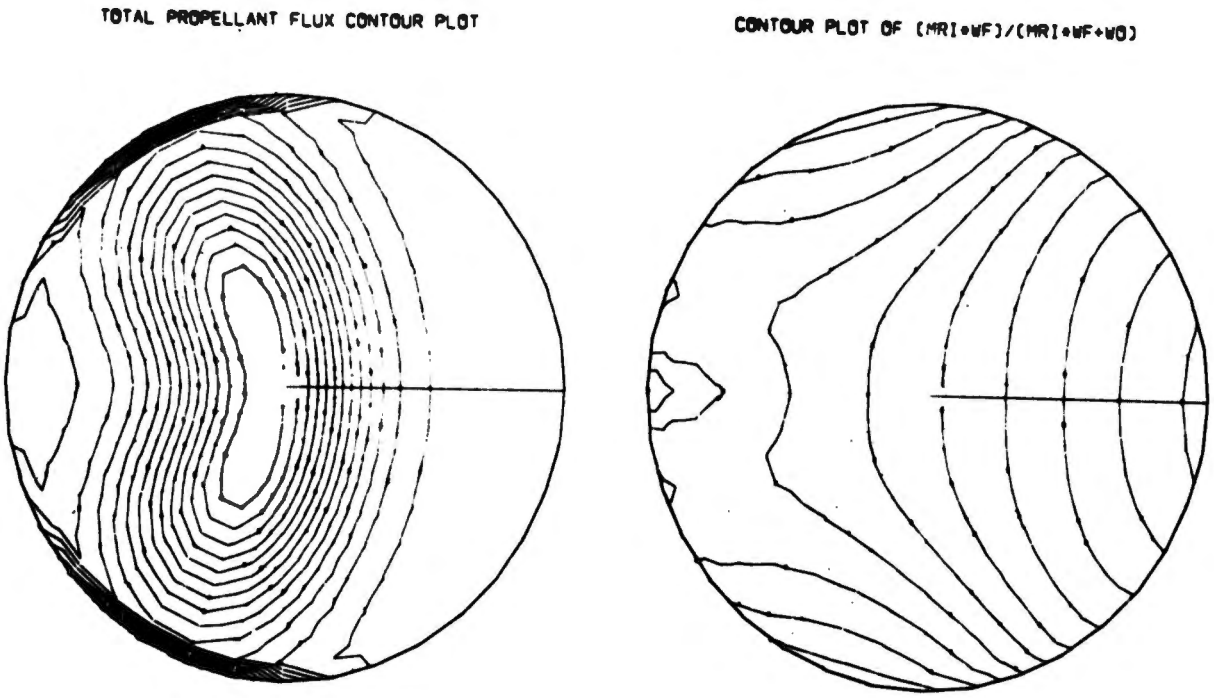

Figure 32. Propellant Spray Mass Flux and Mixing Contour Plots Generated by LISP Model for R-1E (Z_{OM} = 0.5)

VAPORIZATION RATES IN THE SPRAY SPREADING REGION

In the spray spreading region, i.e., the region described by LISP, vaporization is not calculated as a function of local gas and spray conditions as is done in the PMSTC model. Instead, mean values of fuel and oxidizer vaporization coefficients, k_f' and k_o', are employed which must be supplied as input information. These mean values were estimated as fractions of those calculated in PMSTC for the start plane. The effect of varying the fraction of the PMSTC values for the RS1402 thrustor is shown below:

Percent PMSTC k_f' and k_o'	$\eta_{c^*_{mix}}$	η_{c^*}
18	0.9763	0.844
30	0.9748	0.863
60	0.9702	0.854

The 30 percent values are recommended and were used in the rest of the evaluation runs.

MEAN SPRAY DROP SIZES

In addition to the spray mass flux distribution calculations, mean spray drop sizes are calculated in LISP using built-in correlations of mean drop sizes measured for the atomization of impinging jets. These correlations are based on measurements of frozen wax drops formed by impinging hot wax (liquid) jets. Unfortunately, even with the latest available correlations, including physical property corrections (which are also included in LISP), a substantial disparity exists between the drop size predicted from the correlations and the drop size required in the combustion model to predict c* efficiencies compatible with measured hot-fire performance. This disparity is especially great in the case of very small rocket engines, such as reaction control thrustors. Therefore, a drop size correlating factor, $C_{\overline{D}}$, is included in the model to allow for this

difference by adjusting the drop sizes obtained from the correlations. This correlating factor must be supplied as input. In spite of this defficiency, the correlations are still very useful to account for variations in momentum ratios, orifice diameter ratios, impingement angles and ratio of fuel to oxidizer drop sizes.

A series of steady-state computer runs was made to obtain values of the mean drop size correlating factor, $C_{\overline{D}}$, which would cause the predicted and measured c* performance values to agree. This was done separately for both the RS1402 and R-1E thrustors; the results are plotted in Fig. 33. The $C_{\overline{D}}$ value for RS1402 is 0.09664, and the $C_{\overline{D}}$ value for R-1E is 0.0886.

IGNITION DELAY TIME

Many computer cases were run for the RS1402 thrustor with the PULSE subprogram to assess the effect of variations in the ignition delay time on predicted pulsing efficiency (i.e., the ratio of mean pulse specific impulse to steady-state specific impulse). Results from some of these calculations are plotted in Fig. 34, where each curve corresponds to cases in which the input data differs only in ignition delay time. Ignition delay time has a substantial effect with short pulses, moderate to long off-times and long ignition delay times. Generally, however, ignition delay times are expected to be about 0.5 millisecond or less, in which case the predicted performance is only slightly dependent upon the delay time value.

HEAT SOAKBACK RATES TO FEED SYSTEM

Input data to the boiloff model includes the steady-state heat soakback rates to the fuel and oxidizer contained in the feed system dribble volumes. These rates, along with the time interval for boiloff (i.e., the off-time between pulses), substantially control the amounts of dribble-volume propellants which are expelled between pulses. To investigate this effect, a series of PULSE computer runs were executed for various heat soakback rates. The results are shown in Fig. 35 and 36: each curve corresponds to a different set (pair) of heat soakback rates. As shown, substantial changes in pulsing efficiency can be obtained by the selection of heat soakback rates.

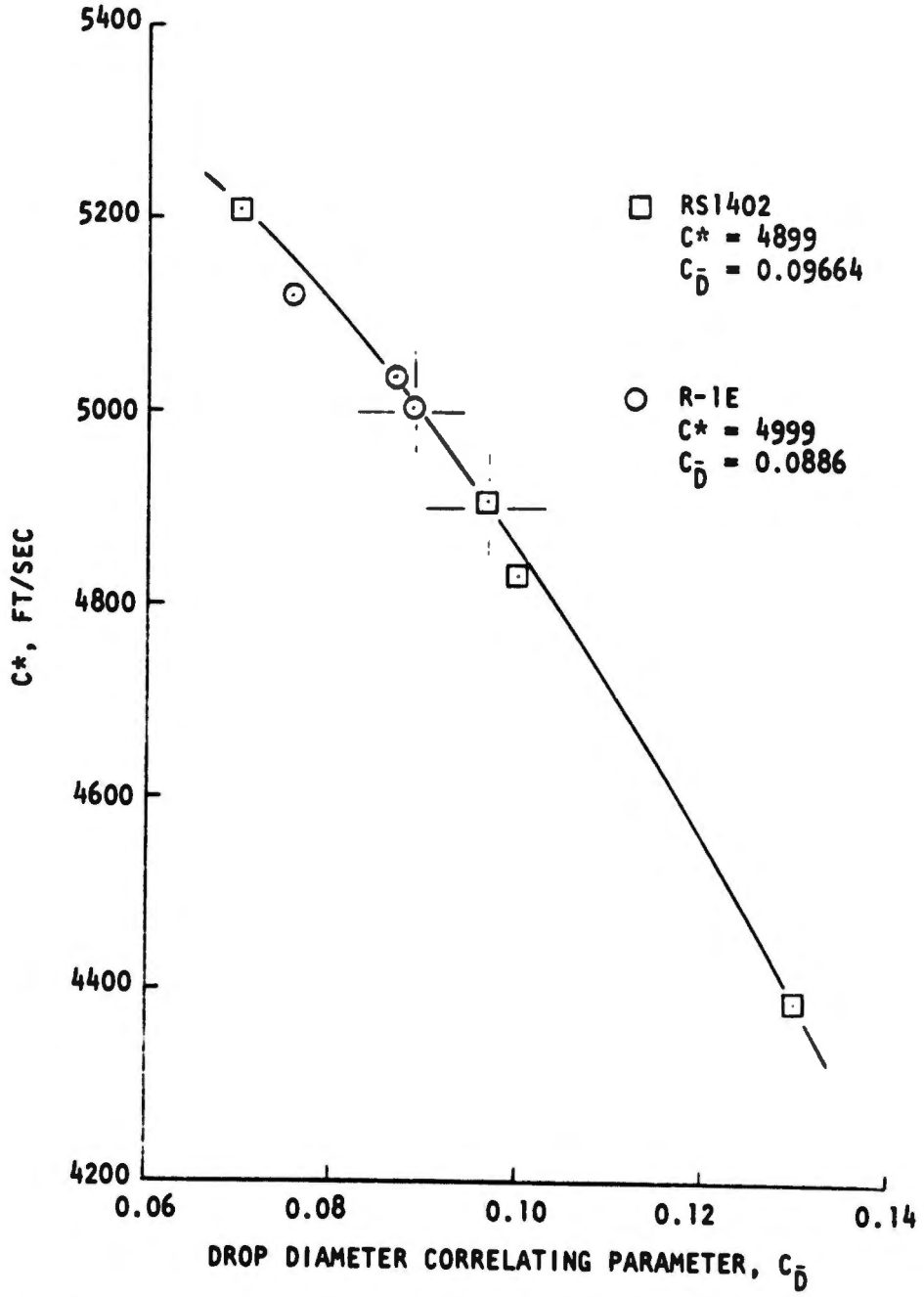

Figure 33. Predicted c* as a Function of Drop Size, Correlating Parameter, $C_{\bar{D}}$, for RS1402 and R-1E Thrustors

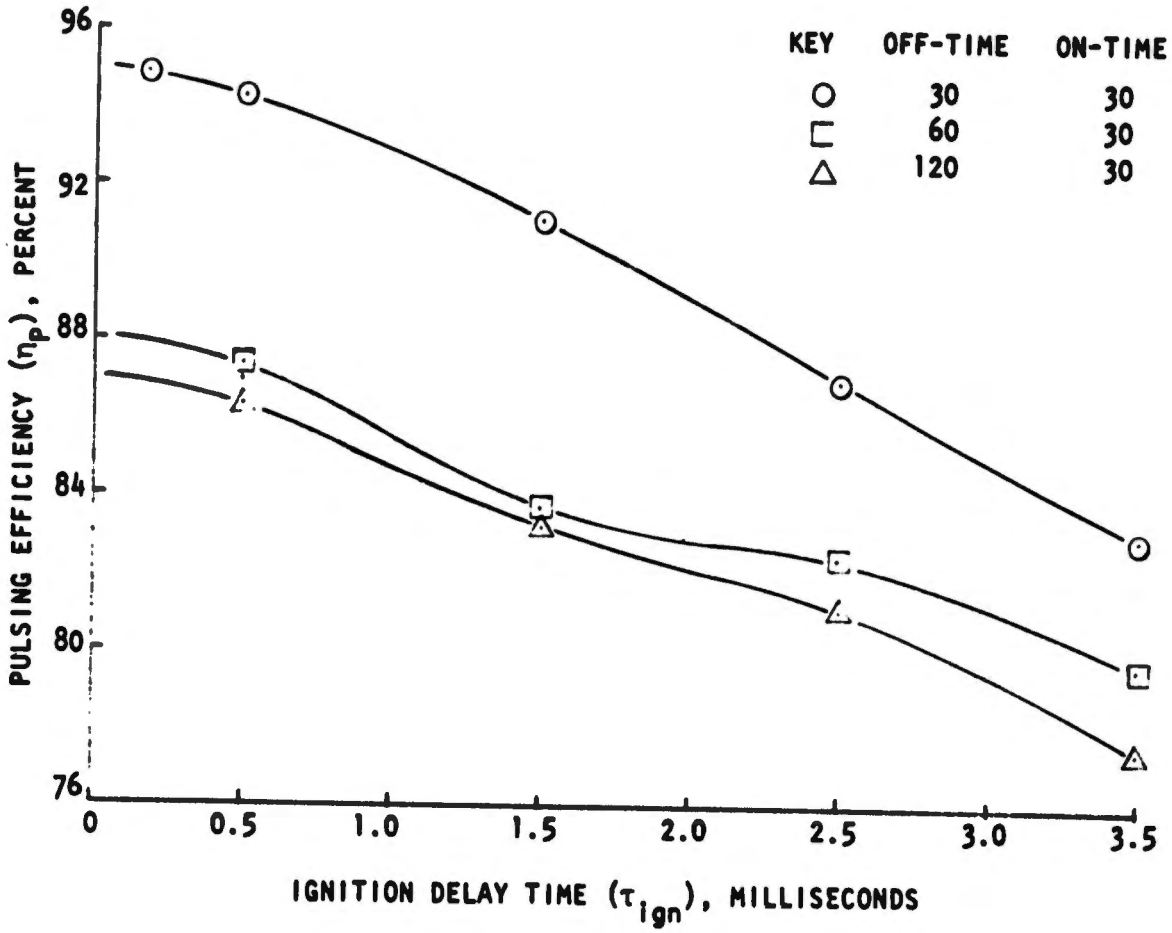

Figure 34. Effect of Ignition Delay Time on Pulsing Efficiency

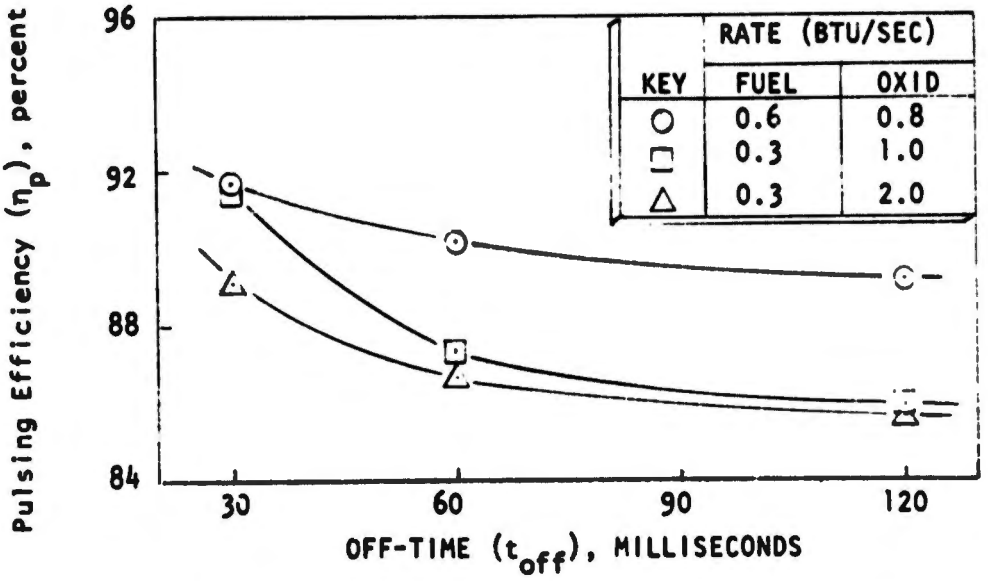

Figure 35. Effect of Heat Soakback Rates and Off-Time on Pulsing Efficiency for RS1402 30-Millisecond Pulses

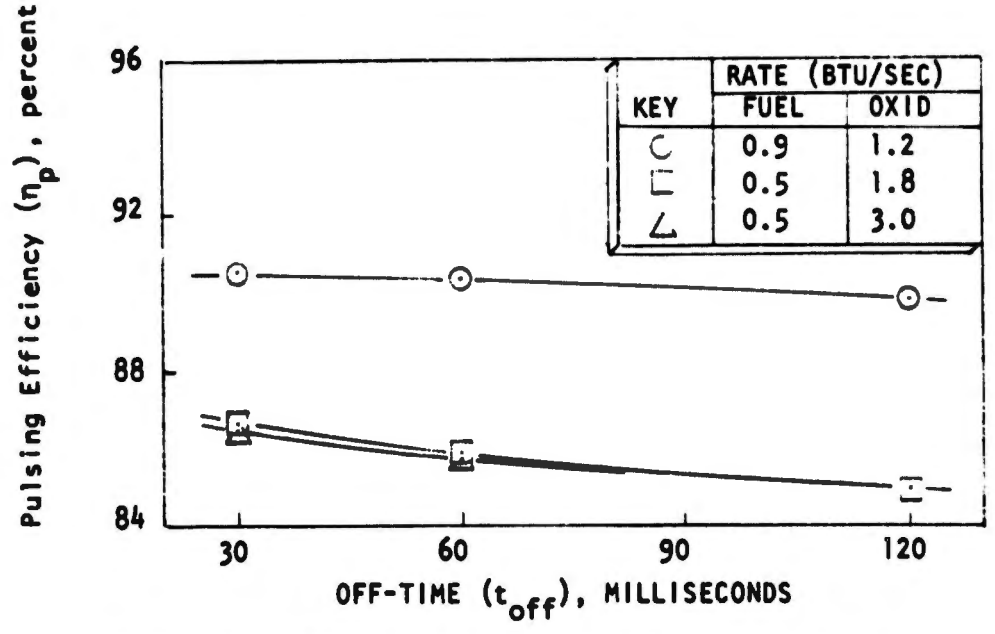

Figure 36. Effect of Heat Soakback Rates and Off-Time on Pulsing Efficiency for R-1E 25-Millisecond Pulses

Physically realistic values are difficult to obtain, requiring a very comprehensive heat transfer analysis of the specific rocket engine system and conditions. An alternative approach was taken and is recommended, i.e., depending on the amount of effort which can be afforded, to use the heat soakback rates as correlating parameters to adjust the model solution of duty cycle performance characteristics to obtain agreement with hot-fire test results. Values plotted in Fig. 35 and 36 may aid in determining approximate values for rocket engines similar to the RS1402 or R-1E engines.

TEMPERATURE OF FEED SYSTEM HARDWARE

Steady-state temperatures of the fuel and oxidizer feed system hardware limits the temperature which the feed system propellants can approach. If one propellant is substantially more volatile than the other (as occurs, e.g., with N_2O_4 oxodizer and monomethylhydrazine fuel), low feed system temperatures may cause its vaporization rate to be high enough to maintain the chamber pressure above the vapor pressure of the less volatile propellant. Thus with N_2O_4/MMH propellants, the chamber gases may become highly oxidizer-rich early in the pulse tailoff period; combustion may even be extinguished (theoretically) by the high oxidizer concentration. Depletion of oxidizer from its dribble volume must eventually permit chamber pressure to decay below the fuel vapor pressure, whereupon the chamber gases during the latter part of the tailoff period should become highly fuel rich. In this case, dribble-volume propellants are inefficiently utilized and the pulse performance efficiency is degraded. Consequently, a series of calculations was made in which the steady-state feed system temperatures were varied with the fuel and oxidizer sides at equal temperatures. Results from these calculations are shown in Fig. 37 and 38. Feed system temperatures appear to be the most critical parameters on pulsing efficiency of short pulses that was investigated during the model evaluation effort. Selection of temperature values was based on correlating duty cycle performance parameters and characteristics predicted by the model with test results, as was done and recommended for the heat soakback rates.

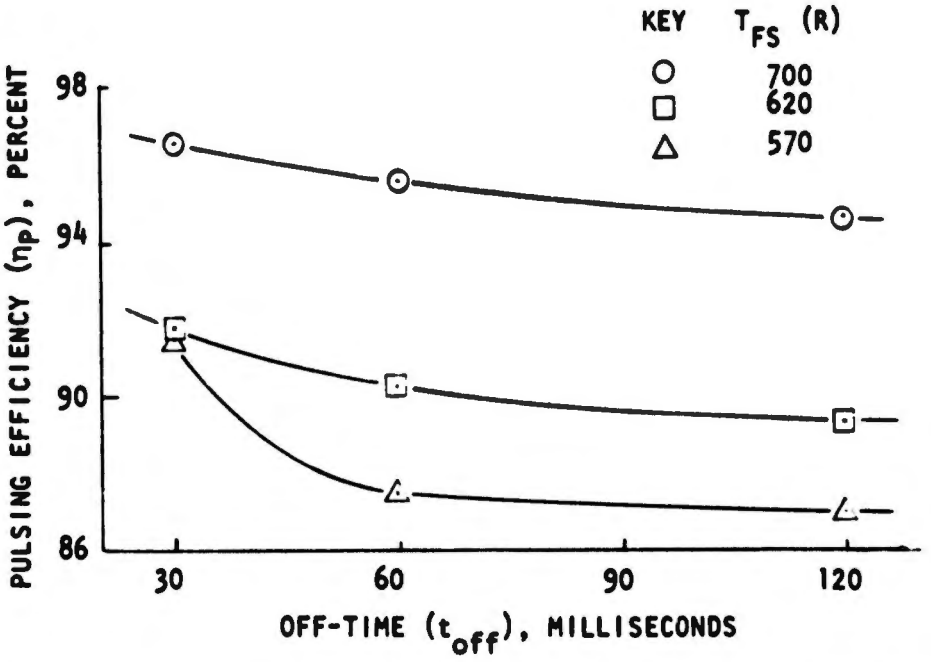

Figure 37. Effects of Feed System Temperature and Off-Time on Pulsing Efficiency for RS1402 30-Millisecond Pulses

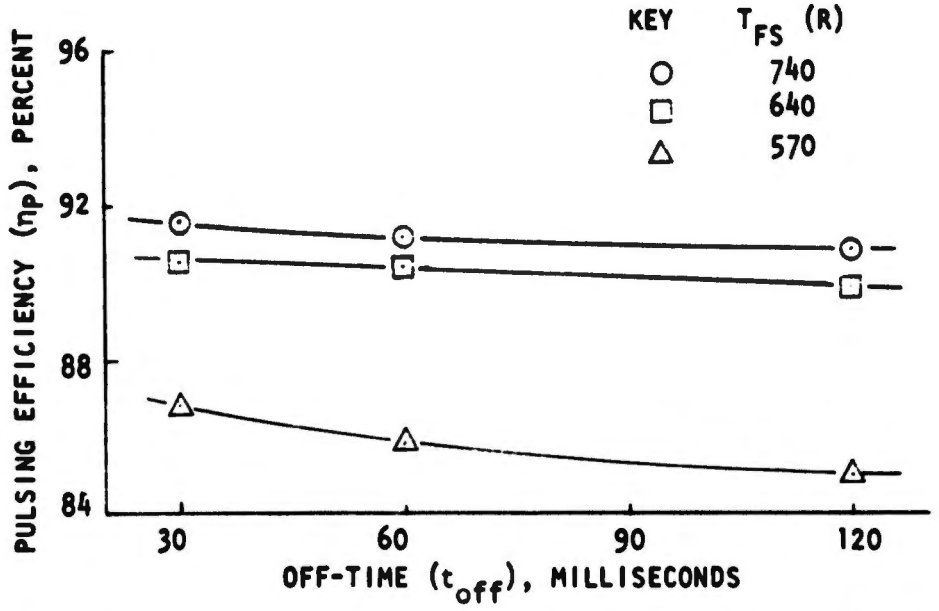

Figure 38. Effects of Feed System Temperature and Off-Time on Pulsing Efficiency for R-1E 25-Millisecond Pulses

COMPARISON OF MODEL RESULTS WITH TEST DATA

STEADY-STATE PERFORMANCE

Steady-state model solutions attained by using the previously discussed values for Z_{OM}, k'_F, k'_O, and C_D's in PMDER were obtained for both the RS1402 and the R-1E thrustors. The results are shown in Table V, along with the corresponding test-derived steady-state performance data. The RS1402 test data represent average performance for all engines tested. Test data for the R-1E were taken from test 3493, run 2271 performed on 13 June 1968, which was selected as an average test case. Clearly, the agreement between measured and predicted values is very good.

PULSE-MODE PERFORMANCE

Several heat transfer related parameters, which are used in the boiloff model and which govern the pulse tailoff performance, were found to be very critical input parameters. Unfortunately, the analytical representation of the heat transfer phenomena is highly simplified and, therefore, probably does not adequately describe this influence on pulsing performance. Consequently, during the model evaluation effort, the heat transfer related input parameters were adjusted widely to match functional pulse characteristics as closely as possible. The input variables used as correlating parameters, along with their final values applied for the nominal RS1402 and R-1E engine cases, are presented in Table VI. An effort was made to duplicate, with PMPM, the experimentally derived RS1402 performance map shown in Fig. 1. PMPM pulse performance efficiency predictions for a 30-millisecond pulse with various off-times are superimposed on this map, Fig. 39. The agreement is good except at the minimum off-time, where PMPM under-predicts performance.

Good agreement is shown on the same figure for variations in pulse efficiency with pulse on-time and with constant off-times of 60 milliseconds. However, such a simple display of overall pulse performance for an engine may be over-simplified. Some specific pulse sequence test data were compared with the performance map and were found to disagree, which suggests other variables are important. Also, the amount of test data scatter was not investigated.

TABLE V. STEADY-STATE PERFORMANCE DATA

Variable	Symbol	Units	RS1402		R-1E	
			Test	PMPM *	Test	PMPM *
Thrust	F	lbf	23.0	23.0	21.7	21.7
Chamber Pressure		$lbf/in.^2$				
Nozzle Stagnation	PNS		95.76	95.84	91.5	91.5
Injector End	P_{IE}			100.9	93.9	93.9
Mixture Ratio	MR		1.600	1.600	1.732	1.732
Propellant Valve Inlet Pressure		$lbf/in.^2$				
Fuel	$P_{V,F}$		199.8	199.8**	198.	198.**
Oxidizer	$P_{V,O}$		214.8	214.8**	198.	198.**
Propellant Flowrate		$lbm/in.^2$				
Fuel (MMH)	$\dot{w}_f$		0.0339	0.0341	0.02860	0.02860
Oxidizer (NTO)	$\dot{w}_o$		0.0543	0.0546	0.04955	0.04955
Characteristic Velocity	c*	ft/sec	4899.	4906.	4999.	5003.
Efficiency	η_{c^*}	%	85.9	86.0	87.7	87.8
Thrust Coefficient	C_F		1.699	1.700	1.789	1.790
Efficiency	η_{C_F}	%	96.3	96.3**	95.3	95.3**
Specific Impulse	I_s	lbf-sec/lbm	258.7	259.2	277.9	278.3
Efficiency	η_{I_s}	%	82.6	82.8	83.5	83.6

*Best results after adjusting input data as discussed in text.
**Values which are part of PMPM data input.

TABLE VI. PULSE CORRELATING PARAMETERS AND VALUES USED

Parameter	Symbol	Units	RS1402	R-1E
Steady-state chamber wall temperature	T_W	R	2000	2400
Steady-state temperature of propellant feed system hardware				
Fuel Branch	T_{FS_F}	R	620	620
Oxidizer Branch	T_{FS_O}	R	620	620
Steady-state heat soakback rates to dribble volume propellants				
Fuel Branch	Q_{SB_F}	Btu/sec	0.15	0.15
Oxidizer Branch	Q_{SB_O}	Btu/sec	0.20	0.20
Exponential coefficients for chamber wall temperature variations				
Heating	λ_h	-	0.0462	0.0306
Cooling	λ_c	-	0.00823	0.00657
Thrust correlation coefficient	C_T	-	0.60	0.82

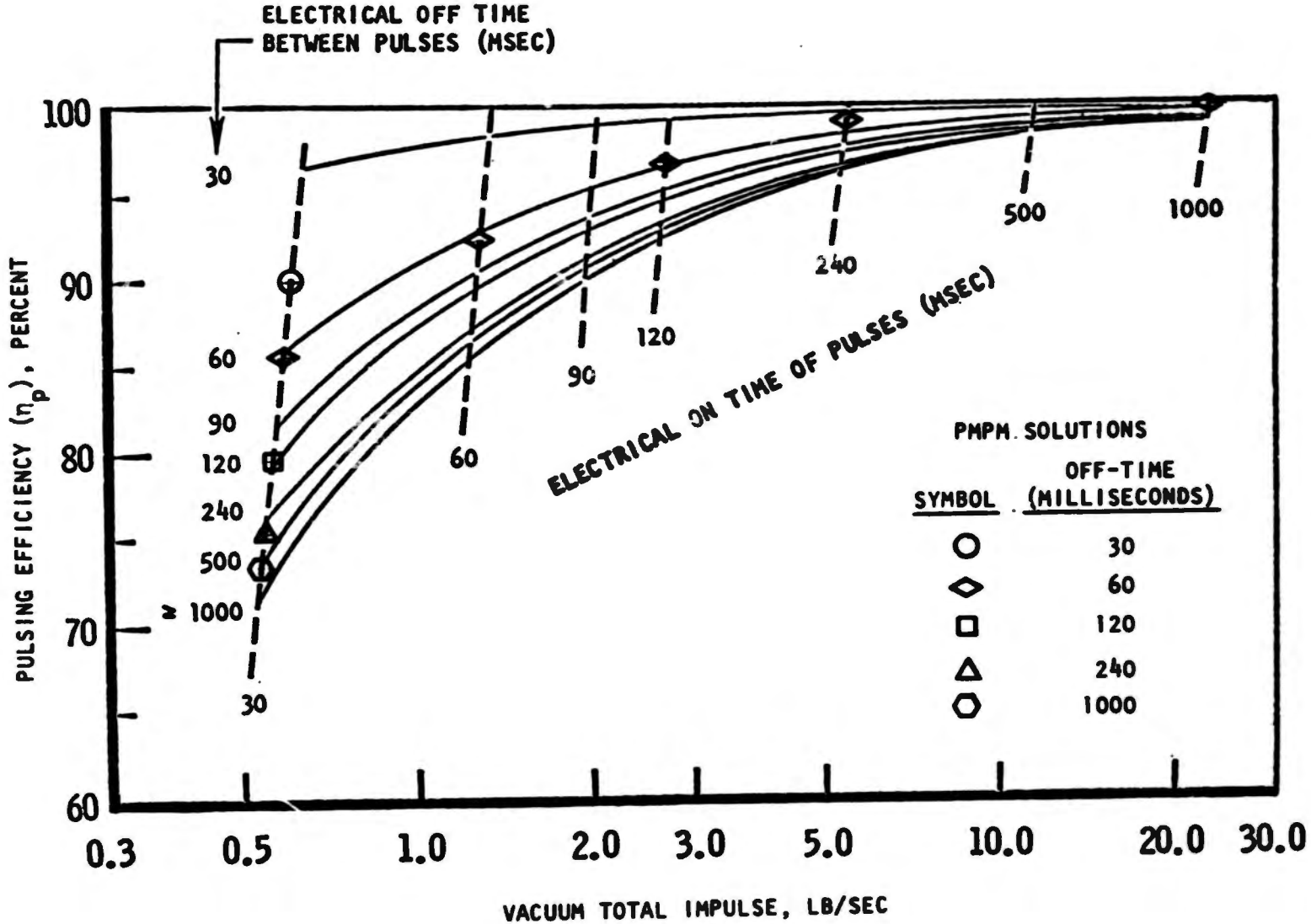

Figure 39. Comparison of PMPM Solutions of RS1402 Pulsing Efficiency With Map of Test Data Trends

A similar comparison was made for the R-1E data but, first, the pulse performance data had to be compiled from data reduction sheets for comparison with model solutions. Results from an attempt to obtain a pulsing efficiency map, with efficiency as a function of valve on-time and off-time between pulses, is shown in Fig. 40, but, the wide data scatter causes a very low confidence level in defining the trends. Nonetheless, an attempt to reasonably match the PMPM solutions with the experimental values was successful. The PMPM predicted results are shown in Fig. 41 superimposed on the test trend curves from Fig. 40.

A spot check was made of pulse total impulse and propellant flows; these indicated significant overpredictions. (Up to 10 to 15 percent for 16.5 millisecond pulse on R-1E engine). The overprediction of oxidizer flow is much greater than that of the fuel flow, which suggests significant effects due to fluid inertance upstream of the propellant valves (which is not modeled). Assuming the fuel and oxidizer facility feed lines upstream of the propellant valves are the same length and diameter, the oxidizer would have a much greater inertance than the fuel. Even though the diameters of the facility feed lines are sufficient to maintain low steady-state velocities, the lengths are probably also sufficient to yield significant (L/A) ratios to which the inertances are proportional. A simple L/A input term added to the PMPM model could correct this deficiency.

Accuracy of the pulse performance efficiency can not be directly assessed because of the considerable data scatter (up to 15 percent in Fig. 40) which exists in the pulse test data. Much leveling of this data was required to obtain smooth trends. Thus, this correlation for mean performance can not be expected to fall within a 3-percent accuracy over all operating ranges, since the test trends are not that accurate. Therefore, the fact that PMPM predicted performance deviated by more than 3 percent from the mean correlated values under some operating conditions does not prove much for or against the accuracy of the model. However, pulse performance characteristics and trends do correspond reasonably well with hot-fire performance.

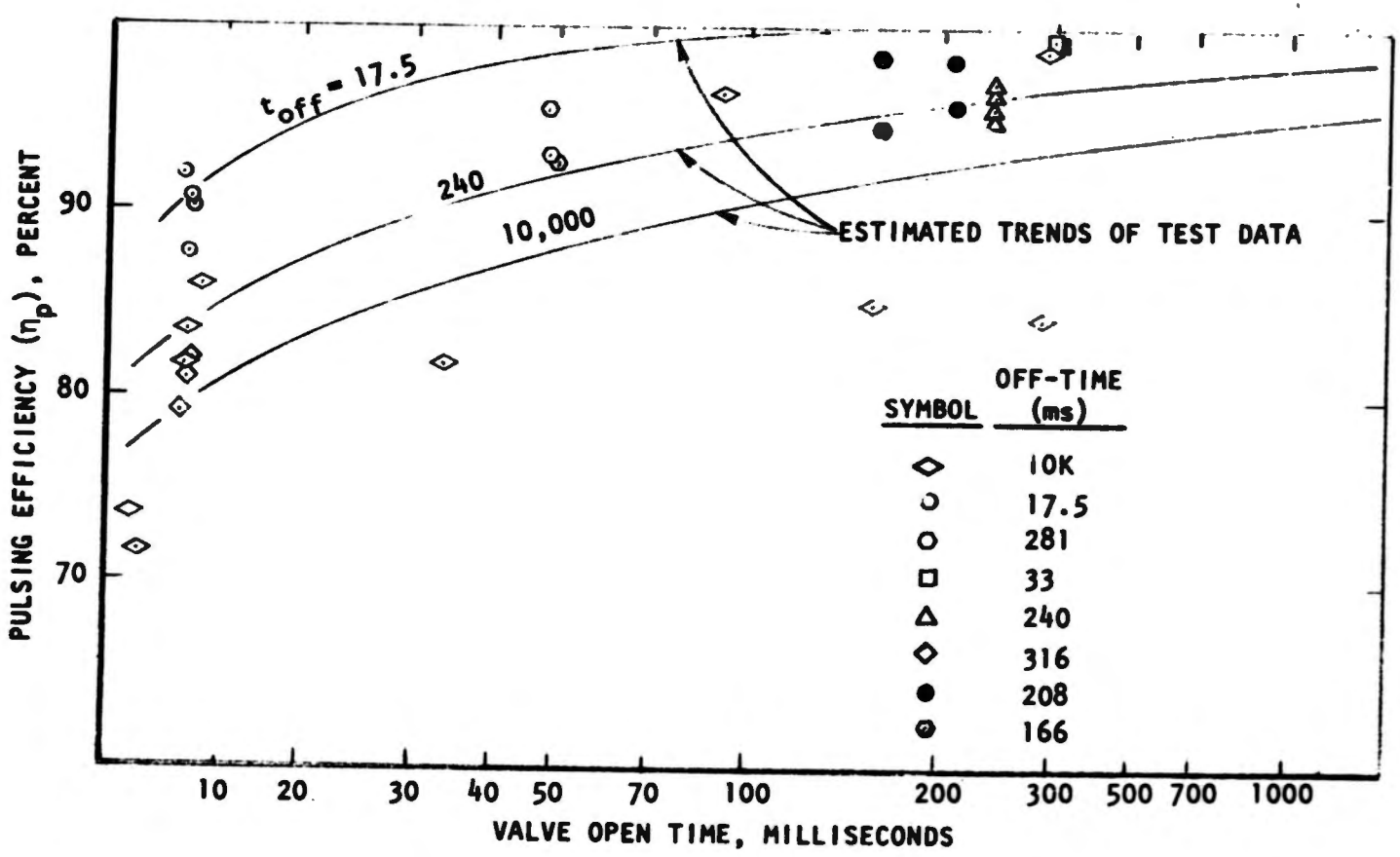

Figure 40. Pulsing Efficiency Test Data for R-1E With Estimated Mean Trend Curves

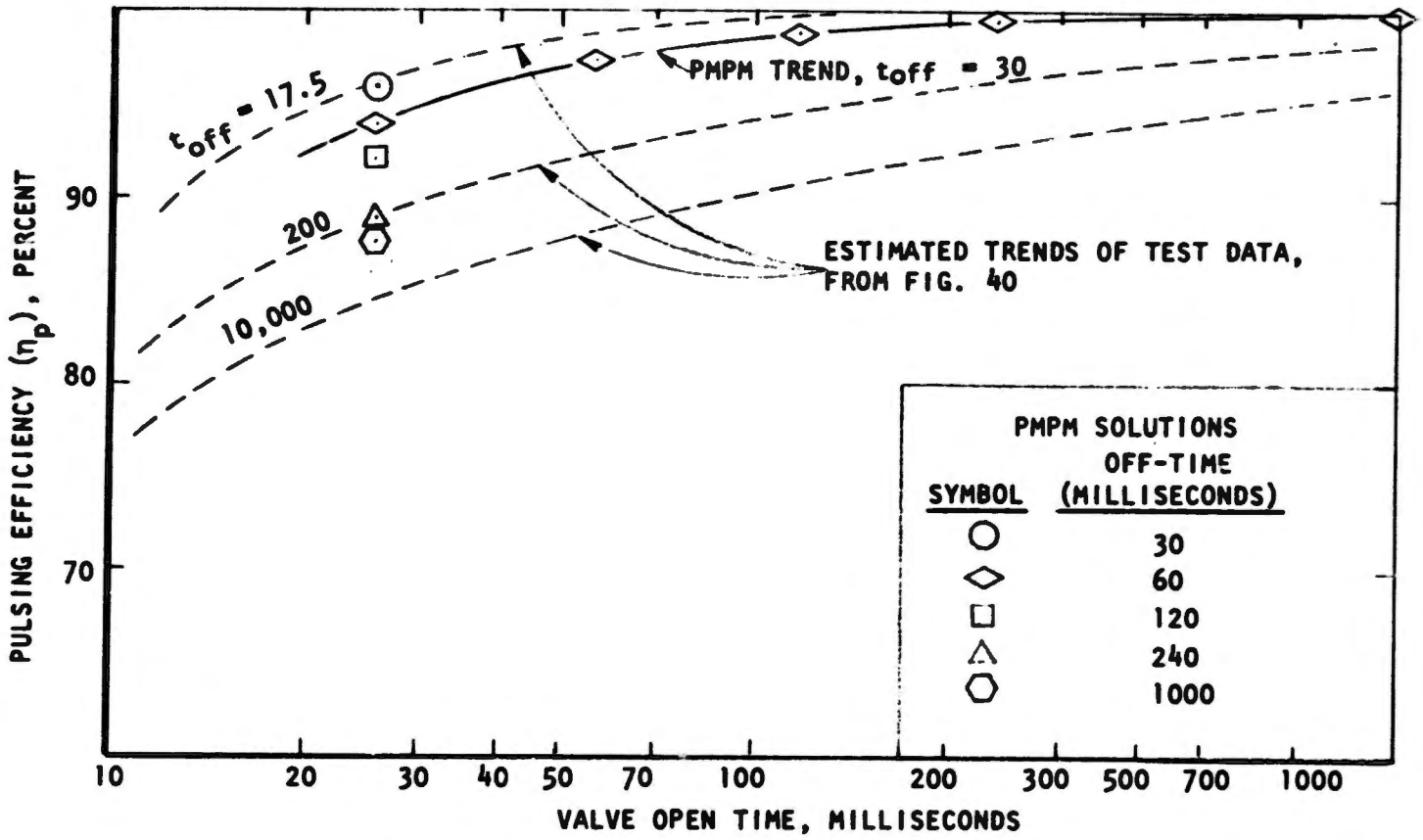

Figure 41. Comparison of PMPM Solutions of R-1E Pulsing Efficiency With Estimated Mean Trend Curves From Test Data

ASSESSMENT OF MODEL APPLICABILITY

A variety of physical phenomena relating to steady and transient rocket engine performance are accurately modeled in PMPM. However, some compromises were necessary which prevent accurate prediction of absolute performance levels without the use of empirical correlating coefficients. Such coefficients whose values do not change appreciably with variations in rocket engine designs or operating conditions are acceptable. However, if their values must be adjusted for each specific application, the usefulness of the model is greatly reduced.

STEADY-STATE PERFORMANCE MODEL

The injector/chamber steady-state combustion performance efficiency may be subdivided into two components, propellant mixing and vaporization efficiencies. Mixing efficiency is predicted primarily in subprogram LISP. The spray distribution correlations built into LISP are applicable to well-designed injectors, but with restrictions. LISP cannot accurately describe cases where jet momentum and diameter ratios are outside reasonable ranges, or where the propellant jets misimpinge. Also, built-in correlations are limited to the commonly used injector element types. Moreover, propellant jet or spray deflection from splash plates or chamber walls is not modeled. Nonetheless, most practical, well-designed and precisely built injector elements can generally be analyzed with the LISP program to adequately predict spray distributions and mixing efficiencies.

Propellant spray drop size is the most critical parameter in determining vaporization efficiency because it has a strong infiuence on efficiency and it is difficult to predict satisfactorily. The drop size correlations built in LISP are based on results from tests in which liquid wax is used as a propellant simulant in a single injector element and, subsequent to atomization, the wax is frozen for size analysis. Physical property corrections are applied to the measured drop sizes to predict drop sizes for specific propellants. The validity of this procedure cannot be checked directly. However, an indirect check or comparison can be made through use of the predicted drop sizes in a spray combustion

model (e.g., PMSTC) and comparing predicted combustion performance with test results. If the procedure were adequate, the best value of the drop size correlating coefficient, $C_{\overline{D}}$, used in the model would be near 1.0. (This coefficient is input in LISP and is used to adjust the drop size based on wax test correlations to an effective value which will cause the predicted performance to agree with measured performance.)

The derived values of $C_{\overline{D}}$ for the two evaluation cases are within 10 percent of each other, but both are an order of magnitude less than 1.0. Moreover, a large disparity exists between $C_{\overline{D}}$'s obtained for these designs and those obtained for larger combustion chambers ($C_{\overline{D}} \sim 1$). Consequently, at present, only experience with related calculations can be used as a guide line for estimating $C_{\overline{D}}$'s for new applications.

The PMSTC combustion model is also limited somewhat by the fact that it contains a k'-type droplet vaporization model. This type of model is based on the assumption that spray droplet temperatures are continuously at their respective, local wet bulb temperatures. More generally applicable vaporization models are available which consider droplet heating, but they should be avoided where possible because they require an order of magnitude more computing time and determination of appropriate input data is considerably more difficult.

PULSE PERFORMANCE MODEL

Propellant Feed System

The propellant feed system description in PMPM is limited to the propellant feed passages from the fuel and oxidizer valve seats through the injector orifices. Moreover, the description assumes one-dimensional flow which is inadequate for flow through some manifold designs. Because it is one-dimensional, the manifold is assumed to fill completely before the propellant enters the injection orifices and then the orifices from that manifold are assumed to fill simultaneously. These are regarded as unimportant restrictions for pulse-mode type engines.

The constant pressure assumed at the valve inlets in the model may not be adequate for analyzing transient flow. This can cause the acceleration of the propellant during the start transient to be overpredicted under some circumstances, and result in excessive flowrate overshoot, quantity of propellant consumed per pulse and pulse total impulse. Also, neglecting inertance differences between the fuel and oxidizer in the facility feed lines upstream of the valves can cause erroneous prediction of the mixture ratio during the start transient and result in a shift in mean pulse mixture ratio.

Ignition Delay Time

Ignition delay time affects pulse-mode performance, but its sensitivity on performance is only moderate for time delays on the order of 0.5 milliseconds. Moreover, the complexity of a preignition model is not justifiable unless the delay times are variable and long enough (>1.0 millisecond) to have a significant variation on performance.

Transient Heat Transfer Solution

Very simple heat transfer expressions have been used in PMPM to predict pulse-to-pulse chamber wall temperatures, heat soakback from chamber walls to dribble-volume propellants, and combustion gas heat loss to chamber walls. The model evaluation results demonstrate that sufficient parameter input flexibility exists so that reasonable correlation between model predicted performance and test data can be obtained by adjusting the parameters to fit. Whether or not the derived values for the parameters are physically reasonable has not been determined. Such a determination would require an extensive transient heat transfer analysis of the thrustor assembly. It appears very likely that the heat transfer expressions are too simple to adequately predict performance variations, tail-off thrust in particular, associated with large variations in wall temperatures.

Transient Combustion

The primary variation which affects chamber combustion rates is time-varying propellant injection rates. This phenomenon is adequately modeled in PMPM. However, other transient phenomena may also be important. Time-varying propellant injection rates cause variations in the atomization process which must alter spray drop sizes. A change in drop size should be accompanied by an adjustment in droplet vaporization rate. Therefore, a variable burning rate function, instead of a constant one, should be applied to the spray ensembles as a function of injection velocities.

Whereas the model does predict normal pressure overshoots, it does not contain the mechanism for simulating pressure spikes caused by detonations. Detonations are critical from a chamber stress standpoint, but relatively unimportant in respect to performance efficiency.

CONCLUSIONS AND RECOMMENDATIONS

The major goals in the development of the Pulse Mode Performance Model (PMPM) were accomplished. The reliability and operational status of the PMPM computer program have been demonstrated through extensive analysis of two designs. Application of PMPM to modeling two real engine designs and comparisons of these results with hot-fire performance have shown (for these engine designs) the capability of predicting performance level and pulse characteristics with reasonable accuracy, as long as certain input values are sufficiently tailored to adjust predicted performance to correspond with reference conditions. Steady-state performance efficiency was duplicated within the 3-percent accuracy goal. Accuracy of the pulse performance efficiency appears to be within the accuracy of the experimental data, and pulse mode performance characteristics and trends correspond reasonably well with hot-fire performance.

In a single computer program, PMPM models most of the important physical processes which occur in the operation of a thrustor assembly, e.g., steady and transient liquid propellant flow, atomization, combustion, and gas flow. There are some physical processes which have been simplified or omitted intentionally. One of these is the heat transfer process within the thrustor assembly. This is a very complex process requiring a sophisticated heat transfer model for adequately determining wall heat fluxes and temperature profiles. The approach taken in PMPM was to decouple (but approximately match) the heat transfer process from the other processes, and to conduct a separate detailed heat transfer analysis to determine the heat fluxes and heating rates which are required as input data to PMPM.

In the application of PMPM, it is strongly recommended that the integrated version of Seamans' ignition model IGN, always be bypassed, by selecting the alternate procedure of using an input-specified, constant, ignition delay time. For the delay times in the range of those estimated for the evaluation cases, predicted performance is not critically affected by small changes in ignition delay time.

Additional effort to improve the usefulness of the PMPM computer program is recommended as follows:

1. A lumped representation of the propellant feed lines from the propellant supply source to the thrustor valves should be added to the feed system model to account, particularly, for fluid inertances which affect propellant flowrates during pulse start transient periods. This addition is necessary to improve the accuracy of predicted pulse flows and total impulses.

2. The modeling of the effect of heat transfer processes on propellant boil-off and combustion-gas heat losses requires a more complete formulation with the use of more precisely defined PMPM input parameters. This effort should replace the input parameters which now require "correlation" type values with parameters that can be accurately determined for any application. An extensive steady-state and transient heat transfer analysis should be performed on the RS1402 and R-1E thrustors, using appropriate heat transfer computer models for predicting their heat fluxes, temperature profiles, and heating and cooling rates. The parametric formulation of heat transfer effects in PMPM should then be reevaluated and reformulated as necessary to obtain a reasonable physical representation of the overall process, thereby eliminating the need for adjusting input data to match model performance with reference conditions. Agreement of PMPM solutions with hot-fire test data for both RS1402 and R-1E should be demonstrated.

3. In the transient combustion model, variation of the overall chamber combustion rate is controlled by the cumulative vaporization of individual spray ensembles, each of which vaporize at a fixed time-distributed rate. The time-distributed rate function should differ between spray ensembles to account for the variation in propellant injection velocities and resulting spray droplet sizes during the inception of each spray ensemble. A moderately simple model

modification is recommended to include a time-scale factor to appropriately adjust the time-distributed vaporization rate function of each spray ensemble. This modification should improve the modeling of the start transient and provide greater accuracy in predicting overall pulse performance of very short pulses.

In conclusion, the PMPM computer program can be applied effectively to relate engine design and operating parameters with steady-state and pulse-mode performance. Design changes necessary to achieve specific performance characteristics can be evaluated directly, rapidly, and inexpensively with a PMPM analysis, as compared with characterization by means of extensive hot-fire tests.

REFERENCES

1. Agosta, V. D. and Kraus, G., "An Investigation of the Impulse Bit Developed by a Pulsed Liquid Propellant Rocket Engine," Aerospace Techniques, Chem. Engr. Progress Symposium Series No. 52, Vol. 60, American Institute of Chemical Engineers, 1964, pages 8-16.

2. Seamans, T. F., M. M. Vanpee, and V. D. Agosta: "Development of a Fundamental Model of Hypergolic Ignition in Space-Ambient Engines," AIAA Journal, Vol. 5, No. 9, September 1967.

3. Seamans, T. F. and P. D. Waser: Effects of Additives on Ignition Delay and Chamber Pressurization of Space-Ambient Engines, Final Report, AFRPL-TR-69-68. Thiokol Chemical Corp., Reaction Motors Division, Denville, New Jersey, July 1969.

4. Ross, C. C. and P. P. Datner: "Combustion Instability in Liquid Propellant Rocket Motors - A Survey," Selected Combustion Problems, AGARD, Butterworths, London, Page 352, 1954.

5. Fontaine, R. J., R. S. Levine, and L. P. Combs: "Secondary, Non-Destructive Instability in Medium-Size Liquid Rocket Engines," AGARD Advances in Tactical Rocket Propulsion, Technivision Services, Maidenhead, England, Pages 383-419, 1968.

6. Harrje, D. T. and Reardon, F. H. (editors), Liquid Propellant Rocket Combustion Instability, NASA SP-194, National Aeronautics and Space Administration, Washington, D. C., 1972.

7. Webber, W. T.: "Calculation of Low-Frequency Unsteady Behavior of Liquid Rockets form Droplet Combustion Parameters," AIAA Paper No. 70-621, June 1970.

8. Combs, L. P., W. D. Chadwick, and D. T. Campbell: Liquid Rocket Performance Computer Program with Distributed Energy Release, NASA CR-11000 (R-8298), Rocketdyne, a division of North American Rockwell Corporation, Canoga Park, California, September 1970.

9. Kliegel, J. R. et al.: ICRPG Two-Dimensional Kinetic Reference Program, Dynamic Science, a division of Marshall Industries, Irvine, California, July 1968.

10. Hines, W. S., L. P. Combs, W. M. Ford, and R. Van Wyk: Development of Injector Chamber Compatability Analysis, Final Report, AFRPL-TR-70-12, Rocketdyne, a division of North American Rockwell Corporation, Canoga Park, California, March 1970.

11. Hines, W. S., M. D. Schuman, W. M. Ford, and K. W. Fertig: Extension of a Thrust Chamber Compatibility Model, Final Report, Contract F04611-70-C-0056, R-8745, Rocketdyne, a division of North American Rockwell Corporation, Canoga Park, California, July 1971.

12. Rupe, J. H. and G. H. Jaivin: The Effects of Injection Mass Flux Distributions and Resonant Combustion on Local Heat Transfer in a Liquid Propellant Rocket Engine, Prog. Rpt. 32-648, Jet Propulsion Laboratory, Pasadena, California, October 1964.

13. Combs, L. P. et al.: Catalog of Injector Spray Correlations, Rocketdyne, a division of North American Rockwell Corporation, Canoga Park, California, in preparation (June 1972).

14. Combs, L. P.: Liquid Rocket Performance Computer Model with Distributed Energy Release, Final Report, NASA CR-114462, Rocketdyne, a division of North American Rockwell Corporation, Canoga Park, California, June 1972.

15. Dickerson, R. A., K. Tate, and N. Barsic: Correlation of Spray Injector Parameters with Rocket Engine Performance, Final Report, AFRPL-TR-68-147, Rocketdyne, a division of North American Rockwell Corporation, Canoga Park, California, June 1968.

16. Falk, A. Y., S. D. Clapp, and C. K. Nagai: Space Storable Propellant Performance Study, Final Report, NASA CR-72487, Rocketdyne, a division of North American Rockwell Corporation, Canoga Park, California, November 1968.

17. Rupe, J. H.: Progress Report 20-195, Jet Propulsion Laboratory, California Institute of Technology, Pasadena, California, August 1953.

18. Nickerson, G. R.: "Instructions for Replacing the Transonic Analysis of the TDK Computer Program," Dynamic Science Letter Report, received April 1970.

19. Kliegel, J. R. and J. N. Levine: "Transonic Flow in Small Throat Radius of Curvature Nozzles," AIAA Journal, Vol. 7, No. 7, July 1969.

20. Zajac, L. J.: Correlation of Spray Dropsize Distribution and Injector Variables, R-8455, Rocketdyne, a division of North American Rockwell Corporation, Canoga Park, California, 1971.

APPENDIX I

REVIEW OF TRANSIENT COMBUSTION MODELS

Most of the reported analytical treatments of transient rocket combustion have dealt with unstable or oscillatory combustion and fall into two categories: (1) those concerned with high-frequency oscillations, in which pressure wave motion within the combustor is a dominant physical reality; and (2) those concerned with low-frequency oscillations, in which wave motion is so fast that the chamber pressure is essentially uniform throughout the combustor at each instant and varies only with time. Analyses of the high-frequency instabilities have embodied a wide range of combustion model complexity, but their major focus is on the wave dynamics and wave-combustion interactions. Injection rate fluctuations, global chamber pressurization, and nozzle efflux--all of which are important in starting and stopping--are usually neglected. Consequently, these high-frequency formulations have little to offer to start-stop analysis.

Formulations for low-frequency instabilities, on the other hand, have embodied analyses of those important combustion chamber phenomena. The models in current use are generally extensions of early work detailed by Crocco and Cheng (Ref. 1).* The combustion process is treated very simply by assuming abrupt gasification occurs a short delay time after propellants are injected. Some models have used separate delay times for fuel and oxidizer, time-varying delay times, etc., but all use this nonphysical simplification of combustion. The combustion space is treated as a lumped-parameter, with a homogeneous combustion gas and uniform pressure at any given time. Stability is analyzed in terms of whether combustion chamber pressure oscillations, driven by time-varying injection rates, grow or decay. Feed system dynamics thus enter strongly in determining stability. These two systems (chamber and feed system) are coupled through the propellant injection orifices, and the transient response (gain and phase) of both must be analyzed. Current models are extended beyond Crocco's work, primarily in the complexity of their feed system dynamics, which range from simple lumped-parameter descriptions

*References for this Appendix are listed on page I-4.

to more-or-less complete treatment of distributed impedance, compressibility, wave motion, structural vibration, complicated flow paths and branch lines, pump and tank dynamics, etc., rather than in the combustion dynamic area.

A natural outgrowth of low-frequency instability analysis is the examination of aperiodic transient behavior of a thrust chamber, using the same model equations. Several investigators are known to have analyzed the response to isolated pressure pulses in the feed system or combustion chamber, although no published reports appeared in the current literature search. Similarly, reported applications to starting or stopping were not found; however, an unpublished pulse model of this type, developed at Rocketdyne in about 1965, is the basis for a modern model discussed later as Boehnlein's model. Perhaps the absence of publications here reflects an appropriate caution in using the low-frequency formulation very far from steady state: the equations have been linearized.

A somewhat more physically realistic formulation for the combustion process was used in an unpublished low-frequency instability model developed at Rocketdyne in 1966. A nonlinear, transient Bernoulli equation was used for injection rates and spray combustion rates were distributed in time following an impingement delay time. Except that the chamber volume was reduced to an effective volume, accounting approximately for the actual axial distribution of combustion gas density, other model assumptions were comparable with Crocco's work. Finite difference solutions with a digital computer were used, however, rather than the usual analog computer solution of Laplace transformed linear equations. Previous use of this model was in calculating stability response to isolated feed line pulses. It has been subsequently shown that this model is capable of analyzing the complete combustion period of a pulse.

The analysis of starting and stopping rocket combustion, *per se*, has been the subject of a very limited number of published reports. A 1964 Polish report (Ref. 2) treated the start transient chamber pressurization in a manner not very different from Boehnlein's work cited next. Unless earlier work was missed in the literature search, U.S. investigators have just recently begun to report their analytical efforts in this area.

Boehnlein (Ref. 3) has developed a digital computer program model for liquid rocket operation, from ignition to cutoff. Major emphasis is placed on detailed analysis of feed system dynamics, although linearized wave equations are still used. His treatment of the combustion process parallels Crocco's efforts, with a time-varying combustion time lag. The ignition process is also represented by a simple, nonphysical delay time. Both these simplifications limit the adequacy of the model for simulating short-duration pulses.

Webber (Ref. 4) has attacked the major combustion chamber simplifications and developed a lumped chamber pressure, but spatially nonhomogeneous, gas formulation which includes distributed spray combustion,* Bipropellant spray combustion is analyzed with a steady-state spray combustion model marching in the axial chamber direction during each time step as the overall model marches in time. Equations are included for calculating initial droplet diameters, burning rates, velocities and position in the chamber, all as functions of time. The computer program is large and complicated and, as a result, execution times are moderately long. The program is capable of analyzing both periodic and aperiodic transient operations. Predicted frequencies and amplitudes of a chug instability were shown to be in good agreement with experimental values. (Neither Webber nor Boehlein made reference to any other comparable published work, which tends to corroborate the dearth of literature found in the current search.)

Mills et al. (Ref. 5) have considered the transient overpressures that may be experienced at the instant of ignition as a result of detonation of explosive liquid intermediates that some propellants form during the preignition period. Presumably all of the chamber contents are completely burned so that subsequent propellant combustion (which may have to wait for injection to recommence) proceeds at rates comparable with propellant injection rates, producing moderate, smooth, and continuous pressurization until the steady-state level is approached or exceeded.

*Since this literature review was conducted, Webber has modified his model substantially in incorporating it into a model for rocket exhaust plume contaminant analysis (Ref. 6).

APPENDIX I REFERENCES

1. Crocco, L. and Cheng, S. I., Theory of Combustion Instability in Liquid Propellant Rocket Motors, Butterworth's Scientific Publications, London, 1956.

2. Szczecinski, S., "Changes in Thermodynamic Parameters During the Starting of a Liquid Fuel Rocket Engine," FTD-TT-65-1016, Foreign Technology Div., Wright-Patterson Air Force Base, Ohio, 1965.

3. Boehnlein, J. J., "Generalized Propulsion System Model," Phase I Interim Report, IL 0112-3055, Rocketdyne, a division of North American Rockwell Corporation, Canoga Park, California, 17 April 1970.

4. Webber, W. T., "Calculation of Low-Frequency Unsteady Behavior of Liquid Rockets from Droplet Combustion Parameters," AIAA Paper No. 70-621, June 1970.

5. Mills, T. R., Breen, B. P., Lawver, B. R., and Tkachenko, E. A., "Transients Influencing Rocket Ignition and Popping," Interim Report, NASA-CR-105315, Dynamic Science, a Division of Marshall Industries, Monrovia, California, April 1969.

6. Hoffman, R. J., Webber, W. T., et al., Plume Contamination Effects Prediction:, The CONTAM Computer Program, Final Report and Program Users' Manual, AFRPL-TR-71-109, McDonnell Douglas Astronautics Company, Huntington Beach, California, December 1971.

APPENDIX II

A REVIEW OF STEADY-STATE LIQUID ROCKET COMBUSTION ANALYSES

The accuracy of a model to predict pulse-mode performance greatly depends on the model's capability of predicting steady-state performance. Therefore, to aid in selecting a steady-state, liquid rocket combustion model for use in PMPM, a literature search was conducted. A review and evaluation of applicable models from the literature search, which supplies background information and technical details about existing and available models, is presented in this appendix. The bulk of this review was taken from an earlier report* and expanded and updated to August 1970.

Analysis of liquid rocket engine combustion involves formulation and solution of a system of coupled algebraic and differential equations representing the various physical and chemical processes which occur during the conversion of injected propellants to combustion products and the exhaustion of those products from the combustor. Realistic formulation of an analytical model requires that the controlling processes, at least, be identified and reasonably well understood.

A verbal description is presented first of the important combustion chamber physical and chemical processes. Next, existing analytical models are categorized and discussed in terms of major simplifications regarding dimensionality, rate-controlling processes and constancy of certain variables. Finally, knowledge of the processes which couple the spray behavior to the combustion gas, and mathematical expressions for them, is discussed.

*Report (not published for dissemination) prepared at Rocketdyne by R. D. Sutton and L. P. Combs under contract AF49(638)-1705, sponsored by the Air Force Office of Scientific Research, Washington, D. C., 1969.

QUALITATIVE DESCRIPTION OF COMBUSTION PROCESSES

After injection of the propellants into the rocket combustion chamber, subsequent steps in their combustion include liquid propellant atomization, spray dispersion and mixing, vaporization, vapor-phase mixing, ignition and chemical reaction. These processes take place in a two-phase flow field of finite length; the limited flow field influences both the process rates and the time available for completing them. A schematic representation of the most important processes is shown in Fig. II-1, which also emphasizes their complex interdependence. The process paths to the left side of Fig. II-1 should tend to be dominant with injectors designed for efficient liquid-liquid inter-propellant contact prior to their atomization. Conversely, paths toward the right side tend to be favored with either gas-liquid propellant injectors or liquid-liquid propellant injections which will accomplish substantial propellant atomization and vaporization before much mixing occurs (Ref.1).* Most practical rocket injectors operate between these two extremes so that combustion proceeds simultaneously along many or even most of the process paths.

The combustion processes occur throughout the combustion chamber in a distributed fashion. It is convenient for this qualitative discussion to divide the combustion chamber into a series of discrete zones. Based in part on photographic evidence from transparent model engine firings (Ref. 2), a logical subdivision is shown in Fig. II-2. The transition and distinction between the various zones in the combustion region is certainly gradual and not sharply defined. However, both the position and abruptness of the transitions are influenced by injector and chamber designs, the propellant combination and operating conditions.

Injection/Atomization Zone

Adjacent to the propellant injector is an injection/atomization zone. Because the injection is usually concentrated at discreet sites, with some degree of separation between unlike propellants, within this zone occur large gradients in

*References for this appendix are listed on page II-32.

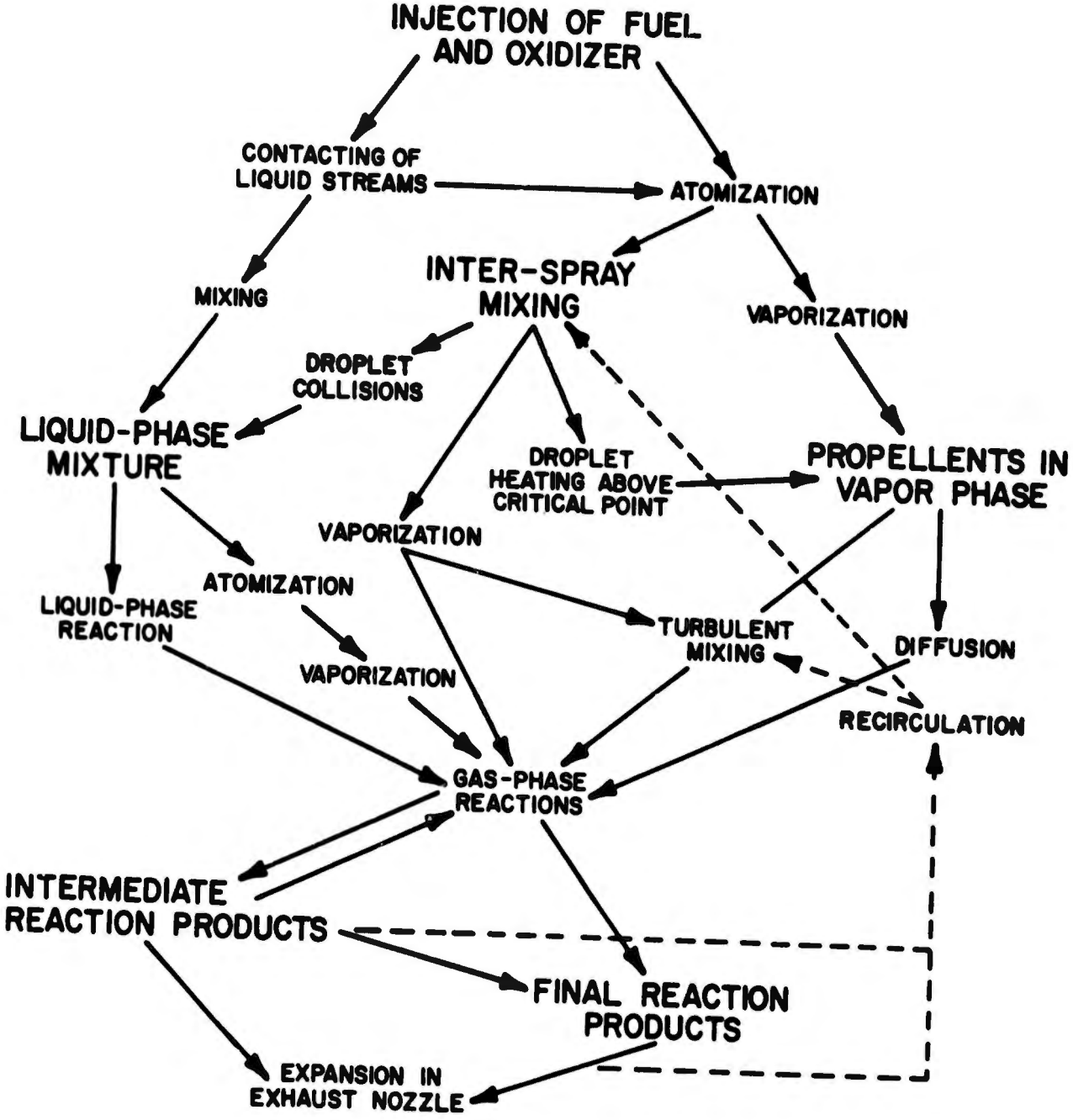

Figure II-1. Schematic Representation of Liquid Propellant Rocket Combustion Processes

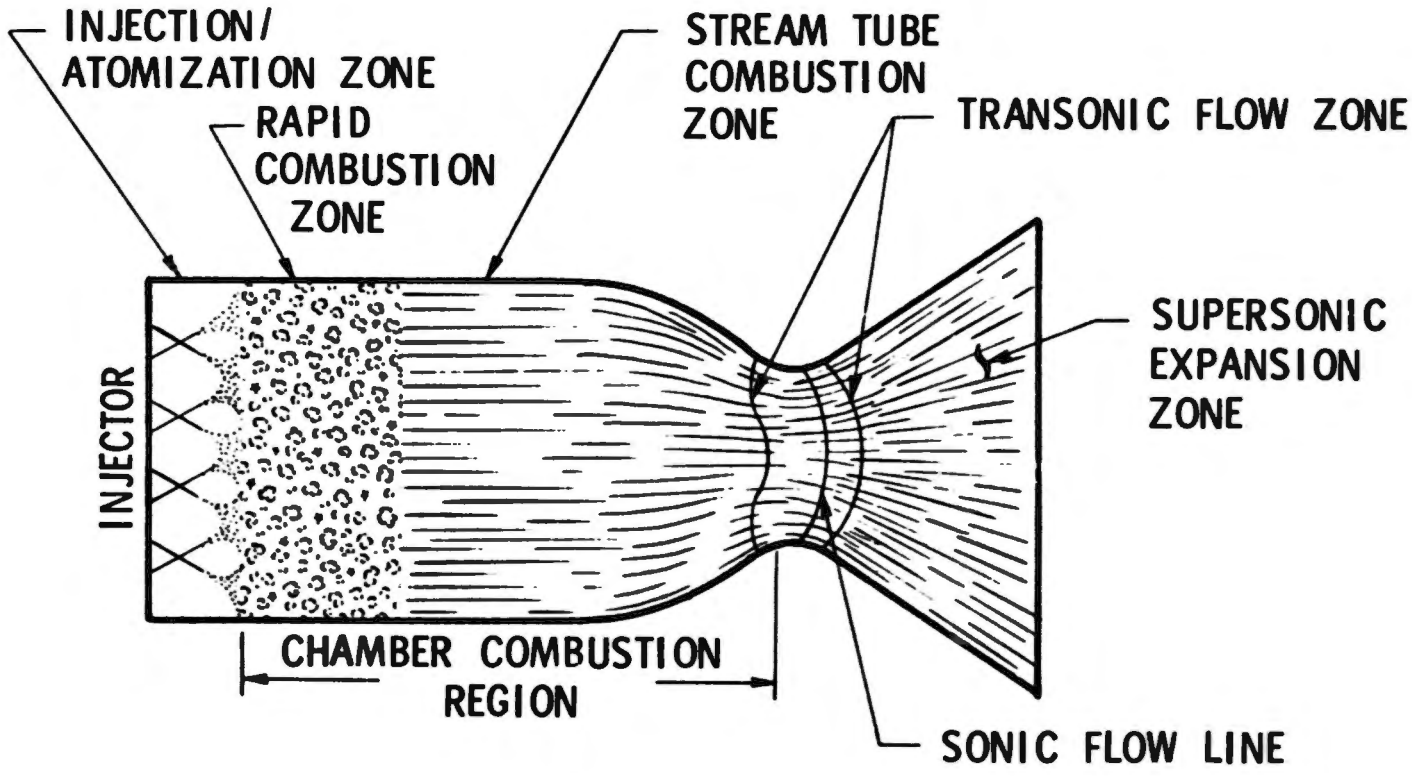

Figure II-2. Subdivision of Combustion Chamber Into Zones for Analysis - Steady-State Operation

each direction with respect to propellant mass fluxes and concentrations, liquid atomization and dispersion rates and properties of the gaseous medium. Some of the gaseous constituents come from local propellant combustion, but they are primarily either gaseous injectants or recirculated combustion produce gases from the next zone downstream. The principal force for driving recirculating gaseous flows is viscous shear between the injected propellants and the surrounding gases. These gases are thereby accelerated in the propellant flow direction and must be continuously supplied by transverse gas flows into the neighborhoods of injection sites. Somewhere in the regions between injection sites, there must be upstream directed flows, as required by continuity of gaseous mass.

The gas-liquid surface shear forces also contribute to distortion and fragmentation of liquid surfaces, i.e., atomization. Some gas/liquid injectors are designed to enhance this shear-breakup mode of atomization, but most liquid rocket injectors provide some kind of liquid-liquid impinegment to enhance atomization due to hydraulic forces.

The primary atomization process is gradual to some extent and requires a finite zone length for completion, which is typically on the order of 1/2 to 2 inches. Spray formation and its dispersion from the (approximately point-source) injection sites proceeds simultaneously. Frequently straight line ray dispersion may be a good approximation, although interactions between sprays from neighboring injection sites may turn the sprays.

As liquid propellant sheets, ligaments and droplets are being formed, they are immersed in the surrounding gaseous medium. Generally, the gases are at somewhat or considerably higher temperatures than the liquid spray elements, so that convective heating of the sprays (and cooling of the gases) will occur. Propellant vaporization is usually negligible at first, because the liquid injection temperatures are far below the propellant saturation temperatures corresponding to the combustion chamber pressure. Continued heating soon raises droplet temperatures enough that vaporization rates become appreciable. During the time required to reach that state, the spray element velocities transport the sprays away from the injector face, through the injection/atomization zone.

For most propellants, liquid-phase reactions are either very fast, essentially preventing mixing between unlike propellants (Ref. 3), or very slow compared to droplet heating and vaporization. Vapor phase chemical reactions, therefore, dominate. Since there is little propellant vaporization in the injection/atomization zone, only a small percentage of the overall combustion occurs in that region. The validity of this argument obviously depends upon the buildup of reaction rates being slower than the approach to complete atomization. The relative balance between these phenomena determines the (approximate) location and the abruptness of the transition between the injection/atomization zone and the next zone downstream.

Rapid Combustion Zone

The second zone in the combustion chamber is characterized by essentially complete primary atomization and comparatively high chemical reaction rates. Dispersion of the sprays and gaseous recirculation in the first zone have reduced the magnitude of transverse gradients in this zone but they are far from being negligible for most rocket engines.

Rapid combustion corresponds to high generation rates of combustion gases. Upon undergoing vaporization and combustion, an element of propellant occupies a volume 100 or more times greater than that which it occupied as a liquid. Expansion of combustion gases from the position where they are formed accelerates the flow axially but also forces transverse flows from high burning rate regions to positions with lower burning rates. These expansion processes simultaneously provide the gases which are recirculated into the injection/atomization zone and close off the recirculation paths by filling them with downstream-flowing gases.

Dense spray droplets accelerate less rapidly than the gases and are only weakly responsive to the combustion gas movements. Acceleration of the combustion gases away from the spray increases the rates of convective heating of droplets and, thus, augments their burning rates. Spray residence times are longer than the gas residence time so that the combustion occurs in a shorter chamber distance

than if the spray and gas velocities were equal. The near-injector gradients in spray mass flux persist, however, being degraded primarily by the dispersion and inter-spray mixing established at injection. Lateral flows of combustion gases will be generated whenever there are appreciable spray flux gradients. Eventually the lateral flow velocities become small compared with axial flow velocities and the combustion field approaches stream tube flow which is characteristic of the next downstream zone.

Chemical reactions within the subsonic flow portion of rocket combustion chambers usually occur very rapidly compared with the spray gasification rates (Ref. 4). Further, local mixing rates between a droplet's vapors and gases flowing around it are high in the droplet wake. Reaction rates are high enough that local thermodynamic equilibrium is rapidly attained.

Stream Tube Combustion Zone

As lateral flows of both burning sprays and combustion gases subside, an essentially streamline flow is developed. Vaporization and burning continue with no more than modest transverse gradients in fluxes and properties, but the flow lacks the strong lateral convective components which are a dominant feature of the rapid combustion zone. Continued mixing depends more upon turbulent exchange between neighboring parallel-flowing striations that upon spray dispersion or lateral convection. High flow velocities in this region, however, lead to short residence times so that turbulent mixing is not very effective. Photographs show the flow to be nearly laminar. To a good approximation, large-scale mixing in this zone can be neglected entirely and the two-phase flow treated formally as stream tube flow.

The gradient in combustion rate decays with increasing axial distance due to early consumption of the smallest spray droplets, decreased residence times as axial velocities increase, and eventually depletion of spray mass flux. Chemical reaction rates, on the other hand, remain high well into the exhaust nozzle. The stream tube combustion region may be considered to extend to the vicinity of the nozzle throat.

Nozzle Expansion Zones

As the combustion products enter and expand through the nozzle, diminishing pressure and temperature gradually reduce the gas-phase chemical reaction rates until it becomes necessary to consider finite-rate chemistry. With most liquid propellants, this effect becomes important downstream of the nozzle throat. For most high efficiency rockets, performance losses due to incomplete propellant gasification and mixing approach their exit values either upstream of the throat or shortly downstream of it; further changes due to spray combustion effects become small compared with chemical kinetic losses and two-dimensional flow effects, which become important in the transonic and supersonic expansion zones (Ref. 5).

REVIEW OF EXISTING STEADY-STATE MODELS

There are on the order of 25 reported analytical models for steady-state liquid rocket combustor operation. Basically, they all start with a set of conservation equations describing the behavior of a combustion gas/liquid flow field. One or more propellant sprays are presumed to be contained within the gas; additional conservation equations are needed for the spray phases. Since the gas stream and sprays coexist and are intermingled, there are exchanges of mass, momentum and energy between them; these exchanges are described analytically by what we will call coupling terms, which appear in both sets of conservation equations. The analytical problem is closed by imposition of initial and boundary conditions corresponding to the particular combustor under study.

In obtaining solutions, each model has been reduced in complexity by introducing simplifying assumptions. In many cases, the simplifications permitted reduction of the coupled partial differential equations to a system of ordinary differential (or, occasionally, integral) equations for the combustion field. Each investigator decided which simplifications were appropriate to his particular combustor situation. As a result there is great diversity in simplifying assumptions among the models.

Despite their apparent differences, however, almost all prior steady-state models share certain common features. First, most are one-dimensional, which implies that all variables are functions only of distance along the axial flow direction. Transverse gradients in the gas-spray flow and recirculation currents of combustion gases are ignored, i.e., conditions are assumed uniform across the combustion space at any axial location. Secondly, most models deal only with the combustion of completely atomized sprays; additionally, in the one-dimensional models they are presumed to be uniformly intermixed at the upstream boundary of analysis. The injected sprays are most often assumed to be represented by a few discrete droplet size groups, each possessing unique values of average droplet diameter, temperature, velocity, etc. depending upon model complexity. Some models are simplified to the point of dealing with a single droplet size. Thirdly, spray vaporization has been adopted as the combustion-rate-limiting process in most models. This choice was corroborated by the definitive work of Bittker and Brokaw (Ref. 4).

Steady-state combustion models may be categorized and discussed according to the complexity with which the governing gas-spray conservation equations are treated, viz.:

a. One-dimensional, decoupled gas and spray flow fields

b. One-dimensional, coupled spray/gas flow fields, constant physical properties for the gas flow field.

c. One-dimensional, coupled spray/gas flow fields, variable gas flow field physical properties.

d. Quasi-one dimensional models (coupled gas/spray flows, variable properties).

   1. Some detailed injector models

   2. Simplified stream tube models.

   3. Coupled stream tube models.

e. Multi-dimensional model (coupled gas/spray flows, variable properties).

Within each of these categories varying degrees of sophistication were applied with regard to the "coupling terms" and the initial/boundary conditions. These will be discussed for each model considered in each category.

One-Dimensional, Decoupled Flows

Chronologically, such models were the first to be tried. By neglecting the coupling with the gas however, no true coupling terms are included, i.e., values cannot be calculated for droplet velocities or residence times, droplet heating or breakup. The mass evaporation rate is calculated to depend only on the first power of the diameter (i.e. droplet diameter regression rate dependent on the reciprocal of the diameter); no convective influence can be considered.

Probert (Ref.6) was the first to report such an analysis; subsequently his work was extended and refined by others (Ref.7 through 10). Williams has given an excellent review of this approach (Ref.11), including effects of various input droplet size

distributions. Usually, because of the many parameters involved, results are plotted in terms of dimensionless parametric groups and only very generalized conclusions can be inferred. Even those reached by Williams in his text regarding the effect of droplet size distribution are now known to be substantially altered by droplet drag and convection.

The main advantage of this method was that it was entirely analytical and did not require numerical solution. While the theory was very incomplete and could not give quantitative answers to engine design questions, nevertheless, it served as the forerunner for more complete models.

One-Dimensional, Coupled Flows, Constant Gas Properties

During the period when such models were being developed, questions arose concerning the correctness of the assumption that spray vaporization was the controlling process. Miesse (Ref.12) and Adler (Ref.13) developed one dimensional models in the 1950's that were concerned primarily with gas phase reaction rates. Miesse's analysis, using an assumption that propellant vaporization was proportional to a linear regression rate of the droplet surface (at rates which were order of magnitude too large), led to an inference that chemical kinetics was the combustion rate limiting process. This conflict was essentially resolved by the work of Bittker and Brokaw in 1960 (Ref.4). They calculated theoretical maximum chemical spatial heating rates in combustion processes and showed that gas phase reaction rates are 10^3 to 10^6 times as fast as typical liquid rocket combustion rates. Thus, spray combustion rates are not significantly influenced by chemical kinetics, but rather are controlled by the physical processes of atomization, vaporization and gross gas phase mixing.

Exceptions to this conclusion might be chemical reactions occurring: (1) within the combustion gas/propellant vapor boundary layer surrounding a droplet (e.g., decomposition of hydrazine), and (2) in low-temperature combustion, which might result from extremely low or high mixture ratios (e.g., gas generator conditions or very poorly designed injectors giving gross nonuniformities in propellant distribution). Consideration of drop vapor kinetics properly belongs in the coupling term expression related to the drop burning rate, which is discussed in a later

section. Mixture ratio striations cannot be modeled with a one-dimensional model, but they can be approximated by a multiple stream tube formulation discussed later. (Even if kinetic losses are not accounted for in such a stream tube model, large mixture-ratio variations are likely to so degrade performance that the design is unacceptable, anyway.) Consequently, the one-dimensional models consider vaporization to be the dominant process in controlling the combustion rate.

One-dimensional models in the coupled flow, constant gas property category correspond to the first attempt to include the combined effects of an interacting spray/gas flow field. The earliest models in this category used an assumption of constant pressure throughout the chamber and considered both propellants (fuel and oxidizer) to be injected as fully atomized liquid sprays. Relative differences between fuel and oxidizer droplet vaporization rates either were not considered or were assumed to be in a constant ratio equal to the injected mass mixture ratio. These assumptions result in a constant (and often excessive) axial gas temperature, a constant gas molecular weight, and constant gas density throughout the chamber. Under these conditions (having knowledge of the approximate flame temperature for the injected mixture ratio) the only gas conservation equation that is really required is the overall continuity equation.

Mayer (Ref.14) was one of the first to develop such a model in 1959. His analysis, however, neglected droplet drag and convective processes by equating all drop velocities to the gas velocity. As a consequence this model would grossly under-predict performance for a given engine length.

Spalding (Ref.15) extended Mayer's analysis to include the interaction of the droplets and gas. To maintain a closed form analytical solution Spalding assumed that all the droplets were of the same size (i.e., a monodisperse spray) and neglected the difference between oxidizer and fuel droplets. Again the burning rate was assumed to be inversely proportional to the first power of the diameter; this is a reasonable assumption if droplet temperature and gas composition and temperature are considered to be constants. (Most burning rate models, such as those of Godsave (Ref.16) or Williams (Ref. 11) etc., reduce to this form under the above conditions.) The analysis at first neglected convection, but was later extended (Ref.17) to include simplified corrections for the convective conditions. This was one of the

first steady-state models that could account for some of the observed trends with liquid rocket engines. Williams has also given an excellent condensation of this Spalding model in Ref.11.

Other similar models were reported during the late 1950's but the application of this approach to analyzing liquid rocket engines largely reached its culmination in 1960 with Priem and Heidmann's work (Ref.18) on propellant vaporization as a design criteria for rocket combustors. They extended the analysis of previous authors to a realistic droplet size distribution and, for the first time within an overall model, considered droplet heating and its effects on vaporization. The formulation of Ref.19, based on spherical heat and mass transfer between a flame and a contained droplet, was used. The analysis required computer solution. Although the assumptions of constant pressure and constant gas properties were retained, this was the first model in which a moderate degree of sophistication was applied simultaneously to both the gas phase and spray equations, to the coupling term expressions (burning and heating rates, drag coefficients), and to the initial conditions. These developments were so important to useful applications of combustion analysis that Ref.18 is sometimes the only work cited in reference to steady-state combustion models.

Priem and Heidmann also applied their model to correlation of experimental data from a range of research scale combustors with several different propellants and varied operating conditions. An empirical equation was developed for correlating changes in design parameters and operating conditions to evaporation efficiency or performance. This correlation has since been used by many investigators for rapid estimation of the effects of design change on performance. An interesting recent application was to multiple stream tubes (Ref.20).

One-Dimensional, Coupled Flows, Variable Gas Properties

Programs in this category represent the most detailed and complicated of the modern, purely one-dimensional combustion models. They employ computerized numerical solutions and remove the restrictions of constant gas physical properties. All of them consider the spray to be input with known or specified drop size distributions. The first such model in this category was that of Burstein, Hammer and Agosta(Ref.21)

in 1962. While retaining the ratio restriction that rates of fuel and oxidizer spray vaporization occur at a constant ratio, this particular model included an integrated gas phase momentum equation and thus accounted for pressure variation along the length of the chamber.

In that same year, work at Rocketdyne culminated in the publication of Lambiris and Comb's state of the art summary regarding stable combustion in liquid propellant rocket engines (Ref.22), which presented the first complete non-restrictive one-dimensional combustion model. A complete set of conservation equations for both the spray and gas phases were included. In addition, appropriate expressions for the coupling terms were included. Godsave's formulation (Ref.16) for droplet burning rate, modified for convective conditions, was applied independently to both the fuel and oxidizer sprays thus allowing inclusion of an axial mixture ratio variation. This, together with axial pressure variation, yielded axially varying gas temperatures and densities. In addition, as in Burstein's work (Ref.21), simplified expressions for droplet breakup were included. The initial sprays were input with specified distributions of droplet sizes. The use of empirical drag coefficient correlations which account for droplet flattening at high Reynolds numbers (Ref.23) was also introduced in this computer program model.

Basically this same model has been modified and enlarged by a number of investigators to include droplet heating (and its effect on mass vaporization rates), supercritical burning of droplets, gas phase injection of one propellant, and the decomposition double-flame front models typically applied to hydrazine-type fuels. The version developed at Dynamic Science (Ref.24) has been disseminated rather widely. Improved numerical methods and extensive functional tables of physical properties were employed in the most recent version (Ref.25).

In practice the gas phase energy equation has been simplified by employing the assumption that the composition and stagnation temperature of the gas are equal to the thermodynamic equilibrium values at the local gas-phase mixture ratio and stagnation chamber pressure. Other gas properties (static temperature, density, etc.) are evaluated from the respective stagnation values by applying local isentropic Mach number corrections under the assumption of frozen composition expansion.

This process, although not strictly valid for a reacting gas, consequently neglects heat and drag energy transfer from the gas to the drops. These terms are, however, properly included in the spray equations and the effect upon burnout of the total droplet energy is properly calculated (energy is conserved). Sutton (Ref.26) investigated this assumption thoroughly by comparing the approximate results with results from an "exact" one-dimensional formulation which retains the complete energy equation and includes extensive tables of gas phase properties as functions of enthalpy, pressure and mixture ratio. He concluded that the simplified energy equation produced gas temperature errors on the order of 3 to 5 percent at low subsonic flow Mach numbers and influenced the droplet burnout location even less. Because the simplified energy equation permits use of simplified tables of combustion gas properties, based on standard thermochemical equilibrium calculations (e.g.,Ref.27), computerized models employing this approximation have been used extensively at Rocketdyne and other locations to aid in the design of new engines and to correlate performance data from existing engines.

More recently, only two significant additional versions of true one-dimensional models have been formulated. The first was by Hammer, Agosta and Peschke (Ref.28) in 1966; this model incorporates the major provisions previously discussed and includes the complete formulation for the energy equation including the equilibrium solution. The second is the previously mentioned due to Sutton and Combs (Ref.26); it incorporates a full energy equation similar to Hammer's et al., but uses tabular data from prior equilibrium analyses. In addition, axial direction effects of gas phase conduction, diffusion and viscosity are also included. The models of Ref.26 and 28 represent the most nearly "exact" formulations to date for steady one-dimensional propellant spray combustion.

One-dimensional models have been extensively used. Their utility stems largely from the basic assumption of one-dimensionality. The analysis is nearly independent of the detailed features of the particular injector used (except for spray droplet sizes and velocities) so that a single model formulation can be applied easily and quickly to a wide range of injectors, propellants, combustors, etc. Hence, when applied to the downstream regions of engines which fall within the approximate domain of one-dimensionality, their performance predictions depend entirely upon the accuracy of input initial conditions and the expressions used for the coupling terms

describing the interaction between the gas and spray phases. It is, in fact, the accuracy of the input conditions (especially the mean drop size and drop size distribution) that relate the one-dimensional model to the particular injector design and make it useful from a design standpoint. As a consequence a great deal of auxiliary work has sought systematic determination of how spray drop size distributions and mean droplet sizes depend on injection element design parameters, e.g., orifice diameters and injection velocities. This has usually been done experimentally by using molten wax to simulate impinging liquid propellants (Ref.29). Results, of course, are applicable to both one- and multi-dimensional programs.

The one-dimensional character of such models is also their major limitation. When applied to engines that have even moderately nonuniform mixture ratio distributions (e.g. wall film cooling), the models fail to predict performance adequately. They are similarly unable to provide information on local miltidimensional problems such as those which arise in studies of injector/chamber compatibility. Adaptations of one-dimensional models such as those described next have offered some approximate, but not complete, solutions to these problems.

Quasi-One Dimensional Models

The simple one-dimensional approximation is inadequate to describe the axial flows and distributions existing near the injector of a liquid rocket engine. As indicated above, it is important to avoid use of one-dimensional models in this region. However, before adoption of the current approach of developing empirical spray mass and drop size distributions through cold flow and molten wax studies, some quasi-one-dimensional combustion models were developed in an attempt to calculate the progress of the propellant combustion within this injection/atomization zone. Typically, multiple coupled one-dimensional flows were assumed to represent the real flow associated with a single injection element. Primary interest was in the degree of partial combustion accomplished and in locating a reasonable starting point for the downstream zone at which the one-dimensional approximation was applicable.

Some Detailed Injector Models. The first of these models (Ref.22) related to self-impinging doublet injection. The model described the region from the center of a fuel spray fan, through a forced mixing region, to the center of a neighboring aligned oxidizer spray fan. A one-dimensional flow zone was established for each

of those regions and a fourth zone was used for a gas flow (without spray) surrounding the other three zones. Spray and/or gas transfer among zones was analyzed as combustion proceeded. A number of poorly understood phenomena were lumped into empirical "incomplete atomization" factors for each spray-bearing zone.

This was a highly physical model involving geometrical zone prescription which drew heavily from high speed photographic records of transparent model motor firings with aligned-element like-doublet injectors. Thus the computer program model was very specific for that type of injector and had limited versatility. It was not possible, for example, to analyze injectors with elements aligned only on one side, etc. As a result it received only limited use and principal reliance was placed on the one-dimensional model for combustion analysis of all impinging-type elements.

A second model, however, because it dealt with the more readily generalized analysis of coaxial gas-liquid injection, has found extensive use. The need for such a model was soon recognized after attempting to correlate performance from such an injector with the basic one-dimensional model. Unlike the impinging type injector, which atomizes the entering jets near the injector face, the gas-liquid coaxial injector may have a liquid jet penetrating 3 to 4 inches from the injector, with simultaneous atomization and burning strongly coupled and distributed throughout that length. Since cold-flow correlations cannot possibly include effects of superimposing combustion on the atomization rates and drop sizes, their principal value for coaxial elements lies in mixing studies rather than in providing combustion model initialization. As a result, a model for this widely used injector type must include both the atomization and vaporization processes in the formulation.

The first generalized coaxial model (Ref.30) was formulated for axisymmetric, cylindrical single element combustion, assumed to be representative of the overall engine combustion. In its original form it applied strictly to injectors having "flush posts," i.e., both an inner cylindrical tube through which the liquid propellant was delivered, and a surrounding annular space for passage of the gaseous propellant were terminated at the injector face. Upon injection, large velocity differences immediately initiate "shear-stripping" of liquid spray from the jet surface. Appropriate equations were contained within the model for calculating both jet stripping rates and local mean drop sizes produced.

Initially, there were two discrete parts to the model. The first, adjacent to the injector, was characterized by an onion-skin type layered structure of spray. This region was assumed to be axisymmetric and non-combusting. When input conditions regarding flammability limits of concentration and flame velocity were satisfied, flame spreading was assumed to be rapid enough that the non-burning region was terminated by a plane flame front standing in the spray laden gases.

The second part of this model was like that of the usual one-dimensional model except that it (1) added a residual liquid oxidizer jet that penetrated into the combustion zone and retained equations for the subsequent atomization of that jet, and (2) allowed for a second zone of axially flowing, fully-burned or non-burning gases surrounding the combusting one-dimensional spray-gas mixture. Mixing between zones was approximated by specifying (input) a linear rate of ingestion of the outer gas flow into the spray-gas flow. In addition, the outer zone was completely coupled to the inner zone through the assumption of no radial pressure gradient. Both zones obeyed their respective conservation equations and their areas were mutually adjusted to match the axial pressure gradient profile and still maintain a full-flowing chamber. This portion of the model is the forerunner of current multiple stream tube models discussed later.

Recently Sutton and Schuman (Ref.31) have redeveloped the model to bring the one-dimensional zone up to the injector face and, in addition, developed equations to describe the process occurring within the recessed "cup." Excellent results have been achieved with this model when predicted performance has been compared with measured values from engines such as Rocketdyne's J-2, J2S and Aerospike. These particular engines are built to deliver relatively uniform flow fields for highest performance.

Simplified Stream Tube Models

In contrast to the foregoing, highly physical models for single element combustion, a quite different quasi-one-dimensional approach considers the entire combustion field to be composed of a large number of stream tubes, with non-uniform striated flows created by the injector persisting throughout the chamber length. Introduced by Wrobel (Ref.32), analyses neglecting mixing between neighboring stream tubes have

been applied to both injector/chamber compatibility (Ref.33 and 34) and combustion inefficiency (Ref.20 and 29) problems. The utility of a stream tube approach depends upon how realistic it is to neglect turbulent mixing and upon accurate description of the injector-imposed striations.

Turbulent mixing between unlike gases flowing in adjacent stream tubes has been shown to proceed slowly (Ref.35) and, within the short gas residence times typical of rocket combustors, is believed to contribute far less to overall propellant mixing than the spray interdispersion associated with injection and atomization, although this has not been unequivocally proven. Injector-imposed striations in the flow are usually characterized experimentally; cold-flow techniques are well-established for bipropellant liquid injection (Ref.36,29). Immiscible propellant simulants are flowed through an actual rocket injector and a collection apparatus is used to sample the flow at a large number of points in some downstream plane. Both mass flux and mixture ratio distributions are derived from the liquid collection data. As an application example, the mean c*-efficiency among n stream tubes, each having flowrate $\dot{w}_n$ and mixture ratio C_n may be approximated as:

$$\overline{\eta_{c^*}} = \frac{\sum_n c^*(C_n)\dot{w}_n}{c^*(\overline{C_i}) \sum_n \dot{w}_n}$$

where $c^*(C_n)$ is a function of mixture ratio and $\overline{C_i}$ is the mean injection mixture ratio.

In addition to the incomplete mixing accounted for by the foregoing, there also may be appreciable degradation of performance due to incomplete spray gasification. While these two sources of performance loss may be coupled, with the presence of one making the other worse, the simplest approach is to treat each separately and assume that their combined effect is the product of the two. Thus, a wide range of experimental c*-efficiency data has been correlated successfully (Ref. 37 and 38) by:

$$\eta_{c^*,\text{pred}} = \eta_{c^*,\text{mix}}\, \eta_{\text{evap}}$$

where $\eta_{c^*,\text{mix}}$ ($\equiv \overline{\eta_{c^*}}$ predicted) is the mass-weighted mean c* efficiency among the stream tubes, assuming complete evaporation within each stream tube and that there

is no mixing between them, and η_{evap} is a mean spray evaporation efficiency, calculated by one-dimensional combustion model analysis for mean initial-plane conditions obtained by mass-weighted averaging over all stream tubes, i.e., assuming complete mixing. Neglecting the coupling between mixing and evaporation losses appears to be justified, to a certain extent, by the degree of correlation attained; in the cited references, the predicted efficiencies were consistently within about ±1 percent of the experimental hot-firing values, which ranged from about 85 to 99 percent.

A somewhat different, uncoupled stream tube approach was taken in Ref. 20, where the stream tubes were initialized near the injector and a separate one-dimensional spray combustion analysis was performed for each stream tube utilizing Priem's empirical correlation equation referred to earlier (p. 13). Imperfect mixing was accounted for by mixture ratio variation from stream tube-to-stream tube and the combustion analysis accounted for incomplete evaporation. Regarding interactions between mixing and evaporation within a given stream tube, then, this formed a coupled model. Uncoupling took the form of absolutely no interactions between stream tubes. Initialized with a given percentage of the chamber cross-sectional area, each stream tube was thereafter assigned that same percentage of local flow area. As a result, neighboring stream tubes with unequal mass fluxes or unequal specific burning rates could be said to be flowing side-by-side with quite unlike pressures. Starting with a uniform injection-end pressure could not, therefore, result in calculation of sonic flow at the geometric throat positions for all stream tubes simultaneously. Such physical unrealities made little difference to the Ref. 20 application of the results; only an integrated, overall approximation of energy release inefficiency was required for subsequent use in analyzing the nozzle expansion efficiency. As with the preceding application to c*, the predicted values of specific impulse were shown to be in agreement with some experimental values.

Coupled Stream Tube Models

The lack of physical reality associated with the foregoing simplified stream tube models makes them applicable to situations in which local details of the combustion flow field are of interest. For example, analysis of combustion chamber wall heat transfer, ablation and erosion requires detailed local combustion gas temperatures, velocities and compositions as well as information about spray splashage on walls. Two related stream tube combustion models have been developed which

provide improved approximations to reality in coupling together a multiplicity of one-dimensional combustion models, one for each stream tube, and solving them simultaneously. One model, developed in conjunction with injector/chamber compatibility analyses (Ref. 34), was designed for use downstream of a three-dimensional model of the rapid combustion zone (see the next section). It was extended (Ref. 39) to axisymmetric flow in the second version, which includes the earlier stream tube initialization directly from injected flows and utilizes a spatial distribution of pressure in the nozzle to make the transonic flow portion of the solution more nearly realistic. By using a one-dimensional, coupled spray gas flow formulation, these models were made fully coupled. They are still based on the assumption of no mixing (i.e., no mass, momentum or energy exchange) among stream tubes.

The model formulations differ from the one-dimensional formulation in several important ways, which arise from the fact that a given tube is not physically confined by walls but is permitted to be squeezed to a smaller size by higher flowrate, faster burning neighboring stream tubes (and vice versa). That is, in the previous one-dimensional models, the cross-sectional flow area is a known, independent parameter, while in the multiple stream tube formulation, it appears as a dependent variable for which solutions must be found. Cross-sectional areas of individual stream tubes can vary, however, only under the constraint that the sum of all stream tube areas must equal the local chamber cross-sectional area. This constraint, in the form of an area conservation equation, is what couples one stream tube's combustion model to the others.

If there are d stream tubes, there are d sets of one-dimensional model equations. Only one equation (area conservation) has been added in the multiple stream tube formulation, while d dependent variables (areas) have been added. To close the problem, therefore, either $d-1$ equations must be added or $d-1$ dependent variables removed. The approach taken in Ref. 34 was removal of dependent variables by assuming that static pressure is constant across any given plane normal to the mean flow, rather than varying from stream tube to stream tube. The computer program solved for the pressure level at each plane, beginning at an initial plane near the injector and marching to the throat.

Programmed for computer solution, this stream tube combustion model was one in a series of related computer programs for overall injector/chamber compatibility analyses. While it was possible to assemble input data manually from full injector cold-flow data (as with the preceding simplified stream tube models) or from a Liquid Injector Spray Pattern computer program output, it was structured to receive punched-card input data generated by its immediate predecessor in the series, a three-dimensional combustion model described in the next section. Similarly, it generated punched-card output for subseqeent Boundary Layer Heat Transfer program analysis (Ref. 34).

The stream tube model of Ref. 34 was "formless" in the sense that not very specific knowledge was needed concerning a tube's position or cross-sectional shape. As a result, the downstream boundary condition was assumed to be one-dimensional sonic flow through the nozzle throat plane. The model was given a specific spatial form in Ref. 39 by specifying axisymmetric annular stream tube flow. Adopted to conform to the JANNAF (ICRPG) reference Two-Dimensional Kinetic computer program (Ref.40) analysis for the supersonic nozzle expansion, this configuration gave stream tube positional data which permitted much more satisfactory nozzle analysis, by means of two model extensions. First, the longer path lengths taken by stream tubes nearer the wall than those near the chamber axis could be accounted for analytically by using each tube's actual path as the independent variable, rather than chamber axial length. Second, the stream tubes' pressures in the nozzle could be made to conform to those for transonic flow. (In practice, these were simplified to local conical convergence – or divergence – and to the pressure distribution for a homogeneous, constant flowrate transonic flow.)

The axisymmetric stream tube combustion computer program was combined, in the work of Ref. 39, with other distinct computer programs to form an overall engine performance analysis computer program which begins with analytical computation of bipropellant spray distributions produced by a prescribed injector design and ends with calculation of specific impulse and thrust coefficient for vacuum exhaust of combustion products from the nozzle. The three-dimensional combustion model, because its results currently need to be examined for consistency before proceeding with further analysis, was omitted from this combined model. Thus the axisymmetric stream tube model was initialized directly from the calculated injected spray distributions, unlike its predecessor. Similarly, it provided partial initialization

of flow data along a supersonic start-line for analyzing the flow in the divergent section of a nozzle.

Multi-Dimensional Model

As a part of the injector/chamber compatibility analysis of Ref. 34, a three-dimensional steady-state spray combustion model has been developed for analyzing the "rapid combustion zone" of Fig. II-2. The model formulation is based on three major simplifying assumptions concerning the combustion field. First, it is assumed that immediately downstream of the injection/atomization (prereaction) zone there are strong enough transverse gradients in spray mass flow (and, therefore, in burning rate) to produce transverse convective flow forces which are large compared to gas-phase viscous forces. The viscous terms in the gaseous momentum equations are, therefore, neglected. The second assumption, that accounting for turbulent motion is not required, follows directly from the first. The third simplifying assumption concerns the transverse pressure gradients; before stating it, the model formulation will be described.

The mathematical formulation for the 3-D combustion model utilizes the cylindrical coordinate system (r,θ,z). Because there are three independent spatial variables, the mass, momentum, and energy conservation equations (for both the combustion gas and propellant spray phases) are partial differential equations. These sets of governing equations are coupled through mass, momentum, and energy exchange between phases; several additional equations provide values for the coupling terms. The gas phase energy equation has been replaced by tables of combustion gas stagnation properties as functions of mixture ratio (for a given chamber pressure) and the adiabatic expansion equation. Specification of appropriate initial plane and boundary conditions completes the model.

The system of equations is solved by means of a digital computer program. "Marching" in the axial (z) direction is used, with simultaneous solutions at discrete nodal points in the r,θ plane found sequentially in predictor-corrector cycles. The gas-phase conservation equations are partially elliptic and, because elliptic partial differential equations are not well-posed as initial-value problems, the third simplification was introduced to avoid the numerical instability certain to result

from that fact: the pressure gradients in the r,θ directions are prescribed, rather than calculated as dependent variables.

Unless the pressure gradients are prescribed properly, the transverse gas velocities will differ from reality approximately as the square root of the errors in pressure gradient. Because of this, the 3-D model is properly viewed as a transition model which acts to distribute the propellant sprays more realistically before starting a stream tube analysis than if the stream tube structure had been begun immediately after the prereaction zone.

As reported in Ref. 34, transverse pressure gradients were effectively forced to vanish by making axial gas velocity a function of z only. Recently, an improvement was made by making the axial pressure gradient uniform rather than the axial gas velocity a function of z only.

EVALUATION OF COUPLING TERMS

The coupling terms are the expressions which describe transport of mass, momentum and energy between spray and gas phases in the combustion flow field conservation equations. All of the steady-state liquid rocket combustion models discussed above depend upon the adequacy of the expressions of the coupling terms for their accuracy.

The current level of understanding concerning spray droplet mass loss rates (due to vaporization, breakup and other mechanisms), droplet heating rates and gas-droplet drag forces are discussed briefly in the following paragraphs.

Vaporization or Burning Rate

Except for the thesis of Strahle, Ref. 41, all existing models for this contribution apply to quasi-steady conditions. The theories range from purely vaporization models (El Wakil, Godsave, Ref. 19 and 16, respectively) to thin-flame front (flame surrounding droplet) models such as Penner's or Williams', Ref. 42 and 11, respectively, Fig. II-3.

All of these aforementioned models avoid mathematical treatment of reaction kinetics within the boundary layer. For the stagnant environment case, recent analytical solutions using the method of matched asymptotic expansions (Ref. 43) have shown that vaporization and thin-flame models actually represent limiting cases of the more general treatment which considers finite rate chemistry. Further, the combustion enhanced gasification rate can be expressed compactly in terms of these two limiting solutions and an appropriate Damköhler number (ratio of characteristics diffusion time to chemical reaction time). This Damköhler number, D_1, may be calculated from

$$D_1 = (\text{const.}) \frac{k\,(T_{f,ad})\,\rho_g^{\,n}\,D_d^{\,2}}{\mathcal{D}\,\rho_g} \sim p^{(n/2)}\,D_d$$

where a single chemical reaction step or order "n" has been assumed. The rate constant, k, is evaluated at the adiabatic flame temperature.

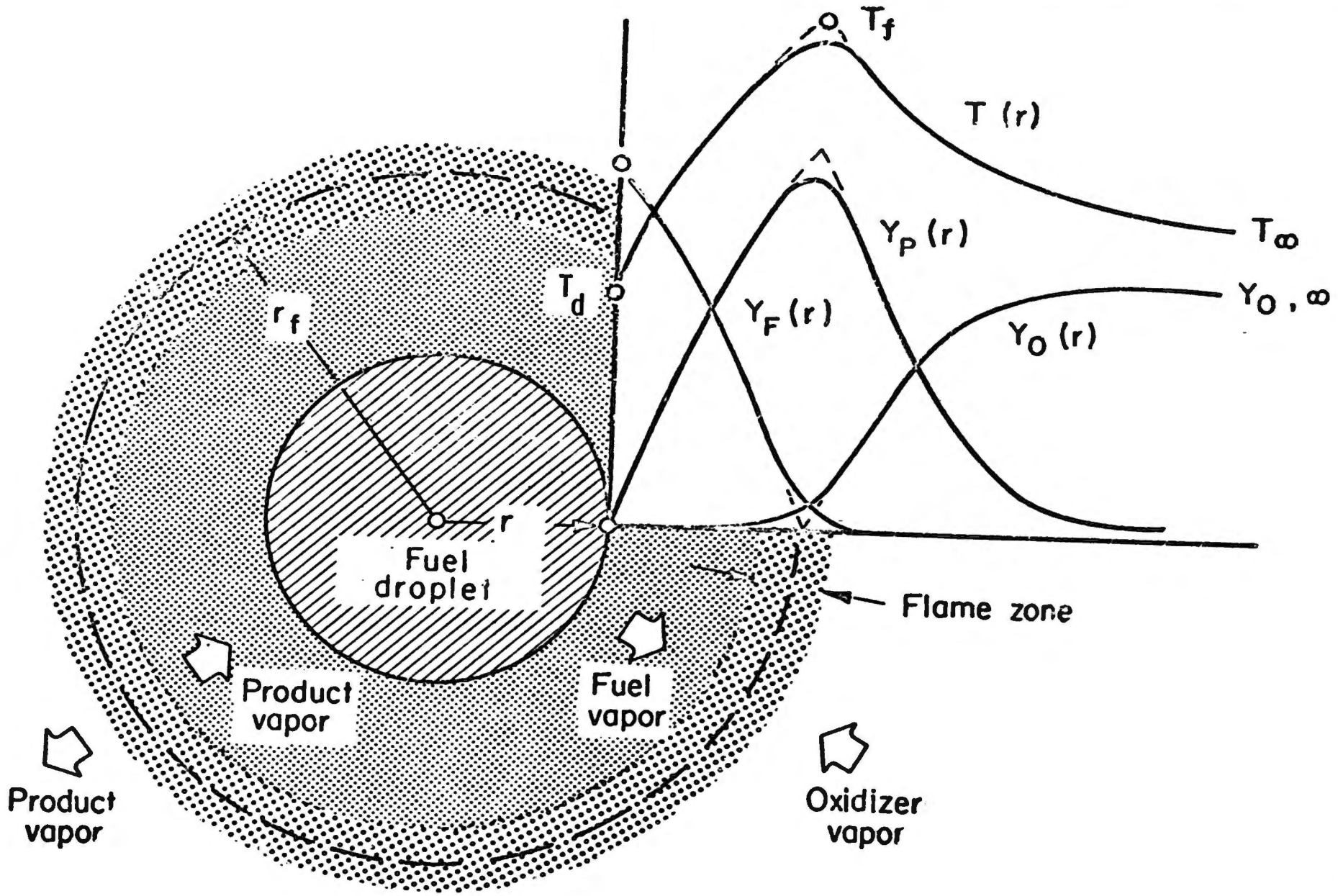

Figure II-3. Thin Flame Zone Droplet Burning Model

For most practical cases, a multivalued solution of the burning rate as a function D_1 is found, with an unstable branch as illustrated in Fig. II-4. As a result, gasification should closely approximate either of the two limiting cases until an auto-ignition or auto-extinction region is reached, whereupon a rapid transition is to be expected. The analysis can predict this transition for completely stagnant conditions; however, moderate convection has been found experimentally (Ref. 44), Fig. II-5, to force the flame into the droplet wake. In any case, the flame enhancement of gasification is removed, resulting in a vaporization process. It is known, also, that flame-holding capability of the droplets is quite sensitive to the free-stream gas temperature. Insufficient data are available as yet to define the relationship between these effects well enough to predict with confidence the extent of flame enhancement on droplet gasification under any prescribed environment. It must be emphasized that both the theoretical treatments and droplet burning experiments (from which the foregoing concepts derive) pertain, almost without exception, to the nonconvective situation. Application of models based on this information to the higly convective environment prevalent in a rocket thrust chamber must be made with caution and with maximum reliance on empirical verification.

In cases with highly convective environment, the El Wakil equations often give a correlation between predicted and observed behavior. In any event heating and gasification rates are enhanced by forced convection; the empirical Nusselt number correlation of Ranz and Marshall (Ref. 45) is invariably employed. Burning rates may also be further enhanced by vapor phase decomposition (Ref. 24).

Droplet Breakup Rate

Although extensive and excellent work has been done on this phenomenan, notably by Nicholls, et al, at the University of Michigan (Ref. 46), problems arise when applying any available breakup model in combustion analysis. This difficulty is probably due to the fact that the experiments have been conducted under conditions which differ substantially from rocket conditions, expecially droplet loading density. As a consequence, all present models greatly overpredict the breakup rate within rocket engines.

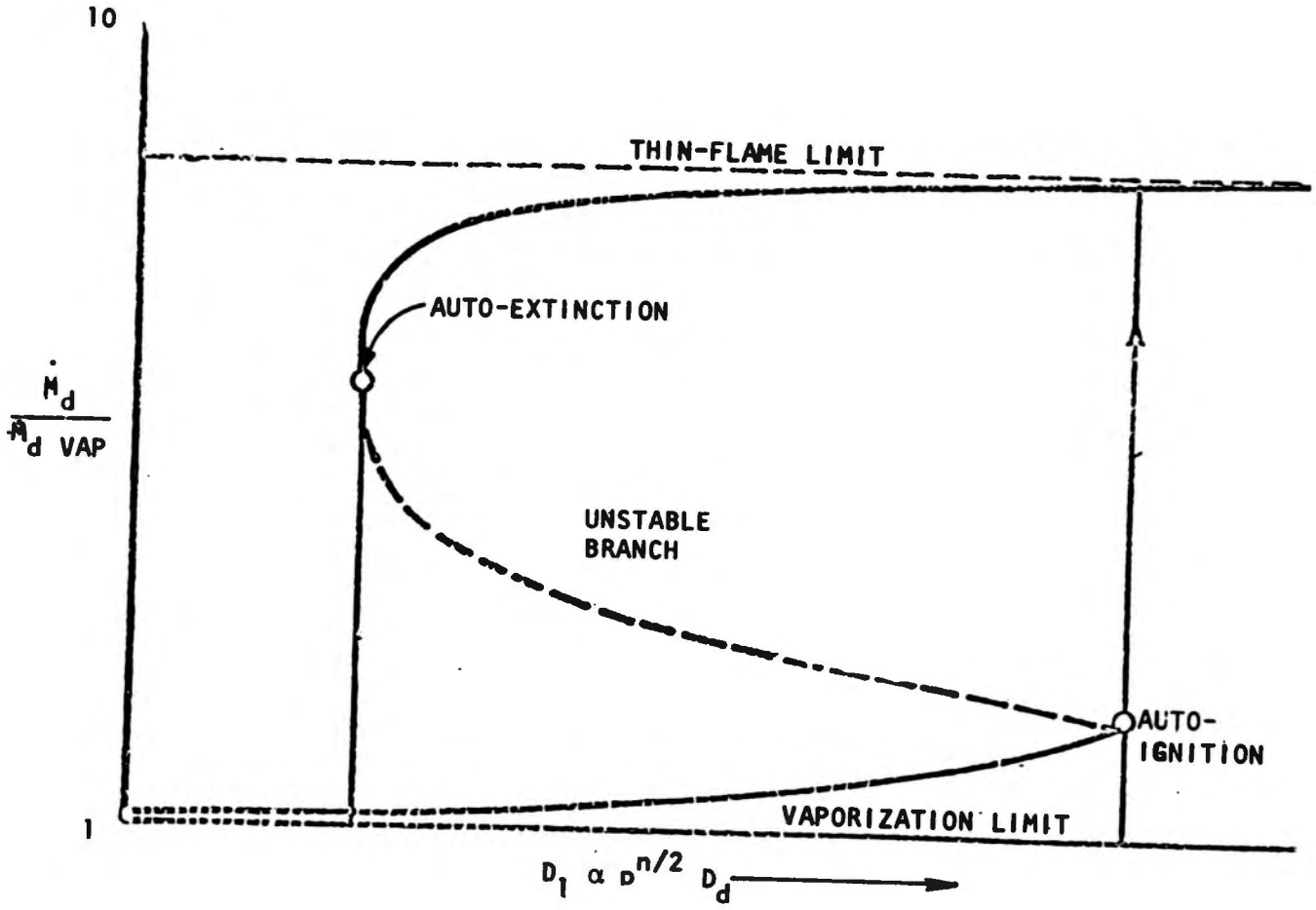

Figure II-4. Vaporization and Burning Rates as Functions of Damköhler Number

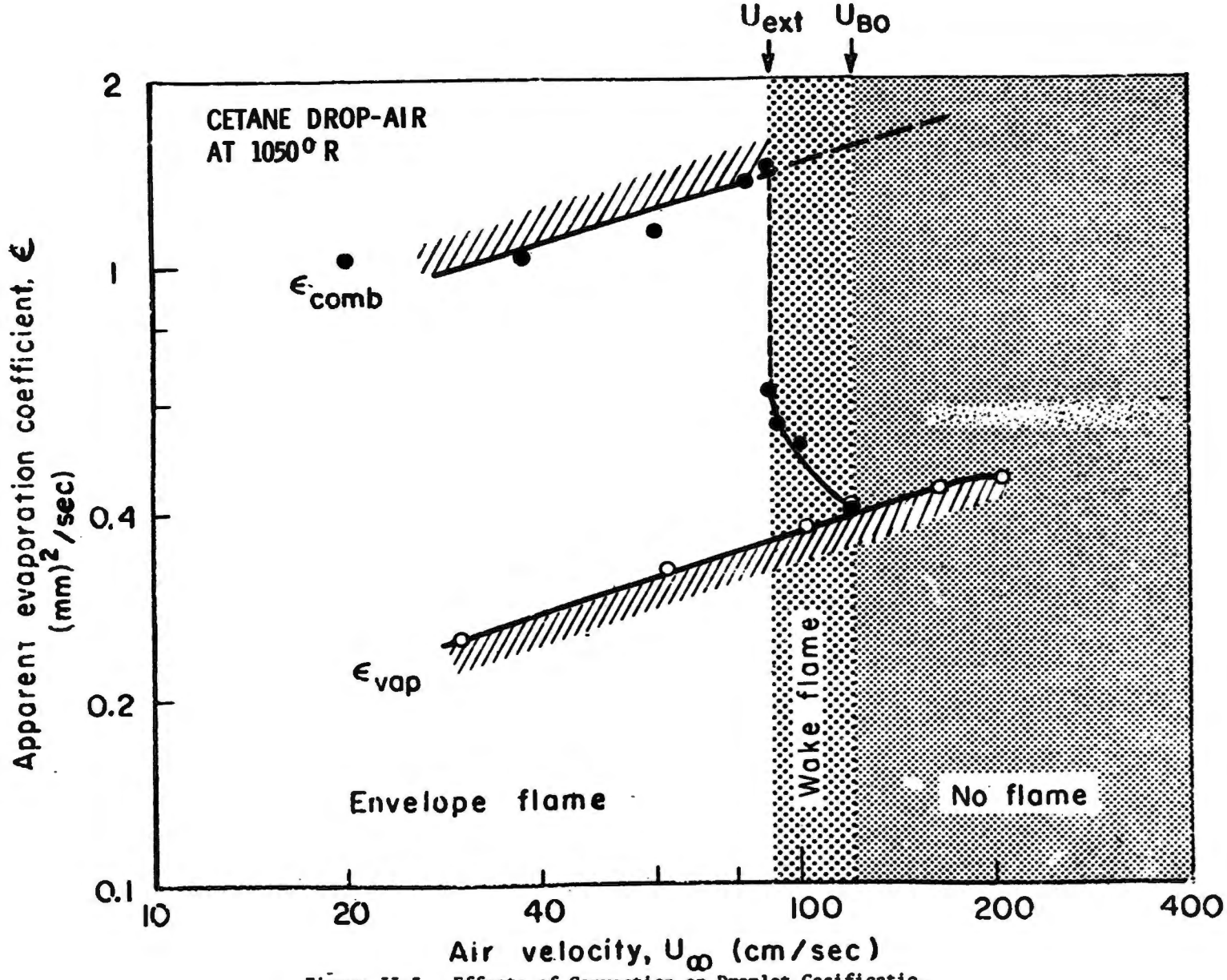

Figure II-5. Effects of Convection on Droplet Gasificatio..

Other Mass Loss Mechanisms

This contribution includes mass addition to the gas phase from processes other than vaporization or breakup. This may include micro-mixing phenomena such as the burning of super-critical drops (Ref. 47 and 48) for which no adequate model considering the effects of convection exists. It may also include effects such as "flashing" (where the drop or portions of it reach a sufficiently high temperature so that drop vapor pressure becomes higher than chamber pressure and hence "flashes" into a vapor) which may occur during periods of transient burning. Or it may include drop vapor accumulation effects in the drop wake or a variety of other phenomena that have received little or no analytical attention.

Droplet Heating

Droplet heating is important and can control the vaporization rate of droplets even in steady-state conditions because of the time required to heat the drop to the usually assumed "wet bulb" condition. Under transient conditions it may be one of the most powerful phenomena, controlling flashing and the vapor pressure. Models to calculate droplet heating range from the El Wakil equations (which assume uniform drop temperatures) to the models of Grossman (Ref. 49) and of Agosta (Ref. 50) which consider radial temperature gradients. For supercritical conditions the behavior is presently unknown once the temperature of the bulk of a drop passes beyond the critical temperature.

Drag Force

Calculation of the drag force on the droplets is accomplished primarily through specification of the droplet drag coefficient. Usually empirical expressions derived from experimental studies of single droplet dynamics are employed (Ref. 51). Drag coefficients for droplets deviate substantially from those for solid spheres because of internal circulation, distortion, and vaporization. Rudinger (Ref. 52), has observed in his experiments that even small numbers of flowing solid particles

apparently have higher effective drag coefficients than do single particles. Similar studies have not been made with loaded sprays; indeed, drag coefficients have not been determined under conditions corresponding to a rocket engine.

Concluding Remarks

From the foregoing brief discussion of coupling terms, it is apparent that the phenomena represented are not fully understood at present, and that, although a good deal of definitive research is continually pursued (e.g., Ref. 26), it may be sometime before really adequate knowledge of all the important coupling terms is attained. In the meantime, a continuing demand may be expected for combustion analysis to support solution of engine development and improvement problems. Therefore, what is known must be used, even though its use introduces substantial uncertainties in derived solutions. In the past, the uncertainties have been reduced by empirically adjusting initial conditions and/or coupling terms to force model predictions to agree with results from some experimental conditions, and then using the model to predict results for as yet untested conditions. To some extent, it has been possible in this process to compensate for uncertainties in coupling terms by making adjustments in initial conditions, which are equally (or even more) uncertain. For example, particular expressions for coupling terms are commonly assumed to be valid and initial plane spray drop sizes and distributions are arbitrarily varied to minimize discrepancies between analytical and experimental results. This kind of empirical justification of combustion model inputs will undoubtedly continue to be required, but as continuing research provides better knowledge of coupling terms, improved knowledge of initial conditions also will be needed (and vice versa) in order that the full potential of the steady-state combustion models may be realized.

APPENDIX II REFERENCES

1. Lewis, J. D.: "Studies of Atomization and Injection Processes in the Liquid Propellant Rocket Engine," Combustion and Propulsion, Fifth AGARD Colloquim: High Temperature Phenomena, MacMillan Co., New York, 141-169 (1963).

2. Lawhead, R. B.: "Photographic Studies of Combustion Processes in Liquid Propellant Rockets, Eighth Symposium (International) on Combustion, Williams and Wilkins, Baltimore, 1140-1151 (1962).

3. Elverum, G. W., Jr. and Staudhammer, P.: The Effect of Rapid Liquid-Phase Reaction on Injector Design and Combustion in Rocket Motors, Progress Report 30-4, Jet Propulsion Laboratory, Pasadena, California (August 1959).

4. Bittker, D. A. and Brokaw, R. S.: Journal of the American Rocket Society, Vol. 30, No. 2, 179-185 (1960).

5. Mitchell, R. C.: The Effect of Nozzle Combustion on Engine Performance, R-7103, Rocketdyne, a Division of North American Rockwell Corporation, Canoga Park, California (January 1968).

6. Probert, R. P.: Phil Magazine, Vol. 37, 94 (1946).

7. Tanasawa, Y.: Tech Report, Tohuher University, Vol. 18, 195 (1954).

8. Tanasawa, Y. and Teisma, T.: Bulletin JSME, Vol. 1, 36 (1958).

9. Williams, F. A.: Phys. Fluids, Vol. 1, 541 (1958).

10. Williams, F. A.: Eighth Symposium (Int.) on Combustion, Williams and Wilkins Co., Baltimore, 50-69 (1962).

11. Williams, F. A.: Combustion Theory, Addison Wesley, Chapter 11 (1965).

12. Miesse, C. C.: Industrial and Engineering Chemistry, Vol. 50, No. 9, 1303-4 (1958).

13. Adler, J.: A One-Dimensional Theory of Liquid Fuel Rocket Combustion, Part II, The Influence of Chemical Reaction, ARC Tech Report No. 20-189, Current Paper No. 446 (1959).

14. Mayer, E.: Journal of the American Rocket Society, Vol. 29, No. 7, pp 505, (1959).

15. Spalding, D. B.: Aero Quart., Vol. 10, No. 1 (1959).

16. Godsave, G. A. E.: Fourth Symposium (International) on Combustion, Baltimore, Maryland, Williams and Wilkens, Co., 818-830 (1953).

17. Spalding, D. B.: A One-Dimensional Theory of Liquid Fuel Rocket Combustion, A.R.C. Tech Report No. 20-175 Current Paper No. 445 (1959).

18. Priem, R. J. and Heidmann, M. F.: Propellant Vaporization as a Design Criteria for Rocket Engine Combustion Chambers, NASA TR R-67 (1960).

19. El Wakil, M. M.: Experimental and Calculated Temperature and Mass Histories of Vaporizing Fuel Droplets, NACA TN 3480 (January 1956).

20. Kors, D. L., Bassham, L. B. and Walker, R. E.: "A Liquid Rocket Performance Model Based on Vaporization Interactions," AIAA Paper No. 69-470 (June 1969).

21. Burstein, S. F., Hammer, S. S. and Agosta, V. D.: "A Spray Combustion Model With Droplet Breakup, Analytical and Experimental Results," Progress in Astronautics and Rocketry, Vol. 6, Academic Press, New York (1962).

22. Lambiris, S., Combs, L. P., and Levine, R. S.: "Stable Combustion Processes in Liquid Propellant Rocket Engines," Combustion and Propulsion, Fifth AGARD Colloquium on High Temperature Phenomena, McMillan Co., Baltimore (1962).

23. Rabin, E. A., Schallenmuller, A. R. and Lawhead, R. B.: Displacement and Shattering of Propellant Droplets, Final Summary Report, AFOSR-TR-60-75, Rocketdyne, a Division of North American Rockwell Corporation, Canoga Park, California (March 1960),

24. Breen, B. P., Zung, L. B., Lawver, B. R., Kosvic, T. C. and Coates, D. E.: Injection and Combustion of Hypergolic Propellants, AFRPL-TR-69-48, Dynamic Science, Monrovia, California (April 1969).

25. Campbell, D. T. and Chadwick, W. D.: Combustion Instability Analysis at High Chamber Pressures, AFRPL-TR-67-222, Rocketdyne, a Division of North American Rockwell Corporation, Canoga Park, California (August 1967).

26. Sutton, R. D., and Combs, L. P.: Research on Pressure Wave Growth in a Homogeneous Spray/Gas Mixture, AFOSR Contract AF49(632)-1705, 1967-1970. Final report to be published September 1970.

27. "ICRPG One-Dimensional Equilibrium Reference Program-Preliminary Description of ODE, a Computer Program for the Calculation of Chemical Equilibrium Compositions With Applications," ICRPG Performance Standardization Working Group (July 1968).

28. Hammer, S. S., Agostor, V. D., and Peschke, W. T.: "Combustion Instability in Liquid Propellant Rocket Engines: Bi-Propellant Spray Combustion,"

29. Dickerson, R., Tate, K., and Barsic, N.: Correlation of Spray Injector Parameters With Rocket Engine Performance, AFRPL-TR-68-147, Rocketdyne, a Division of North American Rockwell, Canoga Park, California (June 1968).

30. Combs, L. P. and Schuman, M. D.: Steady-State Rocket Combustion of Gaseous Hydrogen and Liquid Oxygen, Part II: Analysis for Coaxial Injection, RR64-29, Rocketdyne, a Division of North American Rockwell, Canoga Park, California (March 1965).

31. Sutton, R. D. and Schuman, M. D.: Development of a Generalized Steady-State Combustion Model, Part I: Application to Recessed Coaxial Injectors, Part II: Design Application for the Space Shuttle Injector, Research Memorandum, Rocketdyne, a Division of North American Rockwell, Canoga Park, California (May 1970).

32. Wrobel, J. R.: "Some Effects of Gas Stratification on Choked Nozzle Flows," AIAA Paper 64-266 (1964).

33. Pieper, J. L., Dean. L. E., and Valentine, R. S.: "Mixture Ratio Distribution--Its Impact on Rocket Thrust Chamber Performance," J. Spacecraft Rockets, Vol. 4, No. 6, pg 786-789 (June 1967).

34. Sutton, R. D., Hines, W. S., and Combs, L.P.: "Comprehensive Analysis of Liquid Rocket Combustion," AIAA Paper No. 70-622 (June 1970). Also see Hines, W. S., et al., Development of Injector Chamber Compatibility Analysis, AFRPL-TR-70-12, Rocketdyne (March 1970).

35. Sutton, R. D.: Gas Phase Mixing Under F-1 Combustion Conditions, Research Memo 1278, Rocketdyne, a Division of North American Rockwell, Canoga Park, California, 21 December 1966.

36. Dynamic Properties of a Pair of Impinging Streams and the Uniformity of Mixture Ratio Distribution in the Resulting Spray, Progress Report No. 20-209, Jet Propulsion Laboratory, Pasadena, California (28 March 1956).

37. Falk, A. Y., Clapp, S. D., and Nagai, C. K.: Space Storable Propellant Study - Final Report, R-7677, NASA Contract NAS11199, Rocketdyne, a Division of North American Rockwell, Canoga Park, California (1968).

38. Chamber Technology for Space Storable Propellants, Fourth Interim Report, for Period 29 June 1967 - 26 August 1969, R-7985, Rocketdyne, a Division of North American Rockwell Corporation, Canoga Park, California (September 1969).

39. Combs, L. P., Chadwick, W. D., and Campbell, D. T.: Liquid Rocket Performance Computer Program With Distributed Energy Release, R-8298, Rocketdyne, a Division of North American Rockwell Corporation, Canoga Park, California (September 1970).

40. Pieper, J. L., ICRPG Liquid Propellant Thrust Chamber Performance Manual, CPIA Publ. No. 178, Chemical Propulsion Information Agency, Silver Spring, Md. (September 1968).

41. Strahle, W. C.: 11th Symposium (International) on Combustion, The Combustion Institute, Pittsburgh, Penn., 747-754 (1965).

42. Penner, S. S.: Chemistry Problems in Jet Propulsion, Pergarmon Press, New York (1960).

43. Harrje, D. T. and Reardon, F. H.(editors): ICRPG Reference Book on Liquid Rocket Combustion Instability, Princeton University, Princeton, N. J. (inpress, 1970).

44. Agoston, G. A., Wise, H., and Rosser, W.: "Dynamic Factors Affecting the Combustion of Liquid Spheres," Sixth Symposium (International) on Combustion, Reinhold Publ. Corp., New York, 708 (1957).

45. Ranz. W. E., and Marshall, W. R., Jr.: Chem. Eng. Progress, 48, 141-146, and 173-180 (1952).

46. Nicholls, J. A. et al.: Detonation in Two-Phase Media and Drop Shattering Studies, NASA CR-72421, University of Michigan, Ann Arbor, Michigan (May 1968).

47. Spalding, D. B.: ARS Journal, 29, 828-835 (1959).

48. Faeth, G. M. et al.: "Supercritical Bipropellant Droplet Combustion," Twelfth Symposium (International) on Combustion, Combustion Institute, Pittsburgh, Penn., 9-18 (1969).

49. Sotter, J. G.: Nonsteady Evaporation of Liquid Propellant Drops: The Gross-Man Model, Tech Report 32-1061, Jet Propulsion Laboratory, Pasadena, California (January 1968).

50. Agosta, V. D.: "Nonlinear Combustion Instability: Longitudinal Mode," 6th ICRPG Combustion Conference, CPIA Publ. No. 192 (December 1969).

51. Rabin, E. A., Schallenmuller, A. R. and Lawhead, R. B.: Displacement and Shattering of Propellant Droplets, Final Summary Report, AFOSR-TR-60-75, Rocketdyne, a Division of North American Rockwell Corporation, Canoga Park, California (March 1960).

52. Rudinger, G.: Effective Drag Coefficients for Gas-Particle Flow in Shock Tubes, Project Squid Technical Report No. CAL-97-PU, Cornell Aeronautical Labs, Buffalo, New York (February 1969).

APPENDIX III

PROPELLANT IGNITION MODEL (IGN)

A propellant ignition model was developed as subprogram block IGN of the Pulse Mode Performance Model (PMPM) computer program. IGN was derived directly from the hypergolic ignition model of Seamans (Ref.1)* by adapting it to the pulse mode problem and removing some of its simplifications.

As discussed briefly in the body of this report, IGN was found to encounter serious numerical difficulties, which prevented it from completing its analysis of ignition, when input with typical pulse mode, attitude control engine design, and initial and operating conditions. As a result, it is recommended that the subprogram IGN not be adopted for use in the PMPM computer program. Details concerning development of IGN were not given in the body of the report, but are described and discussed in this appendix.

Following the initial injection of propellants into a space-evacuated rocket combustor, there is a measurable time lag before ignition occurs. Several processes transpiring during that time determine its duration and the characteristics of the actual ignition and the combustion which follows the time lag. The important processes include atomization, vaporization, chamber pressurization, vapor condensation on cold-walls, vapor flow out of the chamber, deposition or accumulation of energy in the combustor and chemical reactions. These low pressure, bipropellant pre-ignition phenomena have been described and discussed in literature concerned with their analysis (Ref. 2 through 5), culminating in the computerized model of Ref. 1.

SUMMARY OF SEAMANS' IGNITION MODEL

Seamans' ignition model consists of mass and energy balances for the preignition flow and reaction processes of hypergolic propellants, including heat losses to the combustor walls, and an ignition criterion. Initial conditions are prescribed

*References for this appendix are listed on page III-13

and the equations are solved numerically, marching in time. Ignition is said to occur when the value of an ignition parameter

$$S_{ign} = \left(\frac{T_g - T_{g_o}}{T_{g_o}} \right) \left(\frac{E_{ign}}{RT_{g_o}} \right) \qquad \text{(III-1)}$$

exceeds unity whereupon the model calculations are terminated. Increasing the reaction rates depends upon raising the reactant concentrations (through vaporization and pressurization) and temperatures (through accumulation of energy in the gases). This can be seen from the Arrhenius equation used to compute the generation rates of reaction products:

$$\frac{dc_i}{dt} = A_{ii}\, c_f c_o \exp(-E_i/RT_g). \qquad \text{(III-2)}$$

Increasing the gas temperature depends upon energy generation or deposition in the combustion space. Hypergolic propellants provide their own energy source. Liquid phase reactions and the production of reaction intermediates may sometimes be important sources (or sinks) of energy, as Seamans shows regarding production of an NO_2/MMH adduct. For nonhypergolic propellants, supply of additional ignition energy is required; extension of Seamans' hypergolic ignition model to these propellants would need an external source term in the energy balance.

Reactant vapor concentrations vary with time, depending upon the previous and current balances among vaporization rates, consumption rates (by reaction and condensation) and vapor outflow through the nozzle. Condensation and vaporization rates are calculated in Ref. 1 using expressions for effusive flow from Kinetic Theory of the form:

$$\frac{\Delta m_v}{\Delta t} = \alpha_s A_s \Delta p \left[\frac{g_c M_v}{2\pi R T_s} \right]^{1/2} \qquad \text{(III-3)}$$

where $\Delta p < 0$ for condensation and $\Delta p > 0$ for evaporation, and the subscript "s" refers to the appropriate mass transfer surface. In the computer program of Ref. 1, total propellant vapor generation in time Δt is calculated by summing over a large number of expressions, one for each discrete spray element existing in

the chamber. Spray elements are "tagged" as they are injected during each Δt interval; equations are provided to calculate their masses, droplet diameters, and temperatures as their residence times in the chamber progress. Spray elements may cease to contribute vapor if they are consumed, become frozen, impinge on the combustor wall, or flow out through the nozzle.

This model is essentially a "first pulse" model, because it assumes the combustor is initially completely evacuated. Flow and energy equations are written (and programmed) as if the chamber gases are composed solely of fuel and/or oxidizer vapors.

Seamans showed good agreement between ignition model predictions and experimental data for ignition delay times and chamber pressurization rates.

MODIFICATIONS FOR PULSE MODE APPLICATION

Two types of modifications were made in implementing Seamans' model into the PMPM computer program: (1) modifications to integrate the model into the more general pulse mode formulation, and (2) modifications to remove some simplifications in the treatment of certain physical phenomena by the model.

The first type of modifications included: (1) restructuring of input data to avoid redundancy with data input in other subprogram blocks; (2) transferring data to and from IGN via label CØMMØN block specifications; (3) subroutinizing the model to achieve a more modular structure, (4) providing logic for nonvacuum, partially filled chamber conditions at the start of a pulse, e.g., which may be initiated at some time during the decay transient of a previous pulse; and (5) provision of time-varying injection rates determined by the feed-system model.

The second type of modifications were mainly concerned with propellant injection, atomization and vaporization, viz: (1) addition of impingement delay times, (2) an attempt to acount for flash vaporization and resultant microatomization, (3) reformulation of the droplet and vapor equations expressing energy conservation, and (4) included provision of a spatial energy source term, e.g., an igniter.

Some advances in the transient treatment of propellant spray processes were reported by Webber (Ref. 6), whose methods for these and other preignition processes are compared with Seamans' methods in Table III-1.

Subroutinization and Nonvacuum Starts

A source deck of Seamans' hypergolic ignition computer program was obtained and modified slightly to: (1) make it compatible with the job control language of Rocketdyne's IBM System 360 computer, and (2) reinstate the N_2O_4/MMH propellants and combustor design used for Seamans' example case in Ref. 1. The example case results were then duplicated in a run on Rocketdyne's computer.

The program was next subdivided into a number of subroutines, essentially as shown in the simplified IGN flow chart, Fig. III-1. Again, as a program development check point, the same example case was run and the results were essentially duplicated.

Referring to Fig. III-1, the first pulse (IP = 1) in a pulse train is assumed to occur under vacuum initial conditions, i.e., the combustor contains no propellant vapors or sprays. For this pulse, the input data and program initialization (VACIN) are essentially duplicated from Seamans' program. Subsequent pulses (IP > 1) are initialized, if appropriate, by subroutine TRCØIN with residual combustor contents (nonburning propellant sprays and vapors) from the immediately preceding pulse. Residual spray of each propellant is arbitrarily assigned to eight spray ensembles with identical velocities but with a distribution of chamber residence times. Each initial ensemble is subdivided into three size group classes, just as the newly injected ensembles will be subdivided subsequently. Residual combustion gases and propellant vapors are entirely reassigned as fuel vapors and oxidizer vapor, conserving mass of each. A finite initial chamber pressure is calculated by means of a state equation, using mixed vapor properties.

Subroutine IGFEED supplies propellant injection parameters for the ignition model. It calls upon subroutine FEEDS, described in the body of the report as part of subprogram PULSE, to compute transient injection rates and velocities as functions

TABLE III-1. COMPARISON OF SEAMANS' AND WEBBER'S ANALYTICAL TREATMENT OF PREIGNITION COMBUSTION CHAMBER PROCESSES

Process or Phenomenon	Seamans' Model (Ref. 1)	Webber's Model (Ref. 6)	Deviation From Seamans' Model for Pulse Mode Model
Delayed vaporization for impinging stream injectors	None	None for flash vaporization; otherwise $t_{imp} = \ell_{imp}/u_{inj}$	Adopt Webber's
Flash vaporization of propellants	None	Isenthalpic: $X_{vap} = \frac{H_{inj} - H_{cond}}{H_{vap} - H_{cond}}$	(Attempted to adopt Webber's)
Microatomization due to flash vaporization	None	For $P_c < P_{vap}$: $\bar{D} = \frac{(1 + K)4\sigma}{P_v - P_c}$	(Attempted to adopt Webber's)
Molecular vaporization	Effusion: $m_D = a_e A_D [P_v(T_D) - P_v]x \Delta t_n (g_c M_d / 2\pi RT_D)^{1/2}$	None (assumes continuum mechanics)	
Droplet cooling (freezing)	$Q_{gD} = 2h_D A_D (T_g - T_D)\Delta t_N$	Initial estimate from flash vaporization	
Droplet acceleration (deceleration)	None (spatial gas velocities not known)	Drag Law: $\frac{d}{dt}(u_d) = f(C_D, D_D, \Delta u_{gD})$	
Droplet-wall impact	After mean delay time: $\Delta t_{DW} = \ell_w / u_D$	None	
Droplet heating by wall	$Q_{wD} \ni f(t)(T_w - T_D)$ if $x_{D,frozen} \leq 0.8$	None	
Droplet outflow through throat	Stop evaporation after: $j_{max} = \ell_{i-t}/(u_D \Delta t_N)$	Stop evaporation when passes through throat	
Vapor recondensation	Via negative $[P_v(T_D) - P_c]$ in effusion eq'n.	None	
Formation of reaction intermediates	$\frac{dc_i}{dt} = A_{1i} c_f c_o e^{(-E/RT_g)}$	None	
Gas phase heating	Arrhenius eq'n. for preignition reactions $\rightarrow Q_{vp}$	None	Add a source term for external ignition energy
Gas outflow $\rightarrow$ nozzle	Supersonic only, no consideration of two-phase flow	Sub- and supersonic, no consideration of two-phase flow	Add subsonic gas flow equation
Wall heat loss--wall temperature	$Q_{vw} = h_c A_c (T_g - T_w)\Delta t_N$	None	
Ignition criterion	$S_{ign} = \left(\frac{T'_g - T_{g_o}}{T_{g_o}}\right)\left(\frac{E_{ign}}{RT_{g_o}}\right) \geq 1$	Delay time: $\tau_{ign} = \frac{RT^2 \rho c_p}{EAE_{ign} c_f c_{ox}} e^{(-E/RT)}$	
Pressure rise after ignition	None	Via continuous analysis, with burning after τ_{ign}	Pulse combustion model
Pressure spike due to explosive reaction-intermediates	None	None	

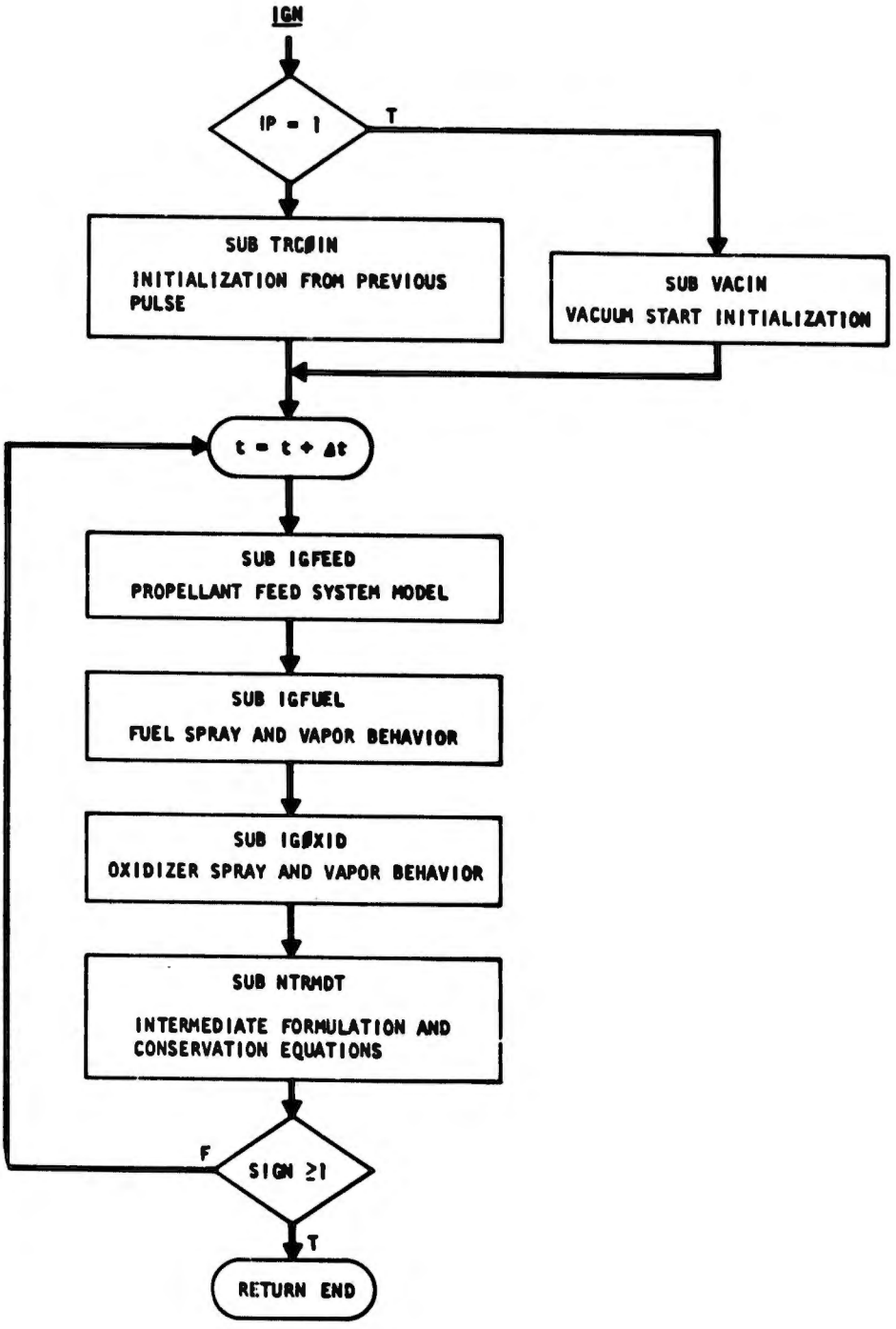

Figure III-1. Block Flow Chart of Subroutine IGN

of injection ΔP. Residual propellants left downstream of the valves from a preceeding pulse may be partially injected before the valve(s) actually begin to open.

Subroutines IGFUEL, IGØXID, and NTRMDT contain, more or less directly, the logic for analyzing spray behavior, intermediate reactions, and nozzle out flow that existed originally. Type 2 modifications were made in these subroutines, as described in the next subsection.

Extension Modifications

At times when the chamber pressure is lower than a propellant's vapor pressure corresponding to its injection temperature, flash-vaporization should attend injection of that propellant. Abrupt partial gasification and atomization to very fine droplets characterize this process. Chamber pressurization should also be accomplished very rapidly so that flashing might not persist for a long duration; however, this condition is very important while it exists.

On the other hand, propellants with vapor pressure lower than chamber pressure will be atomized by some other process. This usually will occur more slowly and produce coarser spray than does flash vaporization. Typically, rocket injectors rely upon some kind of propellant impingement to effect atomization. For that reason, a modification programmed into IGN delays the heating, gasification, etc., of an ensemble until it has been in the combustion chamber longer than an "impingement delay time," calculated as (constant) impingement distance divided by (variable) ensemble injection velocity.

Another, more profound modification was attempted, but was found to introduce severe numerical problems. Webber's (Ref. 6) treatment of flash vaporization (Table III-1) was programmed in a new subroutine FLASH, called by subroutines IGFUEL and IGOXID whenever chamber pressure was lower than injection vapor pressure. Run under Seamans' example case conditions (N_2O_4/MMH propellants, fast-opening fuel valve, slowly opening oxidizer valve, and initially completely evacuated chamber), the model produced droplets so small that their thermal

responses within Δt = 0.025-millisecond time steps were grossly overcalculated. For example, droplets said to be frozen at time t_1, were said to have accepted so much heat during Δt that they were computed to be vaporizing rapidly at time $t_2 = t_1 + \Delta t$. Then, because their vaporization rates were so high, their heating rates could not provide all the required heat of vaporization so they ended the next time step in the frozen condition again. It was not desirable to shorten the time step appreciably, because of the large number of ensembles that would then be produced and the attendant increased run costs. Therefore, several attempts were made toward suppressing the oscillatory numerical behavior, but without success. Consequently, the extension to flash vaporization was abandoned.

During attempts to incorporate flash vaporization, a number of questionable simplifications concerning spray and vapor energy balances were encountered. As a result, a thorough review was made of the model and the energy balances were restructured. Whereas Seamans' model dealt with internal energies, the revision deals with enthalpies. The revised model considers zero enthalpy to occur at absolute zero temperature and uses mean specific heats over the solid, liquid, and gaseous ranges. The enthalpy of a vapor at T_g is thus taken to be

$$H_v = \bar{c}_{ps} T_{FP} + \bar{c}_{pl}(T_{BP} - T_{FP}) + \bar{c}_{pv} (T_g - T_{BP}) + \lambda_f + \lambda_v$$

where FP = Freezing point, BP = boiling point, λ_f = heat of fusion, λ_v = heat of vaporization. By contrast, the earlier formulation simply used

$$U_v = \bar{c}_v T_g$$

which would suffice if the zero of internal energy were at the propellant's normal boiling point. However, negative liquid energies were not printed out. The effect of the energy balance revisions upon computed results for Seamans' example case resulted in a smaller suppression of gas temperature and earlier ignition; the ignition delay time was reduced from 3.86 millisec. to 3.0 millisec.

To simulate addition of energy, e.g., by an electrical or pyrotechnic igniter, a uniform spatial heat source term was added to the vapor phase energy equation. This is a pure heat source term, with no mass addition, because the model cannot handle nonpropellant gaseous species. This was evaluated only to the extent of ensuring that a positive source term actually hastened ignition.

APPLICATION EXPERIENCE

The ignition model IGN was integrated with the PMPM subprogram block .PULSE and checkout runs were made using input data characteristic of the Rocketdyne SE-9 attitude control engine. Numerical instabilities were encountered in the ignition model calculations which grew sufficiently in amplitude to terminate the calculations prior to attaining ignition. Input data were arbitrarily changed in an effort to reduce the numerical difficulty, without success. None of the runs completed the preignition period. Examination of the data suggested that either the time steps were too large or the propellant flow buildup rates were higher than the numerical method can accommodate. Although the SE-9 valve opening times were comparable (~1 millisecond) to Seamans' fuel valve opening time, the injection ΔP's were high enough that the preignition flowrates were substantially higher than those in Seamans' example case.

One final check was made. The flowrates and their buildup rates from the SE-9 case were input into the nonintegrated version of IGN, which had given somewhat faster ignition for Seamans' example case than did his original model. A limit was again reached beyond which numerical instability prevented completion of the run. Thereupon, no further exploratory runs were made and the model was replaced by a constant ignition time-delay option.

CONCLUDING REMARKS

Application of the ignition model was stopped before its worth or capabilities had been fully explored. The numerical problems with flash vaporization and high flowrates and high buildup rates suggest that an improved numerical solution method might be required to develop a workable subroutine IGN.

Any work directed toward improving Seamans' or this related ignition model should include a reexamination of the ignition criterion. The one used here, $S_{ign} \geq 1$, Eq. (III-1), may be derived for the physical situation of slow, uniform heating of a stationary spherical volume of gas initially at temperature T_{go}. Rearrangement of Eq. III-1 shows that the gas must be heated until

$$T_g' \geq T_{go} + \frac{RT_{go}^2}{E_{ign}} \qquad \text{(III-4)}$$

before ignition will occur. In other words, the hotter the gas is initially, the more it must be heated to obtain ignition. This is a rather tenuous result, at best. Its applicability to ignition of a reacting, two-phase flow situation is highly questionable and the derivation of a better criterion is recommended.

NOMENCLATURE

A	area
A_{ii}	pre-exponential factor in Arrhenius rate equation
c	species concentration
c_p	specific heat at constant pressure
$\overline{D}$	mean drop size
E	activation energy
E_{ign}	ignition energy
g_c	gravitational coefficient
H	enthalpy
h	heat transfer coefficient
ℓ_{imp}	impingement length
ℓ_{iw}	injector-to-wall path length
ℓ_{i-t}	injector-to-throat path length
M	molecular weight
m	mass
Q_{gD}, W_{vw}, W_{WD}	heat transferred from: gas to drop, vapor to wall, wall to drop
R	gas constant
S_{ign}	ignition criterion parameter
T	temperature
t	time
U	internal energy
u	velocity
X_v	mass fraction vaporized
x	mass fraction
Z	heat blockage parameter

Greek

α_e, α_s	accommodation coefficient for effusion
ρ	density
σ	surface tension
τ_{ign}	ignition delay time

Subscripts

c	chamber
cond	condensation
D	droplet
f	fuel
g	gas
i	intermediate reaction product
inj	injection
N	n^{th} time step
o	oxidizer or initial value
s	surface
v, vap	vapor
w	wall

APPENDIX III REFERENCES

1. Seamans, T. F. and Waser, P. D., Effects of Additives on Ignition Delay and Chamber Pressurization of Space Ambient Engines, Final Report, AFRPL-TR-69-68, Thiokol Chemical Corp., Reaction Motors Div., Denville, N.J., July 1969.

2. Agosta, V. D. and Krause, G., "An Investigation of the Impulse Bit Developed by a Pulsed Liquid Propellant Rocket Engine," AICHE CEP Symposium Series, No. 52, Vol. 60, 1964.

3. Seamans, T. F. and Dawson, B. E., Hypergolic Ignition at Reduced Pressure, AFRPL-TR-67-129, Thiokol Chemical Corp., Reaction Motors Division, Denville, N. J., June 1967.

4. Seams, T. F., Vanpee, M. M. and Agosta, V. D., "Development of a Fundamental Model of Hypergolic Ignition in Space-Ambient Engines," AIAA Journal, Vol. 5, No. 9, September 1967.

5. Webber, W. T., "Calculation of Low-Frequency Unsteady Behavior of Liquid Rockets from Droplet Combustion Parameters," AIAA Paper No. 70-621, June 1970.